Jurassic to Cenozoic Magmatic and Geodynamic Evolution of the Eastern Pontides and Caucasus Belts, and Their Relationship With the Eastern Black Sea Basin Opening

Haessig, Marc; Moritz, Robert; Ulianov, Alexey; Popkhadze, Nino; Galoyan, Ghazar; Enukidze, Onise

How to cite

HAESSIG, Marc et al. Jurassic to Cenozoic Magmatic and Geodynamic Evolution of the Eastern Pontides and Caucasus Belts, and Their Relationship With the Eastern Black Sea Basin Opening. In: Tectonics, 2020, vol. 39, n° 10. doi: 10.1029/2020TC006336

This publication URL: https://archive-ouverte.unige.ch/unige:143271
Publication DOI: 10.1029/2020TC006336

Tectonics

RESEARCH ARTICLE
10.1029/2020TC006336

Special Section:
Tethyan Dynamics: From Rifting To Collision

Jurassic to Cenozoic Magmatic and Geodynamic Evolution of the Eastern Pontides and Caucasus Belts, and Their Relationship With the Eastern Black Sea Basin Opening

Marc Hässig[1], Robert Moritz[1], Alexey Ulianov[2], Nino Popkhadze[3], Ghazar Galoyan[4], and Onise Enukidze[5]

[1]Department of Earth Sciences, University of Geneva, Geneva, Switzerland, [2]Institute of Earth Sciences, University of Lausanne, Lausanne, Switzerland, [3]Al. Jalenidze Institute of Geology, Ivane Javakhishvili Tbilisi State University, Tbilisi, Georgia, [4]Institute of Geological Sciences, National Academy of Sciences of Armenia, Yerevan, Armenia, [5]M. Nodia Institute of Geophysics, I. Javakhishvili Tbilisi State University, Tbilisi, Georgia

Abstract The magmatic arcs of the Eastern Pontides and Lesser Caucasus lie in continuation from one another. A comparison of the subduction-related magmatic rocks outcropping throughout this segment of the Northern Tethyan belt exhibits chronological disparities, questioning the common subduction history of the Eastern Pontides and the Lesser Caucasus regions. New data and observations including geochronological and geochemical data, relative to subduction- to collision-related magmatic rocks, argue a novel paleogeographic reconstruction illustrating Mesozoic and Cenozoic evolution of this region. Jurassic to Early Cretaceous arc magmatism runs mainly from the Sochi-Ritsa/Bechasyn regions (Greater Caucasus) toward the southeast to the Alaverdi region and further into the Lesser Caucasus. Late Cretaceous and Cenozoic arc magmatism is evidenced throughout the Eastern Pontides extending through the Bolnisi region to the Lesser Caucasus arc. East to west, Jurassic to Early Cretaceous and Late Cretaceous to Cenozoic portions of arc split to the north and south of the Eastern Black Sea, respectively. Throughout Cretaceous subduction, this segment of the magmatic arc of the Southern Eurasian margin was torn in two due to the oblique opening of the Eastern Black Sea as a back-arc to intra-arc basin, from west to east. This reconstitution implies that the Jurassic-Early Cretaceous subduction-related magmatic rocks of the Greater Caucasus are remnant portions of the Eastern Pontides and Lesser Caucasus arcs. This infers the emplacement of subduction- to collision-related magmatic rocks throughout the Mesozoic and Cenozoic along the entire Southern Eurasian margin is solely due to a single long-lasting north dipping subduction.

Key Points:
- Early Jurassic-early Cenozoic subduction/collision-related magmatic arc emplacement is due to a single north dipping subduction
- Early Cretaceous roll-back and Eastern Black Sea opening caused gradual separation of a remnant arc from the active supra-subduction zone
- Jurassic arc-related magmatic of the Greater Caucasus belong to the arc of the north dipping subduction below the Southern Eurasian margin

Supporting Information:
- Supporting Information S1
- Figure S1
- Figure S2
- Figure S3
- Figure S4
- Table S1
- Table S2
- Table S3

Correspondence to:
M. Hässig,
marchassig@gmail.com

Citation:
Hässig, M., Moritz, R., Ulianov, A., Popkhadze, N., Galoyan, G., & Enukidze, O. (2020). Jurassic to Cenozoic magmatic and geodynamic evolution of the Eastern Pontides and Caucasus belts, and their relationship with the Eastern Black Sea Basin opening. *Tectonics*, *39*, e2020TC006336. https://doi.org/10.1029/2020TC006336

Received 2 JUN 2020
Accepted 7 SEP 2020
Accepted article online 16 SEP 2020

1. Introduction

The Eastern Pontides (EP) and the Lesser Caucasus (LC) regions are in continuation from one another, from west to east, as illustrated by the similar geology of the EP and Somkheto-Karabagh (SK) magmatic arcs, the Izmir-Ankara-Erzincan suture (IAES) and Amasia-Sevan-Akera suture (ASAS) zones, and the correlated ophiolitic nappe extending from northern Turkey to Armenia, Eastern Azerbaijan and northeastern Iran (Figure 1). The geology of the EP and the LC is generally accepted as resulting from the successive subduction of Paleotethyan and Neotethyan realms toward the north, below the Southern Eurasian margin along a common and continuous plate boundary (Adamia et al., 2011; Barrier et al., 2018; Dercourt et al., 1986; Khain, 1975; Saintot et al., 2006; Saintot & Angelier, 2002; Sosson et al., 2017; Stampfli et al., 2001). Yet subduction-related magmatic rocks cropping out throughout the EP and the LC are diachronic between western and eastern sectors, respectively (Figure 2; ESD 1). The EP preserve mainly Late Cretaceous and Cenozoic ages, with very few occurrences of Jurassic to Early Cretaceous magmatic rocks, whereas the LC preserves Jurassic to Early Cretaceous, Late Cretaceous, and Cenozoic ages (Figure 2, and references therein).

An alternative model considers the Black Sea as a relic of the Paleotethys realm, which mostly disappeared due to a south dipping subduction just north of the EP and LC throughout the Mesozoic and the early Cenozoic (Bektaş, 1986; Eyüboğlu, 2010, 2015; Eyüboğlu et al., 2013, 2017, 2018, 2019; Liu et al., 2018). In this alternative setup, the Northern Neotethyan realm opened in a back-arc configuration of this south

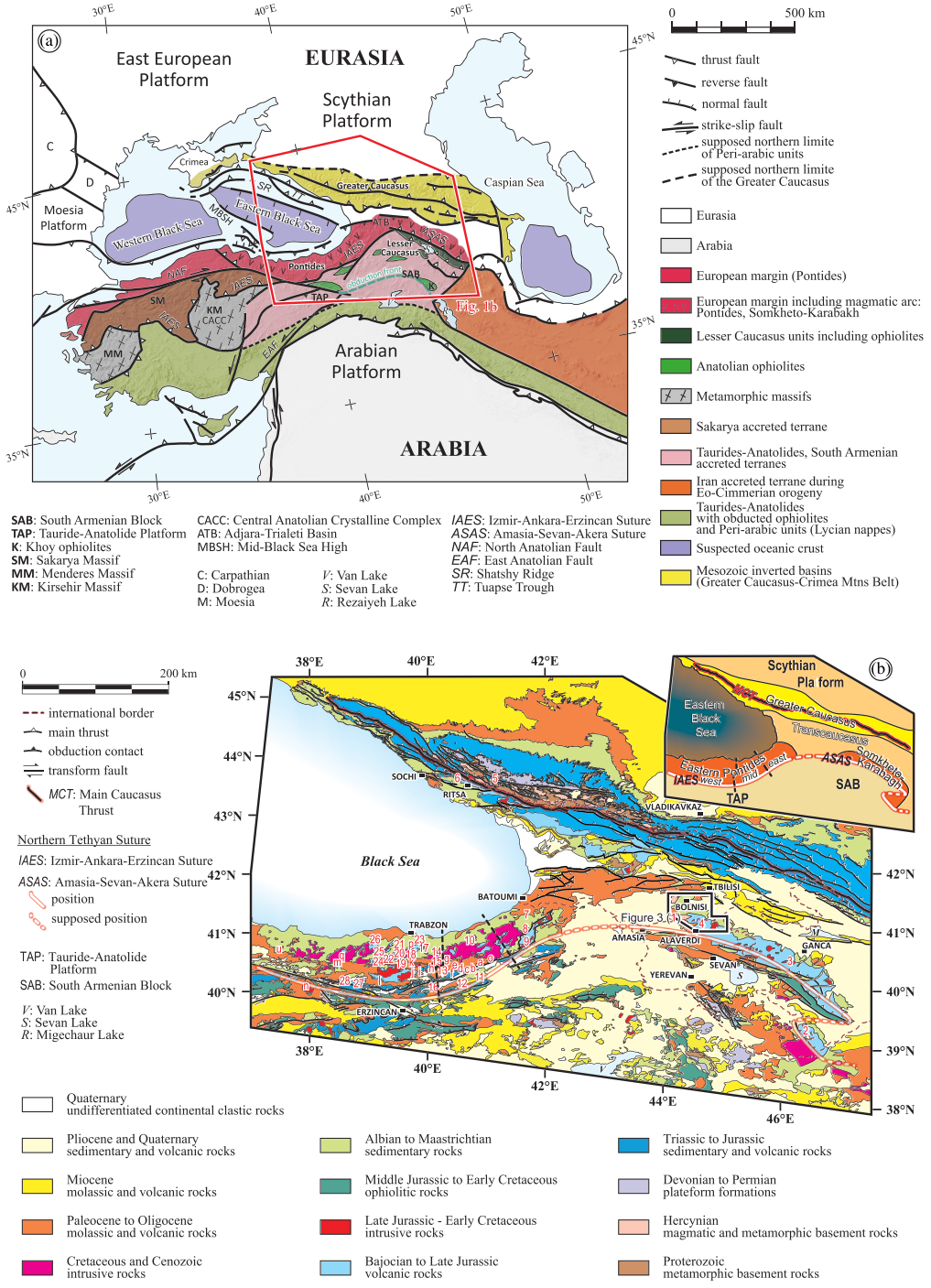

Figure 1. (a)Tectonic map of the Middle East-Caucasus area, with main blocks and suture zones, after Hässig et al. (2019). Location of Figure 1b is indicated. (b) Structural map of North-Eastern Anatolia, the Lesser Caucasus, and Greater Caucasus, after Ali-Zade (2005), Hässig, Rolland, Sosson, Galoyan, Müller, et al. (2013) and Mauvilly et al. (2018), modified. The location of Figure 3 and the locations of additional published geochemical and chronological data to this study are indicated by the red and white outlined numbers and letters: (1) this study, Figure 3; (2) Mederer et al. (2013); (3) Sadikhov and Shatova (2016, 2017); (4) Calder et al. (2019); (5) Hess et al. (1995); (6) McCann et al. (2010); (7) Aydınçakır and Şen (2013); (8) Karsli et al. (2012); (9) Dokuz et al. (2010); (10) Moore et al. (1980); (11) Eyüboğlu (2010); (12) Eyüboğlu et al. (2013) and Altherr et al. (2008); (13) Kaygusuz and Öztürk (2015); (14) Yilmaz-Sahin (2005); (15) Boztuğ and Harlavan (2008); (16) Eyüboğlu, Santosh, and Chung (2011); (17) Kaygusuz and Aydinçakir (2011); (18) Kaygusuz et al. (2014); (19) Arslan and Aslan (2006); (20) Kaygusuz et al. (2013); (21) Aydin (2014); (22) Kaygusuz et al. (2009, 2010) and Kaygusuz and Şen (2011); (23) Karsli et al. (2011); (24) Sipahi et al. (2018); (25) Karsli et al. (2010); (26) Eyüboğlu et al. (2014); (27) Eyüboğlu, Santosh, Dudas, et al. (2011); (28) Topuz et al. (2011); (a: Bademli, b: Meydanlı, c: Meşebaşı, d: Cakırbağ, e: Üzengili, f: Arslandede, g: Kozluk, h: Sorkunlu, i: Sarıçiçek, j: Kaletaş, k: Dölek, l: Çevrepınar, m: Tamdere, and n: Kösedağ) Eyüboğlu et al. (2017); and (o: Ispur-Ulutaş, p: Güzelyayla, q: Emeksen, and u: Elbeyli) Delibaş et al. (2016).

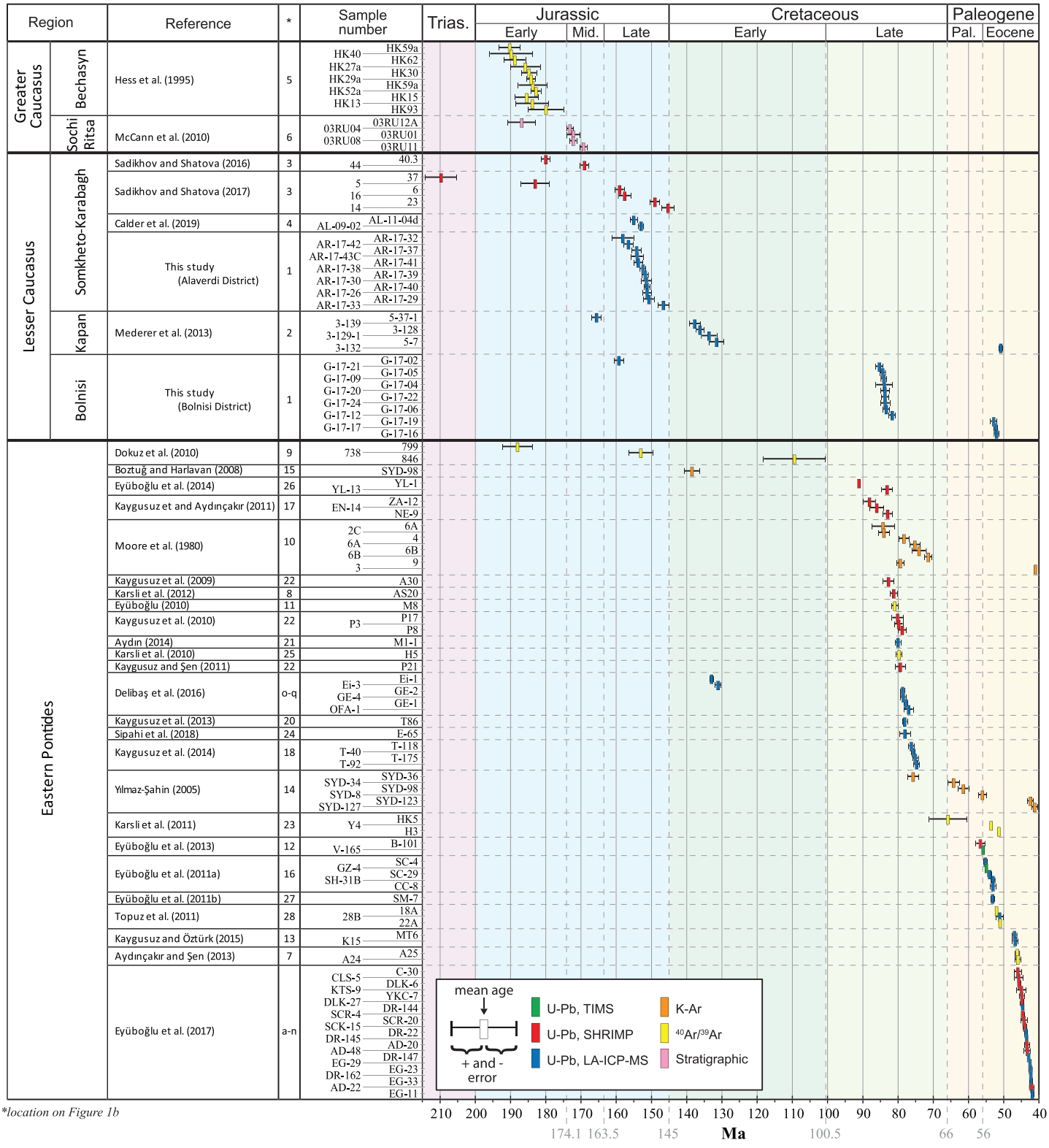

*location on Figure 1b

Figure 2. Summary of geochronological data from this study (Alaverdi and Bolnisi districts) and published studies of magmatic rocks from the Eastern Pontides the Lesser Caucasus and the Sochi-Ritsa/Bechasyn region of the Greater Caucasus. Locations of the published studies indicated on Figure 1b.

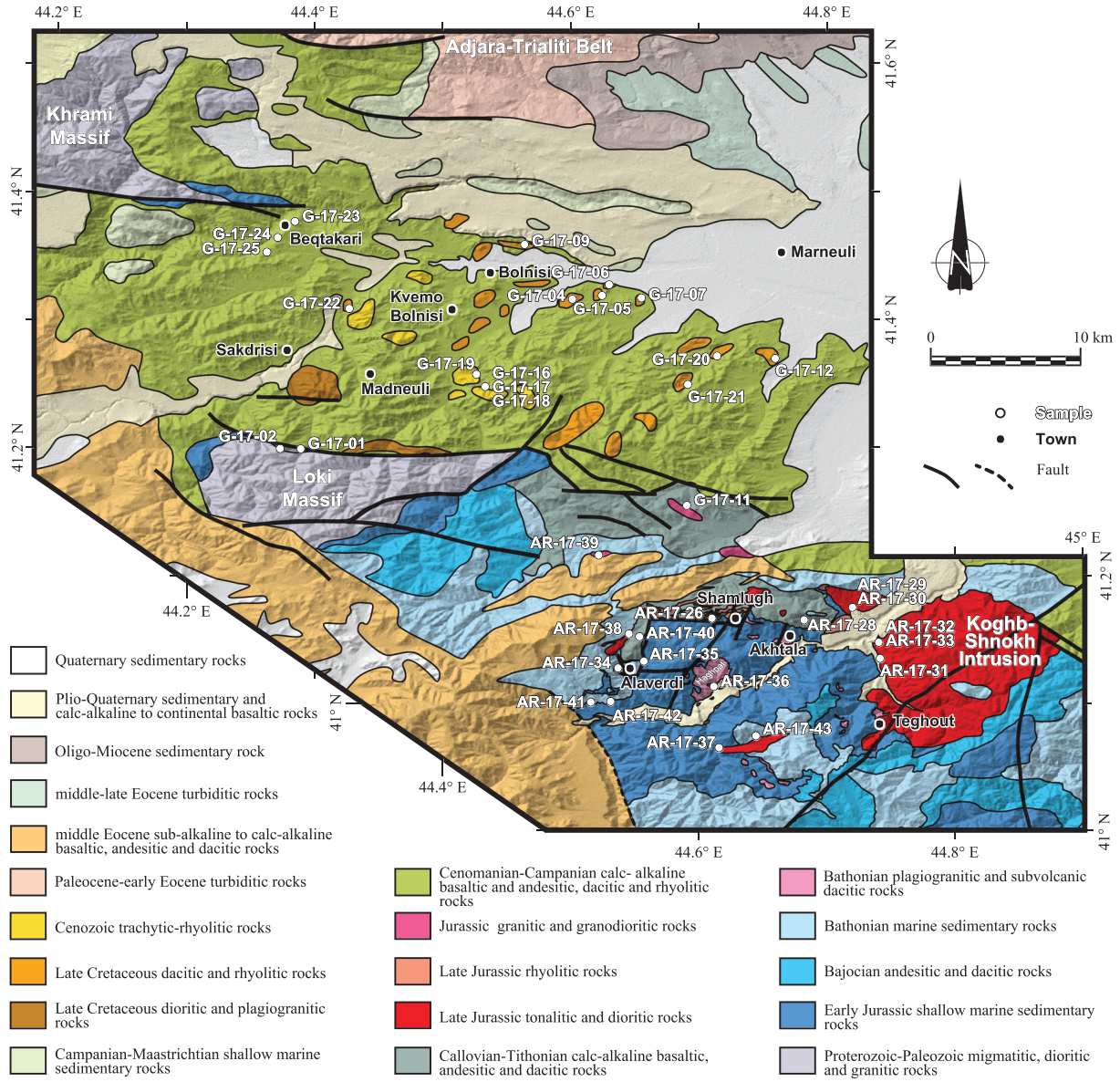

Figure 3. Geological map of the Bolnisi and Alaverdi districts, after Moritz et al. (2016) and Calder et al. (2019), respectively, modified. Locations of newly analyzed samples are indicated.

dipping Paleotethyan subduction just south of the EP and SK arcs (Eyüboğlu et al., 2019; Galoyan et al., 2018). The relative absence of Jurassic and Early Cretaceous subduction-related magmatism in the EP is ascribed to back-arc rifting in relation to slab roll-back and break-off during these times (Bektaş, 1986; Eyüboğlu, 2010; Eyüboğlu et al., 2007). Afterwards, during the Late Cretaceous, north dipping Northern Neotethyan subduction initiated south of the EP and SK arcs all the while south dipping Paleotethyan subduction resumed north of the EP and SK arcs. In this model, Late Cretaceous to Cenozoic magmatism throughout the EP and LC is due to both south and north dipping subductions, jointly.

This study provides new laser ablation-inductively coupled plasma-mass spectrometry (LA-ICP-MS) zircon ages and geochemical characterisations of subduction-related magmatic rocks of the Alaverdi district and of the Bolnisi district, which is the northwestern extent of the SK arc of the LC and just northwest of the Alaverdi district, respectively (Figures 1b and 3). Samples of the Alaverdi district have Jurassic ages and those of the Bolnisi district have Late Cretaceous and Cenozoic ages. There are limited occurrences of

Jurassic and Early Cretaceous magmatism in the EP, yet ages argue a common subduction history of the EP with the LC region from the Late Cretaceous on. Subduction-related magmatic rocks north of the Eastern Black Sea (EBS), within the Southern Slope (SS) of the Greater Caucasus (GC) and along the Main Caucasus Thrust (MCT) in the Sochi-Ritsa/Bechasyn regions provide evidence of Jurassic magmatism (Hess et al., 1995; McCann et al., 2010). Furthermore, recent interpretations of seismic profiles of the EBS (Nikishin et al., 2015a, 2015b) illustrate the presence of continental rift structures constrained to Early Cretaceous times and successive sedimentary fill.

These new data, in conjunction with the magmatic record of the EP and SK, and the structure of the EBS strongly support a model in which the emplacement of subduction-related magmatic rocks along the entire Southern Eurasian margin formed due to only one north dipping subduction. The relative scarcity of Jurassic and Early Cretaceous magmatic rocks in the EP is attributed to the opening of the EBS basin. In this scenario Paleotethyan and Neotethyan realms subduct toward the north below the Southern Eurasian margin along a common and continuous plate boundary. Accompanying this north dipping Tethyan subduction south of the EP and SK, opening of the EBS initiated during Cretaceous times in a back-arc to intra-arc configuration north of the EP to the west toward the SK to east (McCann et al., 2010; Sosson et al., 2016, 2018; Stephenson & Schellart, 2010, and references therein). In this scenario the Jurassic and Early Cretaceous subduction-related magmatic rocks originally emplaced as the EP were displaced farther north of the active supra-subduction zone (SSZ). Intra-arc extension cut across and segmented the Northern Tethyan arc, continuing ultimately to the formation of the EBS. Ongoing subduction is responsible for the development of an active arc separated from a remnant one by an oblique marginal basin. Similar models have already been proposed in the Mediterranean and northeast of New Zealand. There, respectively, Corsica and Sardinia represent remnant relics of the current Apennine arc separated by the Tyrrhenian basin (Karig, 1972; Sartori, 2003) and the remnant Colville and active Kermadec arcs are separated by the Havre Trough (Wright, 1997; Wright et al., 1996).

2. Geological Framework

2.1. Tauride-Anatolide Platform and South Armenian Block

The Tauride-Anatolide Platform (TAP) and South Armenian Block (SAB) originated as slivers of peri-Gondwanan continental lithosphere, which rifted northward away from the northern margin of Gondwana since Triassic times (e.g., Barrier & Vrielynck, 2008; Dercourt & Vrielynck, 1993; Speranza et al., 2012). Distinct Neotethyan suture zones defined by the ophiolitic belts outline successive accretion and collision events involving the closure of Tethyan oceanic basins (Figure 1a). The precise timing of continental collision events associated with the final closure of both Northern and Southern Neotethyan Oceans still remains controversial. The closure of the Northern Neotethys and collision of the SAB and TAP with Eurasia was not synchronous along its southern margin (Sosson et al., 2016). In the LC, collision is interpreted as being Late Cretaceous (~73–71 Ma) (Meijers et al., 2015; Rolland, Billo, et al., 2009; Rolland, Galoyan, et al., 2009) and ranging between Paleocene and early Eocene farther west in the EP (Hippolyte et al., 2017; Okay & Nikishin, 2015; Robertson, Parlak, & Ustaömer, 2013; Robertson, Parlak, Ustaömer, Taslı, et al., 2013; Şengör & Yilmaz, 1981).

2.2. IAES and ASAS Zones

Suture zones are defined in our study region by ophiolite belts and ophiolitic mélanges. The ophiolitic rocks of the TAP-SAB define three main belts (Figure 1a); from north to south (1) the northern ophiolitic belt marking its limit with the Southern Eurasian margin characterized by the EP and SK arcs, (2) the Median or Tauride ophiolite belt limiting the Tauride and Anatolide Terranes, and (3) the Southern or Peri-Arabic ophiolitic belt separating the SAB from the Arabian Block. The northern ophiolite belt defines the IAES-ASAS. The IAES-ASAS represents remnants of the Northern Neotethys Ocean, constituting a continuous limit between the EP and SK arcs with the TAP-SAB (Çelik et al., 2011; Hässig, Rolland, Sosson, Galoyan, Sahakyan, et al., 2013; Hässig et al., 2017; Okay & Tüysüz, 1999; Rolland et al., 2016; Sarıfakıoğlu et al., 2017; Sosson et al., 2010, 2016). An Eocene succession of terrigenous clastic and silicic volcanic rocks typically unconformably covers the TAP-SAB, the IAES-ASAS suture zone, and the EP and LC (SK) magmatic arcs, marking complete suturing (Lordkipanidze et al., 1988; Sosson et al., 2010).

2.3. EP and LC Arcs

The general consensus is that the EP and LC arcs are subduction-related magmatic arcs formed during the Mesozoic and Cenozoic. Two main models for their formation currently prevail: (1) one Tethyan north dipping subduction zone, with Paleotethyan followed by Neotethyan oceanic lithospheres subducting below the EP and SK arcs along the Southern Eurasian margin throughout Mesozoic and Early Cenozoic times (Rice et al., 2006, 2009; Robertson & Dixon, 1984; Şengör & Yilmaz, 1981; Ustaömer & Robertson, 2010; Yılmaz & Boztuğ, 1996), and (2) two Tethyan subductions, one south dipping featuring Paleotethyan oceanic lithosphere subducting below the EP and SK arcs throughout the Mesozoic-Early Cenozoic and one north dipping featuring Neotethyan oceanic lithosphere subducting below the same EP and SK arcs during the Late Cretaceous-Early Cenozoic (Bektaş et al., 1999; Eyüboğlu, 2015; Eyüboğlu et al., 2019).

2.3.1. EP

The Pontides are an east-west striking mountain belt in northern Turkey, located between the Black Sea and the IAES, to the north and south, respectively (Figure 1a). The EP arc is distinguished as the eastern section of the mountain belt. This portion of the Pontides is mainly composed of Late Paleozoic and Mesozoic accretionary complexes as well as Mesozoic and Cenozoic magmatic rocks (Figure 1b) (Okay, 1997; Sayıt & Göncüoglu, 2013).

High-temperature/low-pressure gneiss and schist with Early Carboniferous metamorphic ages are the oldest rocks of the pre-Jurassic basement (Dokuz, 2011; Dokuz et al., 2015; Nzegge et al., 2006; Okay et al., 2006; Topuz et al., 2004, 2007). These basement rocks are overlain by Early to Middle Jurassic sedimentary rocks interbedded with rare basalt and pyroclastic rocks (Dokuz et al., 2006; Kandemir, 2004; Kandemir & Yılmaz, 2009; Şen, 2007).

Based on our compilation, the majority of the geochronologic data (Figure 2; ESD 1) show that the EP recorded two major magmatic pulses during the Late Cretaceous (~90–75 Ma) and the early Eocene (~55–40 Ma). In addition, a small set of data indicate magmatism during the Early Cretaceous (~140–130 Ma) and even as old as the Jurassic (Figure 2; ESD 1). The Jurassic and Early Cretaceous intrusions have a calc-alkaline composition and are attributed to a subduction environment (Boztuğ & Harlavan, 2008; Delibaş et al., 2016). The Late Cretaceous magmatic rocks are calc-alkaline, high-K calc-alkaline, and shoshonitic, including localized adakitic compositions attributed to subduction as well, generally attributed to north dipping Paleotethyan and Northern Neotethyan domains (Akin, 1979; Altherr et al., 2008; Çinku et al., 2010; Delibaş et al., 2016; Karsli et al., 2010, 2011; Okay & Tüysüz, 1999; Şengör et al., 2003; Topuz et al., 2007; Ustaömer & Robertson, 2010; Yilmaz et al., 1997). Alternatively, Eyüboğlu (2010), Eyüboğlu, Santosh, and Chung (2011), Eyüboğlu, Santosh, Dudas, et al. (2011), and Eyüboğlu et al. (2013, 2014) favor a south dipping subduction of the Paleotethyan domain during Jurassic and Early Cretaceous times.

The early Eocene magmatism has high-K calc-alkaline and shoshonitic compositions, with arc and adakitic signatures, variably attributed to a subduction setting (Aydınçakır & Şen, 2013; Karsli et al., 2011; Kaygusuz & Öztürk, 2015; Topuz et al., 2011; Yilmaz-Sahin, 2005) or to a continent-continent collision environment between the TAP and the EP (Aliyazicioğlu, 1999; Boztuğ et al., 2004; Çoban, 1997; Dokuz et al., 2015; Dokuz et al., 2019; Eyüboğlu, Santosh, Chung, 2011; Karsli et al., 2007, 2010, 2011; Okay & Şahintürk, 1997; Okay et al., 1997; Şen et al., 1999; Şengör & Yilmaz, 1981; Tokel, 1977; Topuz et al., 2005, 2011; Yilmaz & Boztuğ, 1996). The EP arc was further uplifted above sea level during the Oligocene, as evidenced by the absence of marine sedimentary rocks and solely the presence of detrital material dated to that time (Topuz et al., 2011). Miocene and younger magmatism is preserved as partly eroded subaerial volcanoes, ascribed to postcollisional magmatism (Robinson, Banks, et al., 1995).

2.3.2. LC

The LC is a region spanning from southern Georgia to northwestern Iran, across Armenia and Azerbaijan. It is composed of the LC (SK) arc, the ASAS, and the SAB, respectively from north to south (Figure 1a). The SK arc has a northwest-southeast strike. It is limited to the northeast by the Transcaucasus basin. The SK arc is defined by Mesozoic-early Cenozoic magmatic series (Figures 1b and 2) (Adamia et al., 1977, 1981, 1987; Knipper, 1975; Maghakyan et al., 1985; Ricou et al., 1986).

The basement rocks of the LC, outcropping as the Akhum and Asrikchai massifs, are interpreted as Late Paleozoic (Hess et al., 1995; Shengelia et al., 2006). Proterozoic and Paleozoic ages have also been

described in the Georgian Loki and Khrami massifs at the northwestern most extent of the SK arc, argued to represent portions of the same basement (Gamkrelidze & Shengelia, 2007; Zakariadze et al., 2007). The assemblages composing this arc unconformably overlay these basement rocks (Sosson et al., 2010).

Our compilation of geochronologic data (Figure 2; ESD 1), featuring new data from the Bolnisi district in southern Georgia and the Alaverdi district in northeastern Armenia (Figures 1b and 3), show that the LC recorded three major magmatic pulses: (1) Jurassic to Early Cretaceous (~190–130 Ma), (2) Late Cretaceous (~90–80 Ma), and (3) early Eocene (~55–40 Ma). The Jurassic and Early Cretaceous series features intrusions, which have tholeiitic to calc-alkaline compositions, as well as volcanoclastic and sedimentary rocks are attributed to a subduction environment (Calder et al., 2019; Mederer et al., 2013; Sadikhov & Shatova, 2016, 2017). The Late Cretaceous magmatic rocks are calc-alkaline, high-K calc-alkaline and shoshonitic in composition. Their formation is attributed to northward subduction of the Northern Neotethys.

2.3.2.1. Alaverdi District, NE Armenia

The Alaverdi district (Figure 3) represents the northeastern portion of the Jurassic SK arc in Armenia. It is mainly characterized by Middle Jurassic magmatic rocks interlayered with sedimentary rocks, followed by Late Jurassic and Cretaceous volcanic and sedimentary rocks, themselves discordantly covered by Eocene and Quaternary rock units (Calder et al., 2019; Ghazaryan, 1971; Lebedev & Malkhasyan, 1965; Mederer et al., 2014; Melkonyan, 1976; Sopko, 1961). The lowermost portion of the Middle Jurassic unit is composed of lava with basaltic, basaltic-andesitic, and andesitic compositions (Bagdasaryan & Melkonyan, 1968). These are conformably covered by tuff and lava breccia of basaltic andesitic, andesitic, and dacitic composition, in turn covered by pyroclastic and lava flows of dacitic and rhyolitic composition (Sopko, 1961). Basaltic-andesitic and andesitic tuff breccia interlayered with sandstone and limestone constitute the Late Jurassic to Early Cretaceous rock sequence (Calder et al., 2019; Ghazaryan, 1971; Sopko, 1961). Unconformably covering this succession are Eocene sedimentary rocks, lava flows and basaltic, andesitic, and rhyolitic tuff (Karapetyan et al., 1982).

Several intrusions crosscut this succession of magmatic and sedimentary rocks (ESD 1), most importantly are those of Haghpat, circa 161 Ma (Melkonyan et al., 2014) and the composite Shnogh-Koghb, dated at circa 164 Ma, 156 Ma (Melkonyan & Ghoukassyan, 2004), and 152.9 Ma (Calder et al., 2019). Much less important in size yet more numerous, multiple basaltic, andesitic, dacitic, and rhyolitic dikes and sills (ca. 155 Ma; Calder et al., 2019) as well as subvolcanic bodies crosscut the Middle Jurassic units.

2.3.2.2. Bolnisi District, South Georgia

The Bolnisi district (Figure 3) is located at the northeastern most portion of the SK in southern Georgia, mainly characterized by Late Cretaceous volcanic and sedimentary sequences emplaced between the Khrami and Loki massifs (Adamia et al., 2011; Zakariadze et al., 2007). These sequences are divided into six suites interpreted to be between Cenomanian and Maastrichtian in age, unconformably overlain by Maastrichtian limestone and marl (Apkhazava, 1988; Gambashidze, 1974; Gugushvili et al., 2014; Popkhadze et al., 2014). An early Eocene formation consisting of terrigenous sedimentary rocks and middle Eocene volcanic rocks unconformably covers the older rocks. In turn, these formations are conformably overlain by late Eocene shallow-marine clastic rocks.

2.4. GC and EBS Basins

2.4.1. GC

The GC belt extends from the northern margin of the EBS basin to the western margin of the South Caspian basin (Figure 1). Its formation resulted from multiple deformation phases during the Phanerozoic, particularly throughout Mesozoic and Cenozoic times (Adamia, 1980; Adamia et al., 1977, 2010; Dotduyev, 1989; Gamkrelidze, 1986; Khain, 1984; McCann et al., 2010; Milanovsky, 1991; Milanovsky et al., 1984; Milanovsky & Khain, 1963; Muratov et al., 1984; Nikishin, Cloetingh, Bolotov, et al., 1998; Nikishin, Cloetingh, Brunet, et al., 1998; Nikishin et al., 2001; Philip et al., 1989; Razvetaev, 1977, 1989). Throughout the Mesozoic and early Cenozoic, several basins developed within the Eurasia Plate, principally the GC basin which initiated its opening in the Early-Middle Jurassic (Adamia et al., 1981, 2011; Barrier & Vrielynck, 2008; Dercourt et al., 1986; Khain, 1975). Its inversion and subsequent formation of the GC mountain belt is related to accretion of Gondwanan and Tethyan terranes along the southernmost edge of the East European Platform (Adamia et al., 2011; Dercourt & Vrielynck, 1993; Dercourt et al., 2000;

Sengör, 1989; Zonenshain et al., 1990). The GC has a doubly verging structure with two fold-and-thrust complexes on either side of a nascent axial zone (Khain, 1997; Mosar et al., 2010; Sholpo, 1993; Sosson et al., 2016).

The southern edge of the axial zone is marked by the north dipping MCT (Figure 1b) (Somin, 2011). The MCT thrusts Variscan basement composed of Late Paleozoic arc-related granitic plutons, migmatite, and both orthogneiss and paragneiss (Nalivkin, 1973) atop the SS. The Variscan basement is covered by Cambrian and Devonian rocks and is in turn unconformably overlain by Late Jurassic and Cretaceous shelf carbonate (Nalivkin, 1976). The upper portion north of the MCT contains a complex system of top-to-north thrust sheets of Jurassic to middle Miocene sedimentary and magmatic rocks (Cowgill et al., 2016; Gudjabidze & Gamkrelidze, 2003; Nalivkin, 1976). South of the MCT, the SS is a of top-to-south thrust system dominated by thrust sheets of Early Jurassic to Pleistocene magmatic and sedimentary rock, featuring Paleogene olistostromes with Cretaceous olistoliths (Adamia et al., 2011; Banks et al., 1998; Cowgill et al., 2016; Dotduyev, 1987; Forte et al., 2010, 2013, 2014; Kandelaki & Kakhazdze, 1957; Philip et al., 1989; Vincent et al., 2007). The SS is limited to the south by late Miocene to Plio-Pleistocene sedimentary rocks of the Transcaucasus basin (Figure 1b) (Adamia et al., 2010; Forte et al., 2010, 2013).

2.4.2. EBS

The Black Sea consists of a roughly east-west orientated depression, north of the Pontides, south of the Crimean Mountains, and southwest of the GC belt (Figure 1) (Dercourt & Vrielynck, 1993; Dercourt et al., 2000; Nikishin et al., 2003; Okay et al., 1994; Robinson & Kerusov, 1997; Stephenson & Schellart, 2010). Currently, the Black Sea features a ~2 km deep abyssal plain separated into two large depressions, the Western Black Sea and EBS basins (Robinson et al., 1996; Sydorenko et al., 2017; Zonenshain & Pichon, 1986). They are filled with a thickness of up to 14 km of Mesozoic and Cenozoic detrital and sedimentary rocks (Graham et al., 2013; Nikishin et al., 2015a, 2015b; Sydorenko et al., 2017; Yegorova & Gobarenko, 2010). These depressions affect a basement of unconstrained composition and tectonic age. The basins formed during the Cretaceous and the early Cenozoic (Cloetingh et al., 2003; Finetti, 1988; Khriachtchevskaia et al., 2010; Letouzey et al., 1977; Okay et al., 2013; Spadini et al., 1996; Stephenson & Schellart, 2010; Vincent et al., 2005). Various scenarios have been proposed to explain their origin (Bektaş, 1986; Eyüboğlu et al., 2014; Okay et al., 1994, 2013; Stephenson & Schellart, 2010), but it remains a subject of debate due to poor understanding of the nature of their basement.

Interpretations of a recent seismic survey (Nikishin et al., 2015a, 2015b) infer that the present EBS basin is underlined by a basement featuring WNW-ESE striking normal faults dipping toward its center, parallel to its northern and southern margins. This argues for the presence of tilted blocks analog to a rifted continental crust bordering an oceanic crust (Bosworth, 1985; Cloetingh et al., 2003; Spadini et al., 1996). Late Barremian to Albian sedimentary sequences are deformed by this faulting. In the northern portion of the EBS basin small Albian-Cenomanian volcanoes seal these normal faults (Nikishin et al., 2015a). Santonian-Maastrichtian sedimentary rocks cover the center of the depression, as well as onlap over localized synnormal faulting Cenomanian-Santonian sedimentary fill (Afanasenkov et al., 2008; Nikishin et al., 2008; Robinson, Spadini, et al., 1995; Shillington et al., 2008). Santonian-Campanian submarine volcanoes 100 km north of the present-day Turkish coast are imaged and are argued to be related to a major E-W trending normal fault system (Nikishin et al., 2003). Paleocene, Eocene, and Oligocene turbiditic sequences constitute the upper part of the sedimentary fill (Letouzey et al., 1977; Shillington et al., 2008). Numerous compressional and transpressional structures appear along the periphery of the EBS basin in the later Cenozoic sedimentary record (Khriachtchevskaia et al., 2010).

3. Sampling

Throughout field studies, a total of 37 representative samples of magmatic rocks was collected, 18 from the Alaverdi district and 19 from the Bolnisi district (Figure 3). From the Alaverdi district, 13 of the samples are intrusive magmatic rocks ranging from pinkish granites with coarse-grained phaneritic textures (marked by potassium feldspar, plagioclase, quartz, and biotite), light gray colored quartz-monzonite with coarse-grained phaneritic to porphyritic textures (marked by less quartz than granites, large fledspar, plagioclase, and biotite), granodiorite with fine-grained phaneritic textures (marked by high plagioclase content), and fine-grained phaneritic diorite (marked by less quartz content). Each sample represents a specific

Table 1
Summary of New U-Pb Zircon LA-ICP-MS Datings With (WGS84) GPS Locations

District	Sample	Longitude (°E)	Latitude (°N)	Rock type	Weighted mean age (Ma) $^{206}Pb/^{238}U$ (1σ)	MSDW
Alaverdi	AR-17-26	44.71123	41.16792	granite	151.20 ± 1.20	1.40
	AR-17-29	44.81810	41.17585	qtz-monzonite	150.70 ± 1.50	1.18
	AR-17-30	44.81810	41.17585	granite	151.40 ± 1.40	1.20
	AR-17-32	44.83866	41.13926	granite	158.10 ± 3.10	0.32
	AR-17-33	44.83839	41.14796	diorite	146.60 ± 1.60	1.02
	AR-17-37	44.71552	41.06629	granite	154.20 ± 1.40	0.54
	AR-17-38	44.64733	41.15480	granite	152.39 ± 0.85	1.30
	AR-17-39	44.62370	41.21660	rhyolite	151.73 ± 0.89	1.04
	AR-17-40	44.65309	41.15228	rhyolite	151.22 ± 0.79	0.66
	AR-17-41	44.61661	41.09775	qtz-monzonite	153.70 ± 1.30	0.12
	AR-17-42	44.63350	41.09814	rhyolite	156.50 ± 1.30	1.20
	AR-17-43C	44.73980	41.07568	granodiorite	154.00 ± 1.70	0.59
Bolnisi	G-17-02	44.39766	41.30809	granodiorite	159.00 ± 1.40	0.66
	G-17-04	44.60182	41.41674	dacite	83.90 ± 2.40	1.40
	G-17-05	44.62590	41.42062	rhyolite	84.36 ± 0.80	1.40
	G-17-06	44.62908	41.42801	rhyolite	83.31 ± 0.90	1.20
	G-17-09	44.56591	41.45947	rhyolite	83.99 ± 0.84	1.60
	G-17-12	44.75991	41.36993	rhyolite	81.64 ± 0.94	0.63
	G-17-16	44.53088	41.34752	granite	52.04 ± 0.70	1.11
	G-17-17	44.53122	41.34672	granodiorite	52.29 ± 0.56	0.96
	G-17-19	44.52847	41.35770	granite	52.85 ± 0.89	0.26
	G-17-20	44.71418	41.37173	rhyolite	83.70 ± 1.30	0.40
	G-17-21	44.69194	41.35037	trachydacite	85.30 ± 1.10	1.30
	G-17-22	44.42693	41.40975	rhyolite	83.70 ± 1.10	1.50
	G-17-24	44.37200	41.46363	rhyolite	83.60 ± 1.30	0.43

occurrence of repetitive subparallel metric wide/thick dikes or sills. The five remaining samples are extrusive magmatic rocks, which outcrop as lava flows of basalt, andesite, or rhyolite.

From the Bolnisi district, five samples are intrusive magmatic rocks including two grayish granites (one with a coarse-grained and one with a fine-grained phaneritic textures marked by large feldspar, plagioclase, quartz, and biotite), two phaneritic granodiorites and one porphyritic quartz-monzonite, which outcrop as metric to decametric wide dikes along regional faults or along the contacts between trachytic-rhyolitic bodies and Cretaceous volcano-sedimentary sequences. The remaining 14 samples are extrusive magmatic rocks with aphanitic to porphyritic textures and compositions ranging from dacitic, to trachydacitic, and to rhyolitic. These outcrop as isolated hills and mounds devoid of greenery among well vegetated Cretaceous volcano-sedimentary deposits.

All 37 samples were analyzed for whole-rock geochemical composition. Twelve samples from the Alaverdi district (all intrusive with massive textures) and 13 from the Bolnisi district (4 intrusive and 9 extrusive, all with massive textures) underwent LA-ICP-MS zircon U-Pb dating.

4. U-Pb Zircon Geochronology

Twenty-five samples, 12 from the Alaverdi district and 13 from the Bolinsi district, were chosen for U-Pb dating by LA-ICP-MS. The analytical techniques and methods used to obtain these new data are presented in ESD 2. All of the spot analyses were carried out on zircons exhibiting clear magmatic zonations as seen on SEM-CL zircon images presented in ESD 3, as well as locations of spot analyses. The detailed results are listed in ESD 4a and 4b and summarized in Table 1 and ESD 1. The results can be divided into three distinct age groups; (1) Late Jurassic, (2) Late Cretaceous, and (3) Eocene (Figure 2).

4.1. Late Jurassic Magmatism

Of the 12 dated samples of the Alaverdi district all yield Late Jurassic ages (Oxfordian-Tithonian, ca. 161–145 Ma). The ages range from 158.1 ± 3.1 Ma for AR-17-32 to 146.6 ± 1.6 Ma for AR-17-33 (Table 1).

When considering their uncertainties, the U-Pb ages overlap with each other between 161.2 and 149.2 Ma, except for Sample AR-17-33 (Figure 2). This is further emphasized by the 159 ± 1.4 Ma age of Sample G-17-02, which crops out along a major fault marking the northern limit of the Loki massif in the southern portion of the Bolnisi district (Figure 3). In addition, similar ages of magmatic rocks are reported by Calder et al. (2019) for the Alaverdi district (Figure 2).

4.2. Late Cretaceous Magmatism

Nine of the 13 samples of the Bolnisi district are dated Late Cretaceous. U-Pb ages range between 85.3 ± 1.1 Ma for G-17-21 and 81.64 ± 0.94 Ma for G-17-12 (Table 2). Emplacement of a major magmatic complex ascribed to part of the LC is bracketed between 86.4 and 80.7 Ma when considering the overlapping uncertainties of the individual dates (Figure 2). The Late Cretaceous magmatic event has not been identified so far in the Alaverdi district (Figure 3).

4.3. Eocene Magmatism

Eocene ages have only been determined for magmatic rocks outcropping in the central portion of the Bolnisi district (Table 1 and Figure 3). Three samples yield ages between 52.85 ± 0.89 Ma for G-17-19 and 52.29 ± 0.56 Ma for G-17-17. Taking into account the uncertainties of these ages, we can constrain the emplacement of a magmatic complex over a short period of time between 53.74 and 51.34 Ma (Figure 2).

5. Whole-Rock Geochemistry by XRF and LA-ICP-MS

Thirty-seven samples, 18 from the Alaverdi district and 19 from the Bolinsi district, were chosen for geochemical analyses. All analyzed samples present minimal alteration, and care was taken to remove weathered surfaces prior to sample preparation. The detailed results are listed in Table 2, and sample locations are plotted in Figure 2.

The sampled magmatic rocks from the Alaverdi district can be divided into two groups on the basis of SiO_2 contents, varying between basic (46 to 54 wt.%) and acid (64 to 77 wt. %) compositions (Table 2 and Figure 4). The basic rocks exhibits generally higher Al_2O_3 (14–20 wt.%), TiO_2 (0.44–1.28 wt.%), CaO (8–11 wt.%), FeOt (8.4–12 wt.%), and MgO (4.4–8.2 wt.%) compared to the felsic rocks (Al_2O_3: 12–16 wt. %, TiO_2: 0.06–0.72 wt.%, CaO: 0.20–4.4 wt.%, FeOt: 1.33–5.0 wt.%, and MgO: 0.04–2.5 wt.%). Binary plots for most of the major elements show a good anticorrelation of Al_2O_3, TiO_2, CaO, FeO_t, P_2O_3, and MgO contents decreasing with increasing SiO_2 (ESD 5). Contrary to those from the Alaverdi district, the samples from the Bolnisi district exhibit a near linear spread in SiO_2, with rather acid values (62–79 wt.%; Table 2 and Figures 4 and 5). As those of the Alaverdi district, most of the major elements show a good anticorrelation with SiO_2, especially in Al_2O_3 (18 to 11 wt.%), TiO_2 (0.73 to 0.14 wt.%), CaO (4.1 to 0.15 wt.%), Fe_2O_3 (56.0 to 0.97 wt.%), and MgO (2.5 to 0.01 wt.%) (ESD 5).

On the AFM diagram (Figure 5), most of the samples from both Alaverdi and Bolnisi districts plot in the calc-alkaline field, even though a small group of samples from the Alaverdi district plots along the limit with the tholeiitic domain and one Late Cretaceous sample from the Bolnisi district plots well within it. The sample group along the limit between the calc-alkaline and tholeiitic domains corresponds to those with lower SiO_2 contents. As in the binary diagrams of SiO_2 against major element oxides, the plots of all of the samples of the Alaverdi district define a clear trend with decreasing FeO_{tot}/MgO and increasing $Na_2O + K_2O$ within the calc-alkaline field (Figure 5). Again, similarly to the binary diagrams, the plots of the samples from the Bolnisi district overlap and continue this trend.

The classification diagram based on the immobile elements Th and Co (Figure 6), which are supposed to avoid the effects of metasomatism and metamorphism (Hastie et al., 2007), shows comparable results. All the samples from both districts plot within the calc-alkaline or high-K and shoshonitic domains except for the basalt sampled in the Alaverdi district (Figures 6 and 7). This sample, which plots in the tholeiitic field of the AFM diagram, is identified as an island arc tholeiite. As in the previous diagrams, the five basic samples of the Alaverdi district plot in a separate cluster compared to the acid ones. Once more, as with the binary diagrams and the AFM diagram, the plots of the samples from the Bolnisi district overlap with the acid samples of the Alaverdi district.

Table 2

Geochemical Whole Rock Data for Magmatic Rocks From the Alaverdi and Bolnisi Districts, Including Isotopic Data (Sr and Nd)

District		Alaverdi	Alaverdi	Alaverdi	Alaverdi	Alaverdi	Alaverdi	Alaverdi	Alaverdi	Alaverdi
Sample		AR-17-26	AR-17-28	AR-17-29	AR-17-30	AR-17-31	AR-17-32	AR-17-33	AR-17-34	AR-17-35
Longitude (°E)		44.71123	44.78142	44.81810	44.81810	44.83866	44.83866	44.83839	44.63589	44.65680
Latitude (°N)		41.16792	41.16649	41.17585	41.17585	41.13926	41.13926	41.14796	41.12922	41.13445
Age		Late Jurassic	Late Jurassic	Late Jurassic	Late Jurassic	Late Jurassic	Late Jurassic	Late Jurassic	Late Jurassic	Late Jurassic
rock type		granite	basalt	qtz-monzonite	granite	diorite	granite	diorite	gabbro	granodiorite
SiO_2	%	73.81	50.56	63.79	76.17	53.06	74.36	51.26	46.30	66.30
TiO_2	%	0.13	1.28	0.63	0.19	0.44	0.06	0.89	0.86	0.72
Al_2O_3	%	13.59	13.90	15.73	12.31	15.60	13.78	20.20	16.10	15.52
FeOt	%	2.53	12.08	4.47	1.33	11.45	1.44	8.40	11.01	4.99
MnO	%	0.03	0.12	0.07	0.02	0.15	0.01	0.15	0.17	0.07
MgO	%	0.16	8.16	2.06	0.17	6.45	0.04	4.37	7.96	0.84
CaO	%	1.41	7.95	3.65	0.42	10.84	0.75	9.21	9.88	1.48
Na_2O	%	3.25	2.11	5.10	3.79	1.26	3.73	4.23	1.69	6.80
K_2O	%	2.09	0.82	2.12	4.16	0.18	5.37	0.29	0.08	0.19
P_2O_5	%	0.02	0.14	0.16	0.03	0.06	0.01	0.22	0.13	0.22
LOI	%	2.88	2.80	1.35	0.55	0.49	0.24	0.94	5.74	2.69
Total	%	99.89	99.99	99.13	99.13	100.09	99.78	100.17	99.96	99.83
Ba	ppm	274	306	339	588	42.1	1332	112	26	65
Rb	ppm	46	12	50	88	2.3	53	3.7	1.1	5.2
Sr	ppm	70	250	285	57	252	99	508	188	78
Ta	ppm	2.4	0.6	1.0	0.8	0.1	5.7	0.17	0.34	0.63
Th	ppm	10	1.7	5.7	7.2	0.9	9.6	0.5	1.7	2.8
Zr	ppm	291	85	178	123	31	176	38	70	161
Nb	ppm	35	8.9	12.8	13	1.0	63	3.2	5.4	10.0
Y	ppm	53	19	24	9.4	13	43	16	19	27
Hf	ppm	8.5	2.3	4.8	3.8	1.0	6.8	1.0	1.8	3.9
V	ppm									
Cr	ppm	18	323	42	20	594	26	54	252	17.6
Ni	ppm									
Co	ppm	1.5	53	14	3.9	31	5.9	22	45	11
U	ppm	2.7	0.3	1.0	1.5	0.2	2.1	0.16	0.38	0.82
Sc	ppm	9.0	28	14	6.6	46	4.7	25	32	14
Cu	ppm	15	82	48	18	23	26	31	80	24
Zn	ppm	170	115	66	43	76	29	75	97	93
Pb	ppm	12	2.5	6.2	9.8	1.4	6.2	2.0	1.7	2.8
Cs	ppm	0.4	0.33	0.6	0.7	0.1	0.3	0.3	0.5	0.4
La	ppm	47	11	23	19	4.4	17	8.5	10	16
Ce	ppm	89	21	44	40	8.6	35	18	20	33
Pr	ppm	9.3	2.5	4.8	3.3	1.0	4.1	2.3	2.4	4.1
Nd	ppm	37	12	19	11	4.9	18	11	10	18
Sm	ppm	7.9	3.2	3.9	1.8	1.3	4.9	2.8	2.4	4.2
Eu	ppm	1.1	1.1	0.98	0.42	0.42	0.85	1.2	0.86	1.3
Gd	ppm	7.9	3.6	4.1	1.6	1.7	5.6	3.2	2.9	4.7
Tb	ppm	1.4	0.56	0.63	0.24	0.27	1.1	0.47	0.50	0.70
Dy	ppm	9.3	3.8	4.3	1.6	2.1	7.3	3.2	3.5	4.9
Ho	ppm	2.0	0.72	0.84	0.32	0.46	1.4	0.63	0.72	1.00
Er	ppm	5.9	2.0	2.5	1.0	1.4	4.7	1.8	2.2	2.9
Tm	ppm	0.90	0.27	0.38	0.15	0.21	0.75	0.23	0.30	0.42
Yb	ppm	6.3	1.7	2.8	1.3	1.6	5.5	1.6	2.1	2.8
Lu	ppm	0.97	0.25	0.39	0.22	0.24	0.81	0.24	0.31	0.44

Table 2
Continued

District	Alaverdi	Alaverdi	Alaverdi	Alaverdi	Alaverdi	Alaverdi	Alaverdi	Alaverdi	Alaverdi	Bolnisi
Sample	AR-17-36	AR-17-37	AR-17-38	AR-17-39	AR-17-40	AR-17-41	AR-17-42	AR-17-43A	AR-17-43C	G-17-01
Longitude (°E)	44.71255	44.71552	44.64733	44.62370	44.65309	44.61661	44.63350	44.73980	44.73980	44.39766
Latitude (°N)	41.11475	41.06629	41.15480	41.21660	41.15228	41.09775	41.09814	41.07568	41.07568	41.30809
Age	Late Jurassic	Late Jurassic	Late Jurassic	Late Jurassic	Late Jurassic	Late Jurassic	Late Jurassic	Late Jurassic	Late Jurassic	Late Jurassic
rock type	granite	granite	granite	rhyolite	rhyolite	qtz-monzonite	rhyolite	andesite	granodiorite	qtz-monzonite
SiO_2	74.92	66.71	77.01	74.23	71.37	64.18	68.93	51.60	65.78	63.96
TiO_2	0.39	0.44	0.14	0.26	0.32	0.51	0.42	0.82	0.51	0.72
Al_2O_3	12.15	14.44	12.93	14.56	14.69	15.88	14.97	17.31	15.37	14.61
FeOt	3.98	2.37	1.62	1.63	3.04	4.48	3.37	10.82	4.30	5.64
MnO	0.04	0.05	0.02	0.01	0.01	0.09	0.08	0.23	0.06	0.13
MgO	0.77	0.29	0.26	0.11	0.43	2.52	0.94	4.35	1.99	2.50
CaO	0.29	4.39	0.37	0.20	0.24	2.02	2.58	10.24	4.17	1.76
Na_2O	5.63	6.14	3.28	5.78	5.44	5.69	3.80	3.18	4.06	5.88
K_2O	0.28	0.59	2.06	1.36	2.26	1.83	3.68	0.36	1.83	1.85
P_2O_5	0.08	0.14	0.02	0.07	0.10	0.17	0.12	0.12	0.14	0.16
LOI	1.66	4.43	1.67	1.14	1.36	2.79	0.96	0.38	1.18	1.99
Total	100.17	99.98	99.39	99.35	99.25	100.15	99.86	99.41	99.38	99.20
Ba	45	62	99	101	245	412	554	57	294	335
Rb	4.5	14	60	21	38	25	92	3.1	38	39
Sr	64	62	36	32	148	197	335	179	240	142
Ta	0.35	0.52	1.6	0.93	1.2	0.46	1.3	0.12	0.63	0.62
Th	2.2	4.0	6.9	4.4	4.8	4.8	11	1.1	4.6	4.9
Zr	118	146	217	142	195	126	200	58	153	199
Nb	5.6	6.3	20	12	17	6.2	17	2.0	7.4	10
Y	33	17	30	19	30	14	21	21	18	31
Hf	3.7	3.8	6.2	4.0	5.3	3.3	4.9	1.7	4.1	5.4
V			4.0	12	19	81	38	278	73	
Cr	23	31	12	14	14	32	19	31	25	34
Ni			4.2	7.0	6.1	17	6.3	13	14	
Co	5.1	6.8	0.49	0.87	2.9	11	5.1	28	9.0	13
U	0.67	0.60	2.0	0.85	1.3	1.0	2.4	0.51	0.74	1.2
Sc	19	12	7.2	5.9	6.4	11	9.5	34	12	20
Cu	53	27	17	6.4	4.8	8.0	8.2	54	86	32
Zn	52	53	30	20	49	57	52	111	33	77
Pb	2.9	2.2	2.1	2.5	1.7	4.3	12	2.4	3.0	6.2
Cs	0.1	0.4	0.8	0.8	0.8	0.6	0.4	0.2	0.4	0.3
La	5.8	14	30	19	25	16	31	6.5	18	18
Ce	15	26	61	36	45	31	56	14	34	38
Pr	2.1	2.8	6.5	4.0	5.5	3.3	5.7	1.9	3.7	4.6
Nd	11	12	24	15	22	13	20	9.0	14	19
Sm	3.3	2.4	5.1	3.0	4.9	2.6	3.7	2.7	2.9	4.6
Eu	0.82	0.90	0.55	0.56	0.89	0.82	0.94	0.96	0.83	1.1
Gd	4.5	2.8	5.0	2.9	5.0	2.5	3.5	3.3	3.0	5.0
Tb	0.78	0.43	0.77	0.48	0.80	0.39	0.54	0.55	0.48	0.80
Dy	5.9	2.8	5.5	3.5	5.4	2.5	3.6	3.8	3.1	5.3
Ho	1.3	0.56	1.2	0.73	1.1	0.50	0.76	0.80	0.65	1.1
Er	4.1	1.8	3.5	2.3	3.4	1.4	2.3	2.4	1.9	3.3
Tm	0.65	0.25	0.56	0.36	0.50	0.20	0.37	0.35	0.31	0.51
Yb	4.6	1.9	4.1	2.6	3.5	1.4	2.6	2.4	2.1	3.5
Lu	0.72	0.28	0.59	0.40	0.53	0.22	0.39	0.37	0.34	0.52

Table 2
Continued

District	Bolnisi	Bolnisi	Bolnisi	Bolnisi	Bolnisi	Bolnisi	Bolnisi	Bolnisi	Bolnisi	Bolnisi
Sample	G-17-02	G-17-04	G-17-05	G-17-06	G-17-07	G-17-09	G-17-12	G-17-20	G-17-21	G-17-22
Longitude (°E)	44.39766	44.60182	44.62590	44.62908	44.65448	44.56591	44.75991	44.71418	44.69194	44.42693
Latitude (°N)	41.30809	41.41674	41.42062	41.42801	41.41711	41.45947	41.36993	41.37173	41.35037	41.40975
Age	Late Jurassic	Late Cretaceous	Late Cretaceous	Late Cretaceous	Late Cretaceous	Late Cretaceous	Late Cretaceous	Late Cretaceous	Late Cretaceous	Late Cretaceous
rock type	granodiorite	dacite	rhyolite	rhyolite	rhyolite	rhyolite	rhyolite	rhyolite	trachydacite	rhyolite
SiO_2	66.33	70.76	78.94	78.21	73.04	76.63	70.38	73.60	66.60	73.62
TiO_2	0.39	0.63	0.15	0.14	0.23	0.15	0.29	0.32	0.39	0.17
Al_2O_3	14.97	15.64	11.01	11.02	14.05	12.14	14.88	13.36	18.13	13.17
FeOt	5.96	4.89	0.97	1.21	2.06	1.31	2.38	1.89	1.93	1.55
MnO	0.08	0.18	0.01	0.01	0.03	0.01	0.03	0.01	0.00	0.03
MgO	2.37	0.08	0.01	0.09	0.15	0.13	0.45	0.50	0.20	0.57
CaO	0.59	0.30	0.97	0.93	1.91	0.15	0.55	0.37	0.36	0.29
Na_2O	2.83	0.02	2.71	2.54	4.76	0.64	2.75	5.39	6.63	3.48
K_2O	1.49	0.15	3.92	4.63	2.99	6.53	7.12	2.64	3.94	5.18
P_2O_5	0.17	0.13	0.02	0.03	0.07	0.03	0.09	0.08	0.09	0.05
LOI	4.16	7.06	0.73	1.33	0.80	2.22	1.11	0.93	1.12	1.02
Total	99.33	99.83	99.44	100.13	100.09	99.93	100.04	99.09	99.38	99.14
Ba	61	182	578	535	464	475	1965	439	539	723
Rb	40	3.0	71	79	60	124	120	42	65	103
Sr	72	88	83	79	150	35	46	76	66	47
Ta	0	0.70	0.53	0.55	0.59	0.71	0.74	0.53	0.56	0.67
Th	3.5	4.9	7.3	8.0	4.8	8.3	4.5	4.3	5.6	6.7
Zr	90	205	100	101	129	82	339	160	203	90
Nb	5.4	12	5.0	5.8	8.6	6.2	11	8.0	6.7	9.7
Y	6.5	56	9.5	9.5	16	6.1	20	22	32	10
Hf	2.4	5.7	2.7	2.8	3.7	2.3	6.9	4.6	5.1	2.3
V								18	19	13
Cr	21	17	32	31	27	31	27	14	14	20
Ni								6.4	4.3	7.9
Co	5.8	4.0	1.7	1.6	4.2	2.7	2.7	1.7	0.6	1.2
U	0.69	1.9	1.4	1.3	1.4	1.2	1.7	1.0	1.8	1.7
Sc	12	19	7.2	7.2	11	6.5	8.3	11	12	5.8
Cu	1743	4.8	4.3	25	7.6	4.2	3.7	6.5	7.0	8.1
Zn	160	116	53	45	66	37	101	35	21	20
Pb	3.5	39	7.9	7.6	9.7	7.1	3.7	5.5	6.2	8.8
Cs	3.5	0.6	0.63	0.85	0.57	3.6	0.69	0.31	0.23	0.80
La	8.5	18	16	18	15	19	25	14	21	22
Ce	20	39	26	29	31	29	48	29	45	43
Pr	2.4	4.7	2.6	2.8	3.0	2.5	5.1	3.5	4.6	3.8
Nd	10	20	9.5	9.0	12	7.7	19	15	18	13
Sm	2.0	5.3	1.8	1.7	2.2	1.4	3.4	3.6	3.8	1.9
Eu	0.60	1.6	0.41	0.34	0.62	0.30	0.91	0.86	0.98	0.48
Gd	1.8	7.2	1.7	1.5	2.3	1.1	3.2	3.7	4.2	1.7
Tb	0.24	1.4	0.26	0.24	0.40	0.18	0.48	0.60	0.71	0.26
Dy	1.4	9.8	1.6	1.6	2.7	1.1	3.3	4.0	5.3	1.7
Ho	0.27	2.0	0.31	0.31	0.63	0.22	0.67	0.86	1.1	0.34
Er	0.8	5.3	1.1	1.0	1.9	0.7	2.3	2.6	3.4	1.1
Tm	0.12	0.74	0.19	0.16	0.34	0.12	0.37	0.41	0.53	0.17
Yb	0.86	4.9	1.3	1.3	2.4	0.8	2.9	3.0	3.8	1.3
Lu	0.14	0.73	0.21	0.19	0.36	0.14	0.52	0.46	0.57	0.21

Table 2
Continued

District	Bolnisi	Bolnisi	Bolnisi	Bolnisi	Bolnisi	Bolnisi	Bolnisi	Bolnisi
Sample	G-17-23	G-17-24	G-17-11	G-17-16	G-17-17	G-17-18	G-17-19	G-17-25
Longitude (°E)	44.38380	44.37200	44.69035	44.53088	44.53122	44.53225	44.52847	44.36521
Latitude (°N)	41.47557	41.46363	41.25616	41.34752	41.34672	41.34659	41.35770	41.45368
Age	Late Cretaceous	Late Cretaceous	Eocene	Eocene	Eocene	Eocene	Eocene	Eocene
rock type	rhyolite	rhyolite	trachydacite	granite	granodiorite	dacite	granite	trachydacite
SiO_2	71.84	78.44	62.09	68.45	67.67	68.29	69.00	63.56
TiO_2	0.37	0.24	0.73	0.22	0.21	0.23	0.21	0.57
Al_2O_3	12.46	11.66	17.28	16.13	15.51	16.10	15.94	16.41
FeOt	3.55	2.14	3.80	2.09	1.85	2.11	2.02	5.30
MnO	0.19	0.03	0.15	0.05	0.05	0.05	0.05	0.08
MgO	1.10	0.11	0.86	0.92	0.50	0.86	1.00	1.29
CaO	0.64	0.33	1.53	3.17	4.09	3.68	1.03	2.88
Na_2O	5.72	5.66	6.35	5.56	4.49	5.03	5.55	5.21
K_2O	1.06	1.09	5.45	1.34	0.97	1.24	2.12	3.01
P_2O_5	0.22	0.06	0.15	0.08	0.08	0.08	0.07	0.14
LOI	1.91	0.53	1.08	1.14	3.76	1.55	2.06	1.05
Total	99.04	100.29	99.47	99.15	99.18	99.21	99.05	99.50
Ba	272	412	2161	447	247	390	437	651
Rb	13	12	93	33	19	26	56	61
Sr	70	129	253	680	422	640	342	262
Ta	0.50	0.60	2.7	0.22	0.21	0.22	0.23	0.45
Th	4.0	5.8	24	1.5	1.5	1.4	1.5	4.6
Zr	182	166	428	60	60	59	61	76
Nb	7.7	9.5	51	3.5	3.3	3.3	3.6	5.6
Y	25	21	32	4.1	3.8	4.1	3.5	14
Hf	5.3	4.5	9.6	1.6	1.7	1.7	1.7	2.0
V	2.5	10		36	33	37	35	164
Cr	13	20	45	28	21	24	27	22
Ni	3.7	11		9.1	7.2	6.6	8.7	42
Co	1.1	1.3	3.0	4.5	3.5	4.2	4.1	11
U	1.0	1.2	5.2	0.80	0.77	0.71	0.59	1.0
Sc	15	9.6	8.9	8.3	7.6	7.9	7.5	17.9
Cu	5.2	8.2	5.9	14	5.1	12	17	11
Zn	81	28	102	35	31	37	33	46
Pb	4.1	5.9	20	9.6	7.5	8.6	8.5	4.5
Cs	0.08	0.17	0.31	1.3	1.5	0.51	4.0	0.83
La	17	20	144	8.2	7.9	7.9	4.8	18
Ce	37	41	229	14	14	14	14	27
Pr	4.7	4.5	24	1.4	1.4	1.4	1.1	3.2
Nd	21	18	80	5.2	5.1	5.0	4.1	13
Sm	5.1	3.5	12	0.94	0.91	0.95	0.79	2.5
Eu	1.1	0.68	3.0	0.36	0.34	0.34	0.25	0.85
Gd	4.8	3.4	8.6	0.88	0.88	0.81	0.72	2.6
Tb	0.72	0.56	1.1	0.12	0.12	0.11	0.11	0.37
Dy	4.7	3.9	6.4	0.7	0.7	0.8	0.7	2.4
Ho	1.0	0.82	1.2	0.15	0.14	0.15	0.12	0.50
Er	3.1	2.5	3.3	0.4	0.4	0.4	0.4	1.4
Tm	0.48	0.38	0.51	0.06	0.05	0.07	0.06	0.21
Yb	3.4	2.8	3.6	0.5	0.4	0.4	0.4	1.5
Lu	0.53	0.44	0.51	0.07	0.07	0.07	0.07	0.23

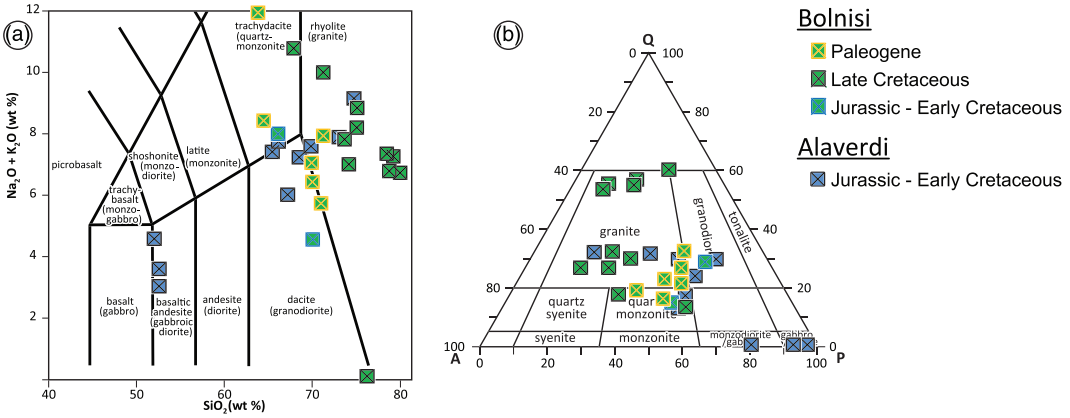

Figure 4. Geochemical classification and discrimination diagrams. (a) Total alkali versus silica (TAS) diagram. (b) Simplified QAPF diagram (Streckeisen, 1976) showing the normative mineralogical composition of intrusive rocks.

The Th/Yb versus Ta/Yb diagram (Pearce, 1982, 1983) for volcanic rocks shows a range of compositions from those which have higher Th/Yb values than depleted mantle to those with higher Th/Yb values than enriched mantle (Figure 8), often attributed to addition of nonconservative elements such as Th during subduction (Pearce et al., 1984).

The samples from both the Alaverdi and Bolnisi districts have similar extended trace element spider diagrams displaying a subduction-related signature (Figure 9). These include general relatively high concentrations of large ion lithophile elements (LILE), lower contents of high field strength elements (HFSE), and negative Nb and Ta, and positive U, K, and Pb anomalies. In addition, various degrees of negative Eu anomalies, variable light rare earth element (LREE) enrichments, and more pronounced depleted medium and heavy rare earth element (MREE and HREE) patterns in chondrite-normalized diagrams (Figure 10) are present for all the samples of both the Alaverdi and Bolnisi districts. In the La/Yb versus Th/Yb diagram (Figure 11) the Alaverdi and Bolnisi district samples plot in continuation from one another from the primitive island arc, to the island arc, to the continental arc fields. In the Sr/Y versus Y diagram (ESD 6), the samples from both the Alaverdi and Bolnisi districts tend to overlap, even though it could be argued that they also plot in continuation from one another from the normal volcanic-arc field to the beginning of the adakite field. Let it be pointed out that even if samples of both districts have comparable chemical compositions, four samples from the Bolnisi district of Eocene age plot well in the adakite field, whereas none of the samples from the Alaverdi district do.

6. Discussion and Geodynamic Implications

6.1. Jurassic to Early Cretaceous Subduction-Related Magmatism: EP-GC-LC

When juxtaposing the ages of the various subduction-related magmatic rocks throughout the study region, it becomes apparent that a significant portion of the rocks corresponding to the Jurassic history of the EP is missing or underrepresented (Figure 2), as the EP form a continuous synchronous arc with the SK arc (Figure 1a). Along the northern margin of the EP, subduction-related tuff and basaltic rocks ascribed to Early and Middle Jurassic times by stratigraphic positioning have been described (Şen, 2007). Outcropping in the Sochi-Ritsa/Bechasyn region of the SS, between the MCT and the northern margin of the EBS, subduction-related magmatic rocks ascribed to Early and Middle Jurassic times also crop out (McCann et al., 2010).

In comparison with the SK, samples of the EP, Bolnisi, and the Sochi-Ritsa/Bechasyn regions plot along similar tends in geochemical diagrams (Table 3). This implies that magmatic rocks of each of these regions are the products of comparable processes and can be attributed to a similar arc setting. The extended trace and rare earth element plots show generally similar patterns. Enrichment in LILE and negative anomalies in Ta-Nb are common in all samples from all three sectors (EP, GC, and LC), diagnostic of subduction-related magmatism (Figure 9). Samples from the GC and SK sectors feature well marked positive Hf anomalies, whereas the samples of the EP tend to be devoid of positive anomalies, even one sample

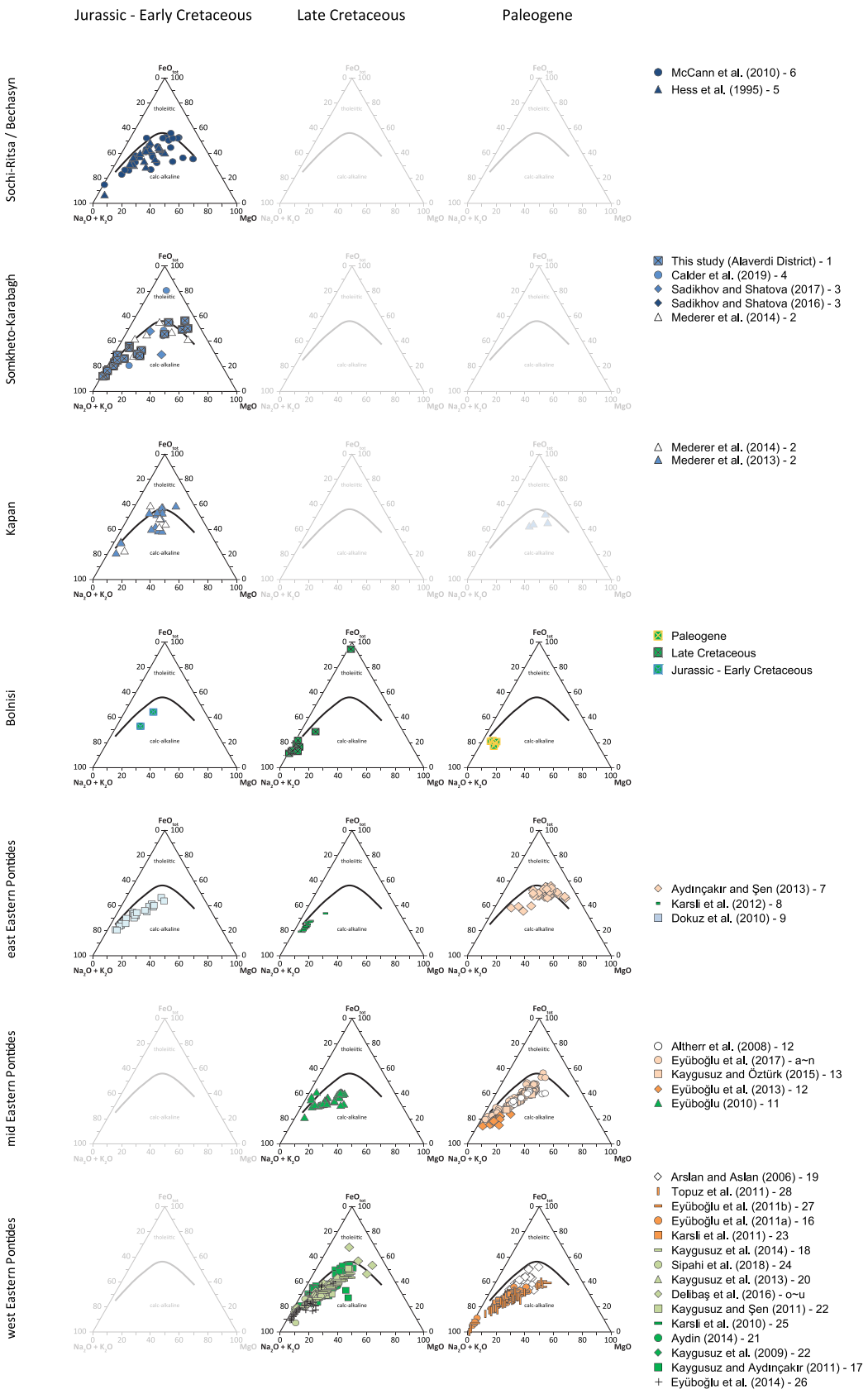

Figure 5. AFM plot (Irvine & Baragar, 1971).

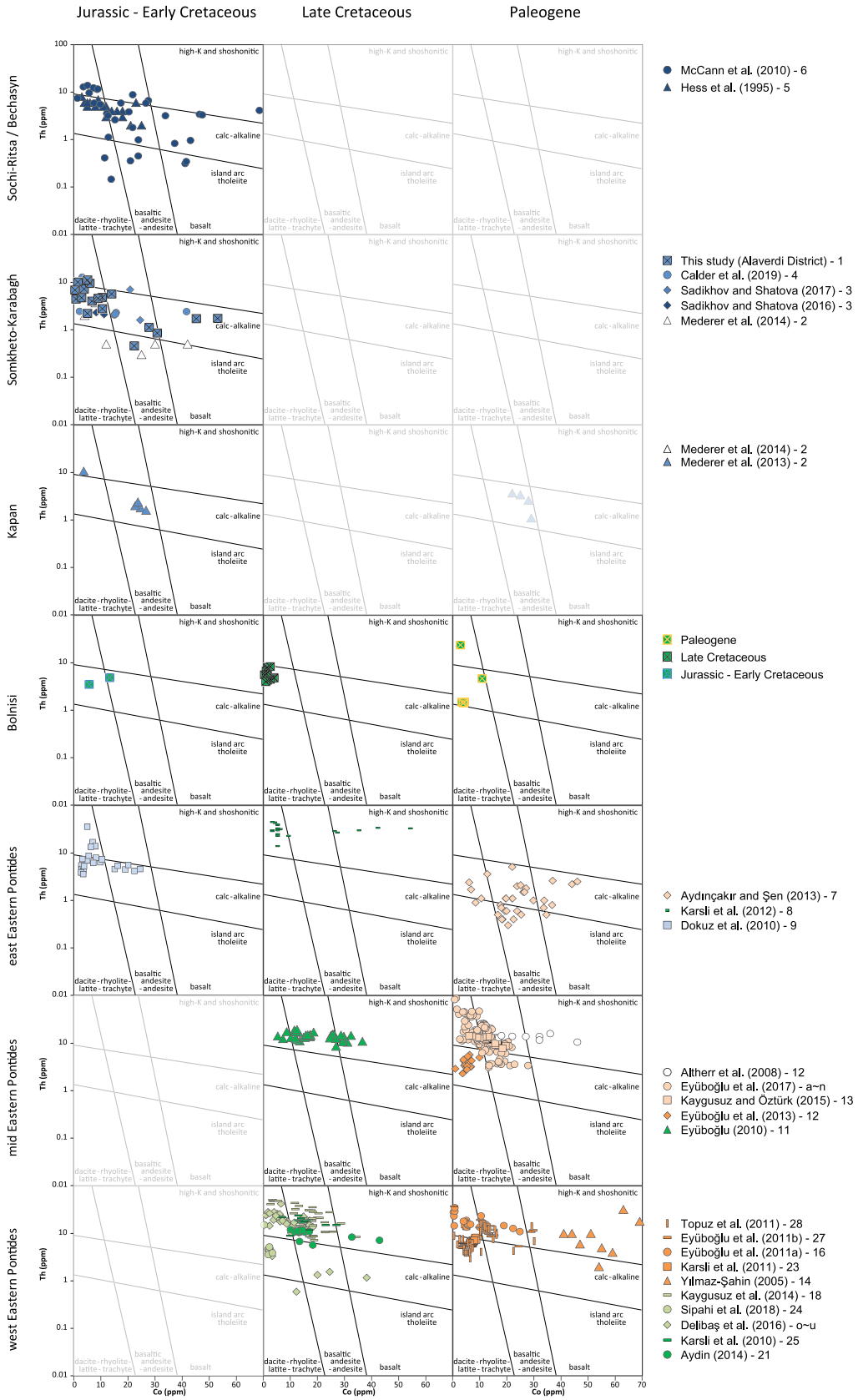

Figure 6. Th-Co discrimination diagram for island arc rocks (Hastie et al., 2007).

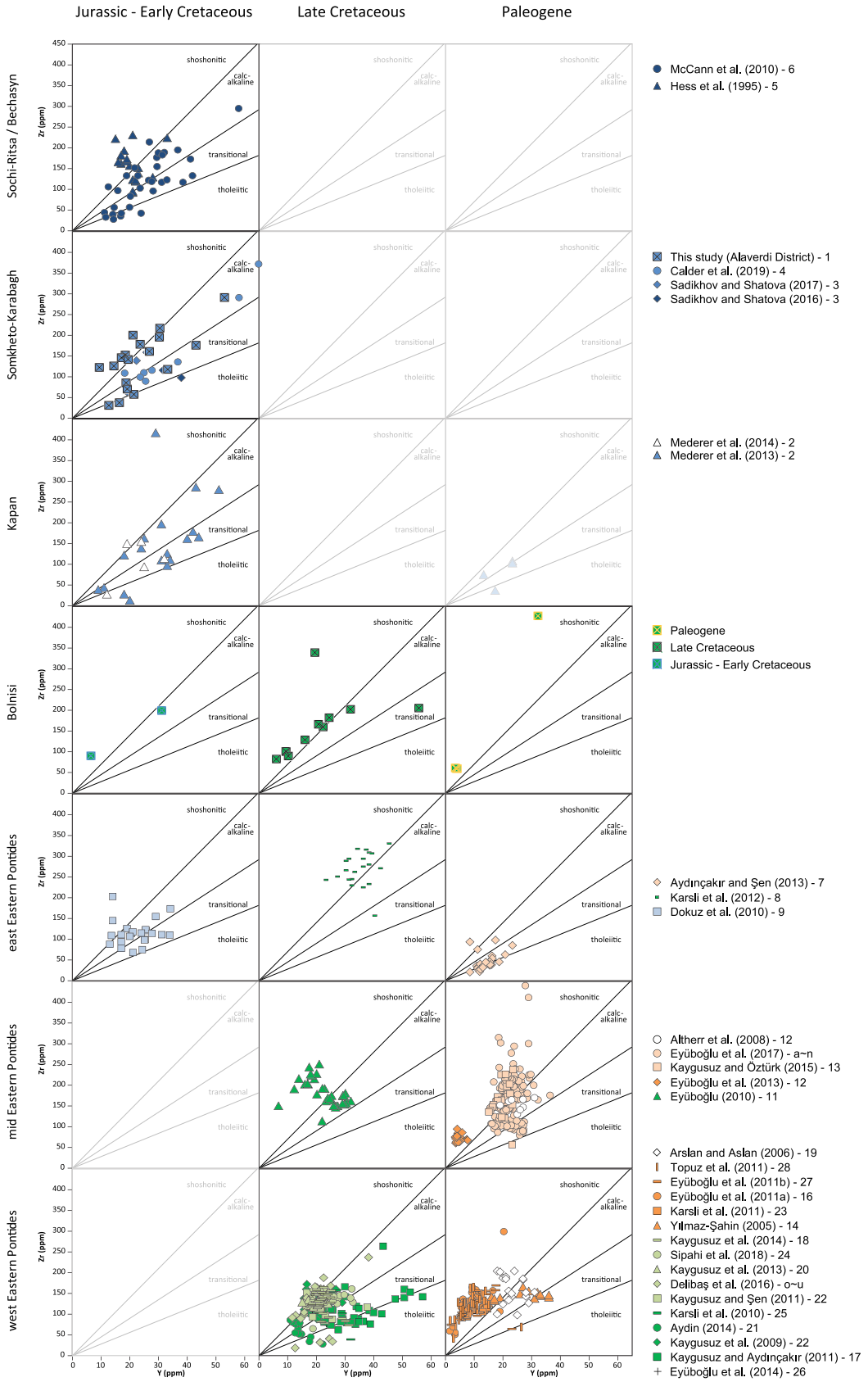

Figure 7. Zr versus Y diagram (Barrett & MacLean, 1994, 1999).

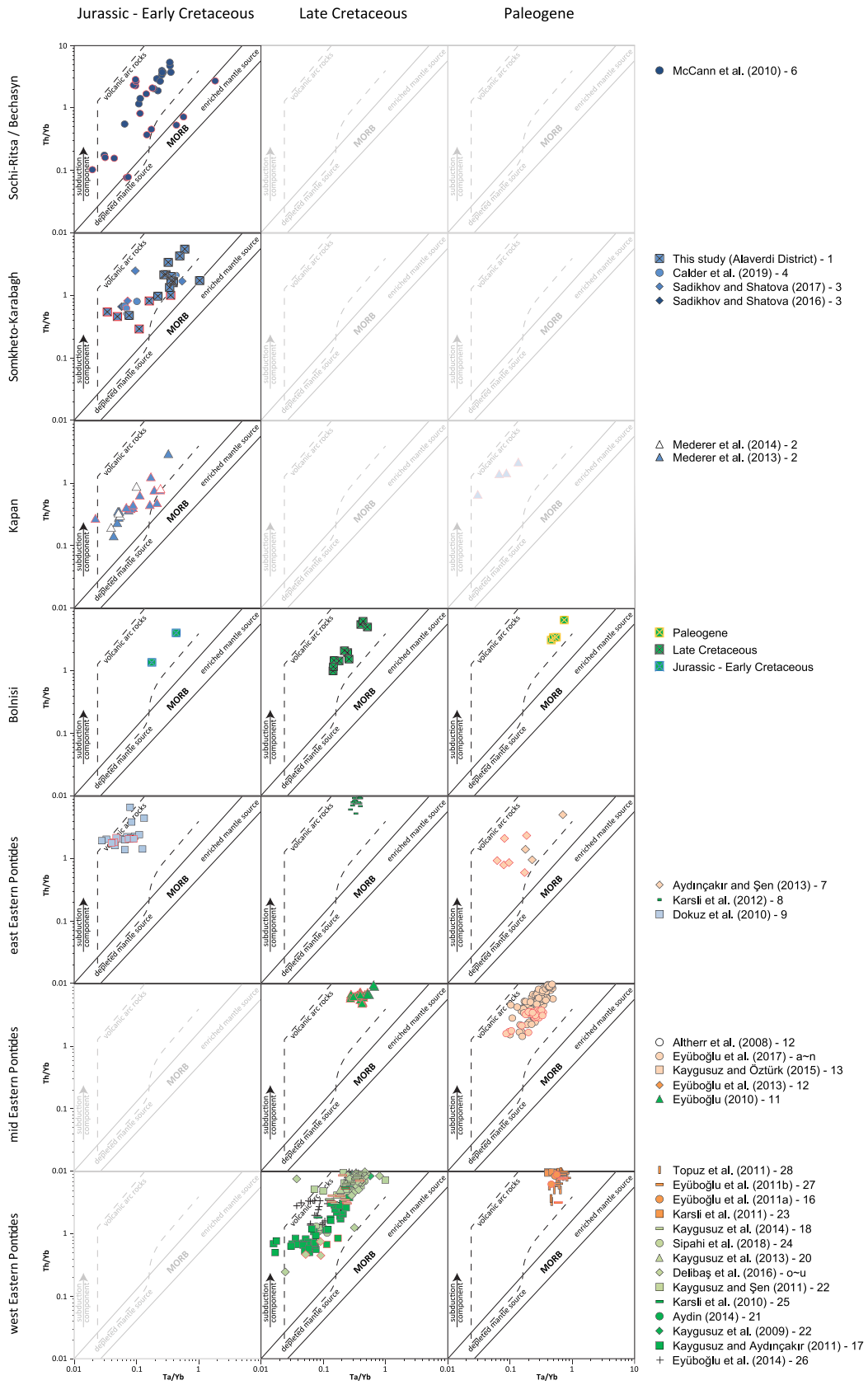

Figure 8. Ta/Yb versus Th/Yb tectonic emplacement diagram (Pearce, 1982). Mafic rocks are represented with red contours.

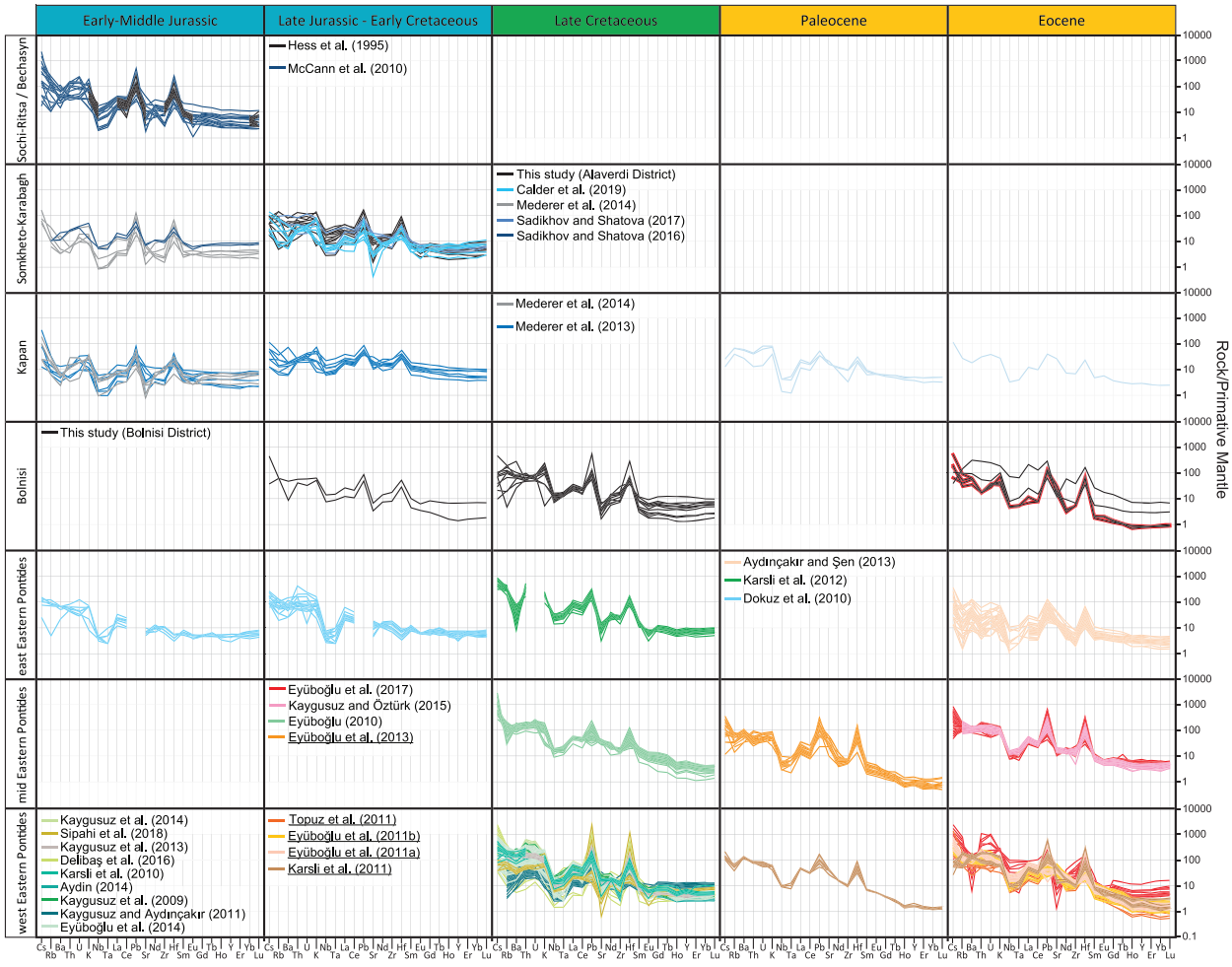

Figure 9. Primitive mantle-normalized extended trace element spider diagrams, normalization with respect to Sun and McDonough (1989). References featuring adakite-like rocks, according to ESD 6, are underlined. Adakite-like rocks from the Bolnisi district are represented with red contours.

showing a negative Hf anomaly. Rare earth element patterns (Figure 10) of Early-Middle Jurassic rocks of the LC and some rocks of Late Jurassic-Early Cretaceous age of the SK show no, to limited, LREE enrichment. Jurassic-Early Cretaceous rocks of the GC and EP sectors and Bolnisi region exhibit well-marked LREE enrichment. These differences may be due to localized involvement of residual, minor phases in the downgoing slab, fluid and sediment addition, and partial melting in the mantle wedge (Dokuz et al., 2010). Th/La versus $(Ce/Ce^*)_{Nd}$ diagrams (ESD 7) show that the subducted sediment component varies between continental and volcanic detritus, except for those of Bolnisi composed solely of continental detritus, with no correlation of Hf anomalies or LREE enrichment. In the La/Yb versus Th/Yb diagram (Figure 11) Jurassic-Early Cretaceous samples from the GC (Sochi-Ritsa/Bechasyn), LC (SK, Kapan, and Bolnisi) and EP plot within the primitive island arc field. Likewise, these samples plot in a common field in the Sr/Y versus Y diagram, as normal arc (ESD 6), further supporting a common geodynamic evolution among the considered regions.

In light of all the geochemical data (Table 3), it appears that the Jurassic-Early Cretaceous subduction-related magmatic rocks of the GC (Sochi-Ritsa/Bechasyn), LC (SK, Kapan, and Bolnisi), and EP share similar geochemical characteristics from site to site and age to age, implying similarity of magmatic processes may be involved, if not a continuous arc setting. The geographic positioning of the EP and SK arcs, and the Bolnisi and Kapan regions further supports a common geodynamic process responsible for their formation (Figure 1a). Yet the Sochi-Ritsa/Bechasyn region is located over 100 km farther north with respect to the

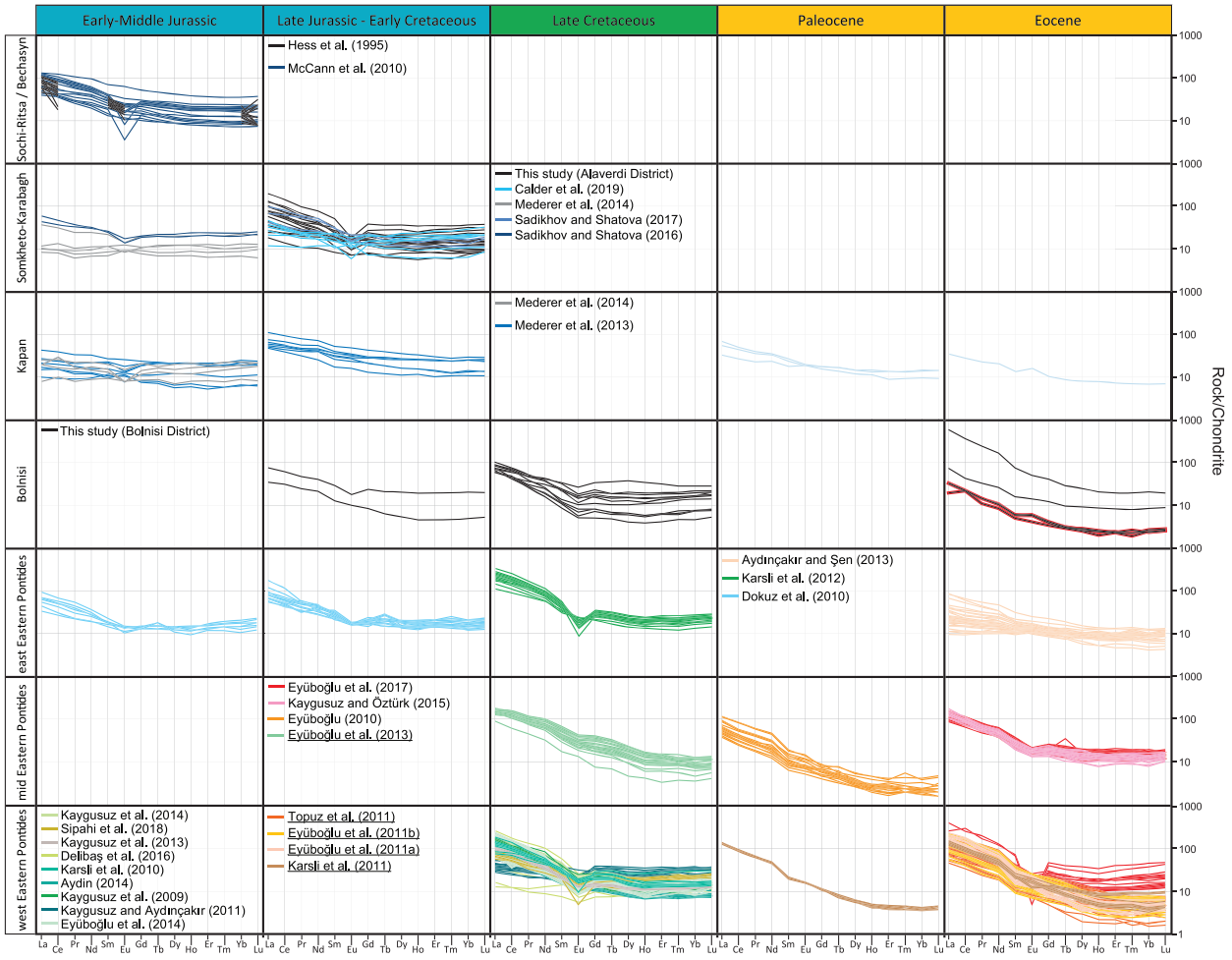

Figure 10. Rare earth element chondrite-normalized diagrams. Normalization with respect to Sun and McDonough (1989). References featuring adakite-like rocks, according to ESD 6, are underlined. Adakite-like rocks from the Bolnisi district are represented with red contours.

EP and the SK. It is separated from the EP by the EBS and from the SK by the Transcaucasus. The Jurassic subduction-related magmatic rocks of the GC present a general NW-SE distribution, in continuity with those of the SK (Figure 3). The position of these subduction-related magmatic rocks found along the SS of the GC can in no way be linked to the formation of the GC belt itself. The GC was formed by top-to-south lithospheric thrusting (Cowgill et al., 2016; Mauvilly et al., 2018; McCann et al., 2010) during the Cenozoic (Mosar et al., 2010; Nikishin et al., 2010). The structure of the GC implies that any related magmatism would be farther north of the MCT, not to its south. Furthermore, the ages of these rocks (Early and Middle Jurassic; Hess et al., 1995; McCann et al., 2010) do not coincide with the timing of the compression within the GC belt (Mauvilly et al., 2018; Mosar et al., 2010).

6.2. Late Cretaceous Subduction-Related Magmatism: EP-LC

An important contribution of this study is the confirmation of Late Cretaceous subduction-related volcanic rocks associated to the LC in its northernmost part, in the Bolnisi district (Figure 3). Previously, there were only little chronometric data available documenting Late Cretaceous subduction-related magmatic rocks in the Bolnisi district. In comparison, the Late Cretaceous magmatic evolution is well documented for the EP arc (Figure 2 and Table 3). By contrast, no Cretaceous or younger subduction-related magmatic rocks have been documented for the SS of the GC.

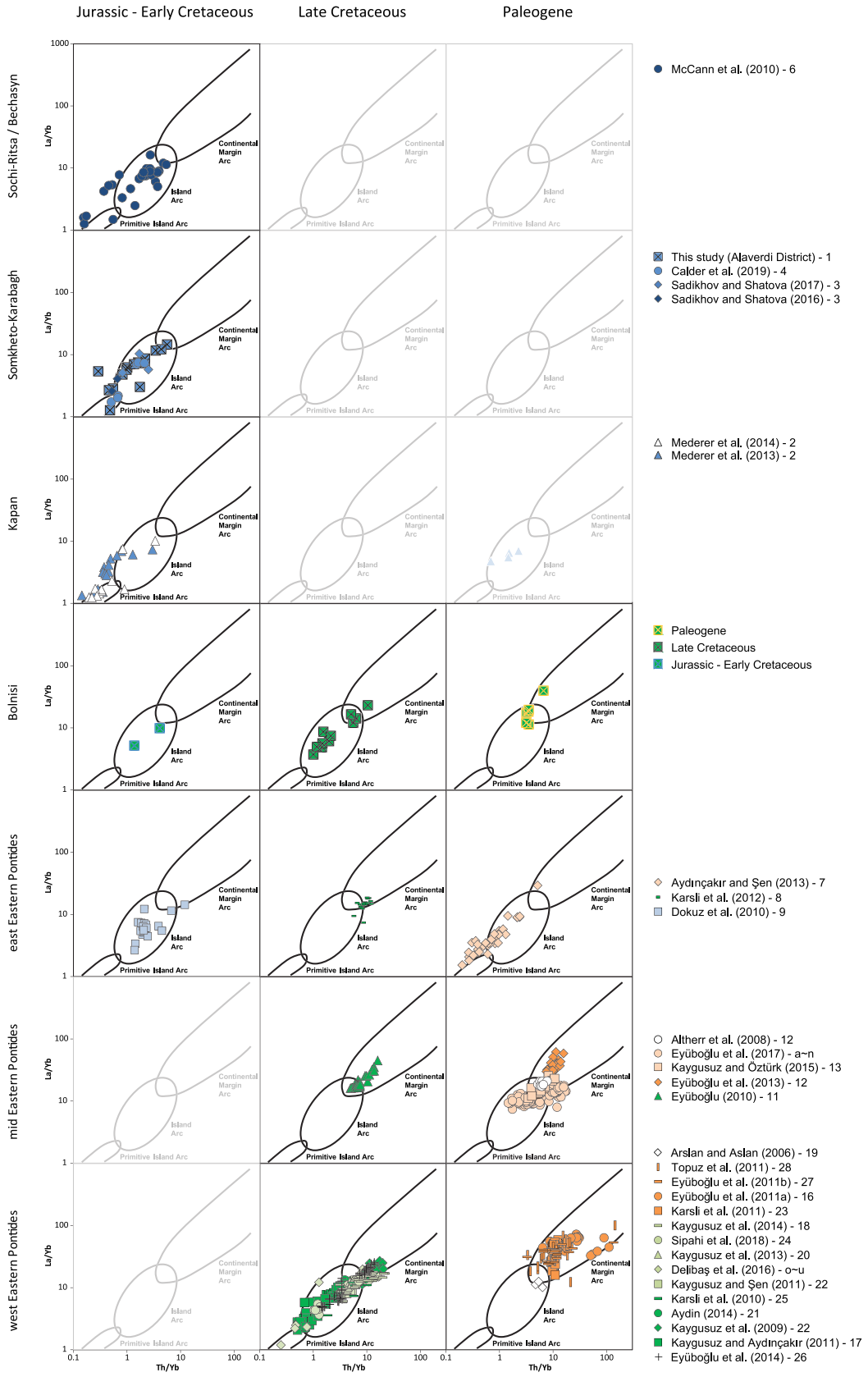

Figure 11. La/Yb versus Th/Yb volcanic rock discrimination diagram (Condie, 1989).

Table 3
Summary of Observations and Tendencies Described in Figures 5–12

Region		diagrams	Figure	Jurassic-Early Cretaceous	Late Cretaceous	Paleogene
Greater Caucasus						
	Sochi-Ritsa/ Bechasyn	major elements versus SiO_2	ESD 5	CaO, Fe_2O_3, and MgO negative trends with increasing SiO_2 Al_2O_3 positive trend with increasing SiO_2 for SiO_2 < 55 wt% Al_2O_3 negative trend with increasing SiO_2 for SiO_2 > 55 wt% two TiO_2 and P_2O_5 negative trends with increasing SiO_2 high angle for SiO_2 < 55 wt% low angle for SiO_2 > 55 wt%		
		AFM	5	subduction-related calc-alkaline trend		
		Th versus Co	6	island arc tholeiite, calc-alkaline, high-K, and shoshonitic		
		Zr versus Y	7	tholeiitic, transtional, calc-alkaline, and shoshonitic		
		Th/Yb versus Ta/Yb (Pearce diagram)	8	depleted to enriched mantle source affected by subduction component plotting as volcanic arc		
		extended trace elements	9	enrichment in LILE negative anomalies in Ta-Nb		
		rare earth elements	10	LREE enrichment negative Eu anomalies		
		La/Yb versus Th/Yb	11	primative island arc to island arc		
		Sr/Y versus Y	ESD 6	normal arc		
		Th/La versus (Ce/Ce*) Nd	ESD 7	continental and volcanic detritus		
Lesser Caucasus						
	Somkheto-Karabagh	major elements versus SiO_2	ESD 5	CaO, Fe_2O_3, and MgO negative trends with increasing SiO_2 Al_2O_3 positive trend with increasing SiO_2 for SiO_2 < 55 wt%		

Table 3 *Continued*

Region	diagrams	Figure	Jurassic-Early Cretaceous	Late Cretaceous	Paleogene
			Al_2O_3 negative trend with increasing SiO_2 for SiO_2 > 55 wt% two TiO_2 and P_2O_5 negative trends with increasing SiO_2 high angle for SiO_2 < 55 wt% low angle for SiO_2 > 55 wt%		
	AFM	5	subduction-related calc-alkaline trend		
	Th versus Co	6	island arc tholeiite to calc-alkaline to high-K and shoshonitic		
	Zr versus Y	7	tholeiitic, transtional, calc-alkaline and shoshonitic		
	Th/Yb versus Ta/Yb (Pearce diagram)	8	depleted to enriched mantle source affected by subduction component plotting as volcanic arc		
	extended trace elements	9	enrichment in LILE negative anomalies in Ta-Nb		
	rare earth elements	10	LREE enrichment as well as no LREE enrichment negative Eu anomalies		
	La/Yb versus Th/Yb	11	primative island arc to island arc		
	Sr/Y versus Y	ESD 6	normal arc		
	Th/La versus (Ce/Ce*) Nd	ESD 7	continental and volcanic detritus		
Kapan	major elements versus SiO_2	ESD 5	Al_2O_3, TiO_2, CaO, Fe_2O_3, P_2O_5, and MgO negative linear trend with increasing SiO_2 two TiO_2 negative trends with increasing SiO_2 high angle for SiO_2 < 55 wt%		

Table 3 *Continued*

Region		diagrams	Figure	Jurassic-Early Cretaceous	Late Cretaceous	Paleogene
				low angle for $SiO_2 > 55$ wt%		
		AFM	5	subduction-related calc-alkaline trend		
		Th versus Co	6	island arc tholeiite to calc-alkaline		
		Zr versus Y	7	tholeiitic, transitional and calc-alkaline		
		Th/Yb versus Ta/Yb (Pearce diagram)	8	depleted to enriched mantle source affected by subduction component plotting as volcanic arc		
		extended trace elements	9	enrichment in LILE negative anomalies in Ta-Nb		
		rare earth elements	10	no LREE enrichment negative Eu anomalies		
		La/Yb versus Th/Yb	11	primative island arc to island arc		
		Sr/Y versus Y	ESD 6	normal arc		
		Th/La versus (Ce/Ce*) Nd	ESD 7	continental and volcanic detritus		
	Bolnisi	major elements versus SiO_2	ESD 5	Al_2O_3, TiO_2, CaO, Fe_2O_3, P_2O_5, and MgO negative linear trend with increasing SiO_2	Al_2O_3, TiO_2, CaO, Fe_2O_3, P_2O_5, and MgO negative linear trend with increasing SiO_2	Al_2O_3, TiO_2, CaO, Fe_2O_3, P_2O_5, and MgO negative linear trend with increasing SiO_2
		AFM	5	subduction-related calc-alkaline trend	,	subduction-related calc-alkaline trend
		Th versus Co	6	calc-alkaline	calc-alkaline	calc-alkaline and high-K and shoshonitic
		Zr versus Y	7	calc-alkaline and shoshonitic	calc-alkaline and shoshonitic	shoshonitic
		Th/Yb versus Ta/Yb (Pearce diagram)	8	MORB to enriched mantle source affected by subduction component plotting as volcanic arc	MORB to enriched mantle source affected by subduction component plotting as volcanic arc	enriched mantle source affected by subduction component plotting as volcanic arc
		extended trace elements	9	enrichment in LILE negative anomalies in Ta-Nb	enrichment in LILE negative anomalies in Ta-Nb	enrichment in LILE negative anomalies in Ta-Nb

Table 3 *Continued*

Region		diagrams	Figure	Jurassic-Early Cretaceous	Late Cretaceous	Paleogene
		rare earth elements	10	LREE enrichment negative Eu anomalies	LREE enrichment negative Eu anomalies	LREE enrichment
		La/Yb versus Th/Yb	11	island arc	island arc and continental margin arc	continental margin arc
		Sr/Y versus Y Th/La versus (Ce/Ce*)Nd	ESD 6 ESD 7	normal arc continental detritus	normal arc continental detritus	normal arc and adakite-like volcanic detritus
Eastern Pontides						
	east	major elements versus SiO_2	ESD 5	Al_2O_3, TiO_2, CaO, Fe_2O_3, P_2O_5, and MgO negative linear trend with increasing SiO_2	Al_2O_3, TiO_2, CaO, Fe_2O_3, P_2O_5, and MgO negative linear trend with increasing SiO_2	Al_2O_3, TiO_2, CaO, Fe_2O_3, P_2O_5, and MgO negative linear trend with increasing SiO_2
		AFM	5	subduction-related calc-alkaline trend	subduction-related calc-alkaline trend	subduction-related calc-alkaline trend
		Th versus Co	6	calc-alkaline to high-K and shoshonitic	high-K and shoshonitic	tholeiitic and calc-alkaline
		Zr versus Y	7	transitional, calc-akaline, and shohonitic	calc-alkaline and shoshonitic	tholeiitic, transtional, calc-alkaline and shoshonitic
		Th/Yb versus Ta/Yb (Pearce diagram)	8	depleted mantle to MORB source affected by subduction component plotting as volcanic arc	enriched mantle source affected by subduction component plotting as volcanic arc	depleted to enriched mantle source affected by subduction component plotting as volcanic arc
		extended trace elements	9	enrichment in LILE negative anomalies in Ta-Nb	enrichment in LILE negative anomalies in Ta-Nb	enrichment in LILE negative anomalies in Ta-Nb
		rare earth elements	10	LREE enrichment negative Eu anomalies	LREE enrichment negative Eu anomalies	flat to LREE enrichment primative island arc and island arc
		La/Yb versus Th/Yb	11	island arc	continental margin arc	normal arc
		Sr/Y versus Y	ESD 6	normal arc continental detritus	normal arc	
		Th/La versus (Ce/Ce*) Nd	ESD 7		continental detritus	continental and volcanic detritus
	mid	major elements versus SiO_2	ESD 5		Al_2O_3, TiO_2, CaO, Fe_2O_3, P_2O_5, and MgO negative linear trend with increasing SiO_2	Al_2O_3, TiO_2, CaO, Fe_2O_3, P_2O_5, and MgO negative linear trend with increasing SiO_2
		AFM	5			

Table 3 *Continued*

Region		diagrams	Figure	Jurassic-Early Cretaceous	Late Cretaceous	Paleogene
					subduction-related calc-alkaline trend	subduction-related calc-alkaline trend
		Th versus Co	6		high-K and shoshonitic	calc-alkaline and high-K and shoshonitic
		Zr versus Y	7		calc-alkaline and shoshonitic	transtional, calc-alkaline and shoshonitic
		Th/Yb versus Ta/Yb (Pearce diagram)	8		enriched mantle source affected by subduction component plotting as volcanic arc	MORB to enriched mantle source affected by subduction component plotting as volcanic arc
		extended trace elements	9		enrichment in LILE negative anomalies in Ta-Nb	enrichment in LILE negative anomalies in Ta-Nb
		rare earth elements	10		LREE enrichment	LREE enrichment negative Eu anomalies
		La/Yb versus Th/Yb	11		continental margin arc	island arc and continental margin arc
		Sr/Y versus Y	ESD 6		normal arc	normal arc and adakite-like
		Th/La versus (Ce/Ce*) Nd	ESD 7		continental detritus	continental and volcanic detritus
	west	major elements versus SiO_2	ESD 5		Al_2O_3, TiO_2, CaO, Fe_2O_3, P_2O_5, and MgO negative linear trend with increasing SiO_2	Al_2O_3, TiO_2, CaO, Fe_2O_3, P_2O_5, and MgO negative linear trend with increasing SiO_2
		AFM	5		subduction-related calc-alkaline trend	subduction-related calc-alkaline trend
		Th versus Co	6		calc-alkaline and high-K and shoshonitic	calc-alkaline and high-K and shoshonitic
		Zr versus Y	7		tholeiitic, calc-alkaline, and shoshonitic	transtional, calc-alkaline and shoshonitic
		Th/Yb versus Ta/Yb (Pearce diagram)	8		depleted to enriched mantle source affected by subduction component plotting as volcanic arc	enriched mantle source affected by subduction component plotting as volcanic arc
		extended trace elements	9		enrichment in LILE negative anomalies in Ta-Nb	enrichment in LILE negative anomalies in Ta-Nb
			10		LREE enrichment	LREE enrichment

Table 3 *Continued*

Region	diagrams	Figure	Jurassic-Early Cretaceous	Late Cretaceous	Paleogene
	rare earth elements			negative Eu anomalies	negative Eu anomalies
	La/Yb versus Th/Yb	11		primitive island arc, island arc, and continental margin arc	continental margin arc
	Sr/Y versus Y	ESD 6		normal arc	normal arc and adakite-like
	Th/La versus (Ce/Ce*)Nd	ESD 7		continental and volcanic detritus	continental and volcanic detritus

The Late Cretaceous samples of the northernmost LC at Bolnisi (Figure 3) and EP arc fall along similar trends in geochemical diagrams (Table 3), akin to those of the Jurassic-Early Cretaceous samples. This indicates that the magmatic rocks of each of these two regions formed due to a comparable process not only during Late Cretaceous times but since Jurassic times. We ascribe the emplacement of these magmatic rocks to a similar arc setting from the Jurassic to at least the Late Cretaceous. Yet the Th-Co discrimination diagram (Figure 6) shows a subduction-related calc-alkaline trend for the samples of Bolnisi, while the samples from the EP exhibit high-K and shoshonitic compositions. Only the samples from the western EP partially overlap with those of Bolnisi in the calc-alkaline field. Zr versus Y diagrams (Figure 7) contradict this by showing Bolnisi, eastern EP, and mid-EP samples plot both as calc-alkaline and shoshonitic.

In light of all the geochemical data (summarized in Table 3), the Late Cretaceous subduction-related magmatic rocks of the LC and the EP share similar characteristics. The geographic positioning of the EP and LC arcs in lateral continuation from one another along the northern Tethyan suture further supports a common geodynamic process responsible for their formation (Figure 1a). Yet important variations in subduction dynamics and margin evolution are apparent along the strike of the intercontinental boundary, suggestive of particular subduction dynamics along mid and east EP compared to west EP and Bolnisi regions (i.e., slab roll-back).

6.3. Paleocene-Eocene Subduction- and Collision/Post Collision-Related Magmatism: EP-LC

Early Paleogene ages are well represented in the LC (Bolnisi and Kapan) and EP (Figure 2). In the LC, ages are constrained to Eocene times, whereas in the EP magmatism ranges from the beginning of the Paleocene and throughout the Eocene. Magmatism in the Kapan region coincides with the early magmatic evolution of Meghri-Ordubad pluton which is linked to the subduction of the southern branch of the Neotethys (Mederer et al., 2013; Moritz et al., 2016; Rezeau et al., 2016, 2017), which is not within the scope of this study. There is no real consensus for the signification of the Paleocene-Eocene magmatism of the entire EP. It has been ascribed not only to subduction-related settings (Eyüboğlu et al., 2013, 2017; Eyüboğlu, Santosh, & Chung, 2011; Eyüboğlu, Santosh, Dudas, et al., 2011) but also to collision (Karsli et al., 2011; Yilmaz-Sahin, 2005) and post-collision-related settings (Aydınçakır & Şen, 2013; Kaygusuz & Öztürk, 2015; Topuz et al., 2011).

Paleogene samples from the LC and EP show similar trends as those of the Jurassic-Early Cretaceous and Late Cretaceous magmatic rock samples (summarized in Table 3). This suggests that the magmatic rocks of each of these two regions formed due to similar continuous process since the Jurassic times. The emplacement of these magmatic rocks can be attributed to a common setting evolving from Jurassic to at least Eocene times. Samples from Bolnisi show the most evolved compositions while those from the EP show a distinct E-W partition, from the least evolved compositions for the Eocene east EP, to the most evolved compositions for the Paleocene-early Eocene (Ypresian) in the west EP region. In the La/Yb versus Th/Yb diagram (Figure 11), the Paleocene-early Eocene (Ypresian) samples of Bolnisi are characterized as continental margin arc, as are those of the mid-EP and west EP. Mid-Eocene (Lutetian) samples from the east EP and the mid-EP have island arc compositions, while samples from the east EP extend to primitive island arc compositions. In the Sr/Y versus Y diagram (ESD 6), the samples of the LC and EP sectors plot

as normal arc and adakite-like rocks. Samples emplaced during the Paleocene-early Eocene (Ypresian) corresponding to mid-EP have normal magmatic arc tendencies, while the Bolnisi and west EP regions plot as adakite-like rocks. Mid-Eocene (Lutetian) samples of the mid-EP show normal arc tendencies, while those of east EP plot within the overlap of the normal arc and adakite-like fields.

In addition to their geographic positioning, the Paleogene magmatic rocks of the LC and the EP share similar characteristics. Yet important variations geochemical tendencies (Table 3) indicative of variations in subduction dynamics and margin evolution are apparent along the strike of the intercontinental boundary, the IAES and ASAS. The Eocene magmatic rocks of the Bolnisi district are coeval with the early Eocene adakite-like magmatism of the EP (Figure 2). Thus, both the EP and the Bolnisi district share a common early Eocene collision and postcollisional magmatic evolution, suggestive of asthenospheric upwelling in relation to slab dynamics (i.e., slab break-off, roll-back, or tearing). The drawing of asthenospheric flow and the accompanying renewed metasomatism of rejuvenated mantle is in accordance with previous studies concerning the Eocene magmatism of the EP (Dokuz et al., 2019; Eyüboğlu, Santosh, Dudas, et al., 2011; Karsli et al., 2010, 2011; Topuz et al., 2005, 2011). However, in addition to mantle-related processes and slab melting, we cannot discount magmatic differentiation in a thickened lower crust, that could also have generated the adakite-like high Sr/Y ratios (Chapman et al., 2015; Chiaradia, 2015; Mamani et al., 2010; Richards & Kerrich, 2007).

6.4. Subduction Polarity

Two models subsist concerning the subduction, or subductions, responsible for the magmatism of the EP and LC. The first describes that the magmatic arcs result from the subduction of Tethyan realms (Paleotethys and Northern Neotethys) toward the north below the South Eurasian margin, from Triassic times until collision during the Paleogene (Adamia et al., 2011; Barrier et al., 2018; Dercourt et al., 1986; Saintot et al., 2006; Saintot & Angelier, 2002; Sosson et al., 2017; Stampfli et al., 2001). In this model, the BS opened in an intra-arc to back-arc setting. The second features a south dipping subduction of Paleotethys throughout the Mesozoic to early Cenozoic times below the northern margin of the Pontides (Bektaş, 1986; Eyüboğlu, 2010, 2015; Eyüboğlu et al., 2007, 2013, 2017, 2018; Liu et al., 2018). Recent modifications of this model also feature two subduction zones, a south and north dipping subductions along the northern and southern margins of the Pontides, respectively, during latest Cretaceous to early Cenozoic times (Eyüboğlu et al., 2019). This second model implies that the BS represents a relic of the Paleotethys ocean, which mostly disappeared through south dipping subduction. In the latter model, the northern Neotethyan realm opened in a back-arc setting related to the south dipping Paleotethyan subduction.

Typical subduction polarity evidence such as obducted ophiolites, subduction/obduction-related metamorphic rocks as well as radiolarite originating from abyssal parts of disappeared oceanic domains are only present along the southern margin of the EP and LC's SK arcs, not along their northern margin (Asatryan et al., 2010, 2011, 2012; Celik, 2007; Çelik et al., 2006, 2011; Danelian et al., 2007, 2008, 2010, 2012, 2014; Galoyan, 2008; Galoyan et al., 2009; Hässig, Rolland, Sosson, Galoyan, Müller, et al., 2013; Hässig, Rolland, Sosson, Galoyan, Sahakyan, et al., 2013; Hässig et al., 2017, 2019; Okay & Tüysüz, 1999; Okay et al., 2001, 2006; Parlak & Delaloye, 1999; Parlak et al., 2012; Robertson, 2002; Robertson, Parlak, Ustaömer, Taslı, et al., 2013; Rolland, Billo, et al., 2009; Rolland et al., 2010; Sosson et al., 2010; Topuz et al., 2013). Furthermore, the seismic profiles of the BS (Nikishin et al., 2015a., 2015b) do not show any structures suggestive of south dipping subduction or the existence of any basins older than Cretaceous. On the contrary, this imagery is interpreted as portraying a rifted continental crust with a central oceanic crust stratigraphically covered by a sedimentary fill indicating basin opening and deepening throughout the Cretaceous (Afanasenkov et al., 2008; Görür, 1988; Nikishin et al., 2008; Robinson, Spadini, et al., 1995; Shillington et al., 2008), followed by subsidence throughout the Paleogene (Letouzey et al., 1977; Shillington et al., 2008).

The geochronological and geochemical data concerning the Sochi-Ritsa/Bechasyn region of the GC's SS (summarized in Table 3; McCann et al., 2010) strongly support a common history with the EP in spite of being over 100 km farther north along the northern margin of the BS. In the second model (south dipping subduction beneath the EP), a common origin for subduction-related magmatic rocks of the GC with those of the LC and EP is incompatible. In this model the GC and LC-EP ensemble are on alternate sides of the subduction: the GC north of the sinking slab, while the LC and EP on the overriding margin. The

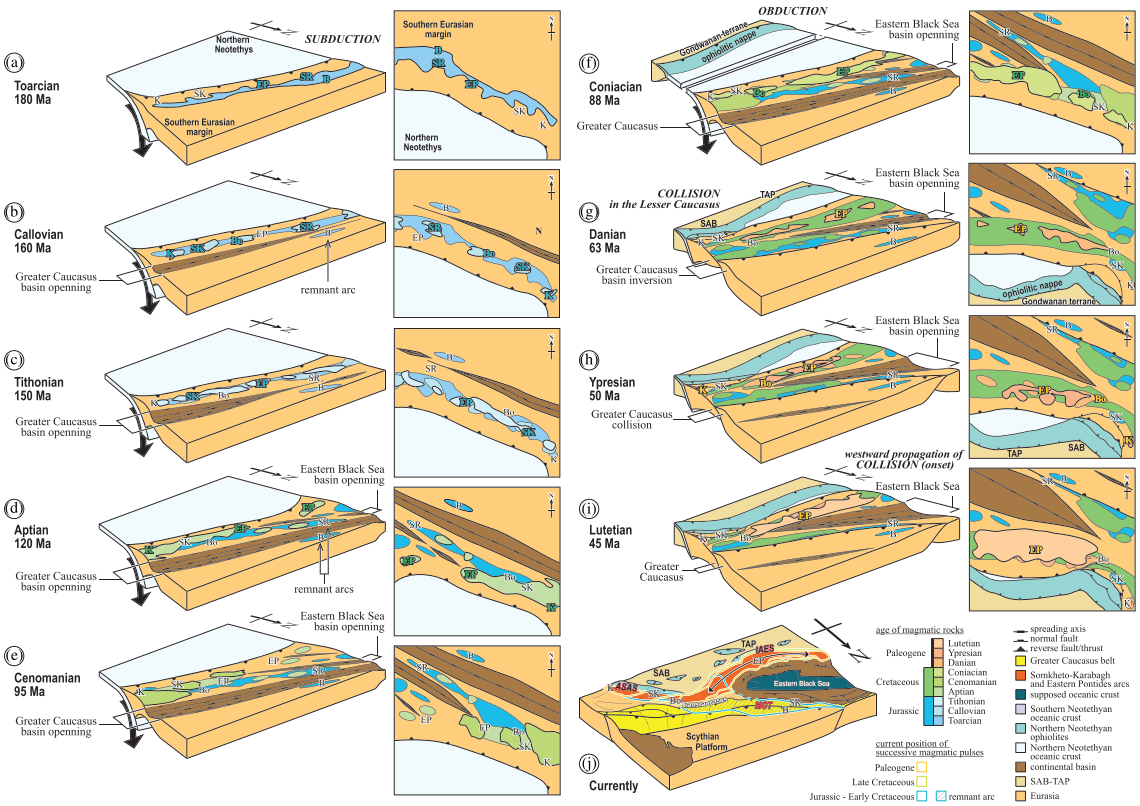

Figure 12. Middle Toarcian (ca. 180 Ma) to present-day palaeotectonic evolution of the NE Anatolian-Lesser Caucasus region. Maps modified from DARIUS Programme paleotectonic maps of the Central Tethyan Realm (Barrier et al., 2018) featuring new interpretations.

significance of the geodynamic evolution of the Jurassic subduction-related magmatic rocks of the GC, and their similarities with those of the LC and EP arcs, is not considered nor discussed. The model proposing solely a north dipping subduction and an opening of the BS as an intra-arc to back-arc basin implies that the Jurassic subduction-related magmatic rocks of the GC were originally part of the same continuous belt from the LC's SK to the EP. Here, the Jurassic subduction-related magmatic rocks of the GC represent part of the missing Jurassic subduction-related magmatic rocks of the EP.

6.5. Geodynamic Reconstruction: Cutting an Arc in Two

Major and trace element geochemistry (summarized in Table 3) generally supports a model derived from regional geology and geochronology where the subduction-related magmatic rocks of the EP and LC arcs as well as those of the Sochi-Ritsa/Bechasyn regions of the GC are all relics of a common arc. This underlines ongoing evolution of a common interplate boundary from Jurassic to Eocene times with evolution and maturing of a common arc throughout, including the opening of a related intra-arc to back-arc basin (Figure 12). In light of the new and available geochemical and geochronologic data, it appears that the studied subduction-related magmatic rocks exhibit coherent, continuous, and similar tendencies throughout the EP, LC, and GC regions during the Jurassic-Early Cretaceous, throughout the EP and LC during the Late Cretaceous. Considering EP and LC Paleogene evolution, analyses of the data manifest differences in subduction, collision, and postcollision dynamics.

The Jurassic-Early Cretaceous subduction-related magmatic rocks of the GC (Sochi-Ritsa/Bechasyn), LC (SK, Kapan, and Bolnisi), and EP to represent relics of a common and continuous arc along the Southern Eurasian Margin (Figure 12a). The arc was deformed and divided throughout its formation due to the opening of marginal basins (Figures 12b–12d) and even further afterward due to collisional processes (Stephenson & Schellart, 2010). Division of an active arc into two segments (one active and another inactive "remnant") separated by an oblique marginal basin has been proposed in the Mediterranean where Corsica and Sardinia represent remnant relics of the current Apennine arc

separated by the Tyrrhenian basin (Karig, 1972; Sartori, 2003). Also, northeast of New Zealand, studies have shown that the Colville arc represents a remnant relic of the active Kermadec arc, displaced from above the active SSZ by the opening of the Havre Trough (Wright, 1997; Wright et al., 1996). The Sochi-Ritsa/Bechasyn region of the GC and the EP are separated by the EBS (Figures 12d and 12e). The Sochi-Ritsa/Bechasyn region and the LC are separated by the Transcaucasus. Only the EP and the LC arcs form a continuous structure along the Southern Eurasian Margin from Late Cretaceous to Eocene times (Figure 12f), considered today to be the Northern Tethyan arc.

There are no reported Cretaceous subduction-related magmatic rocks in the GC (Hess et al., 1995; McCann et al., 2010). This strongly argues migration of the Sochi-Ritsa/Bechasyn region away from the active SSZ becoming remnant portions of the Tethyan arc during, or shortly preceeding, these times (McCann et al., 2010; Figures 12d and 12e). Incidentally, the complete rifting and supposed formation of oceanic crust of the EBS basin is constrained to the beginning of the Late Cretaceous (Nikishin et al., 2015a, 2015b; Sheremet et al., 2017). Generally, Late Cretaceous magmatic rocks from the LC and the EP share similar characteristics (Table 3), comparable arc formation settings (Figure 12f). Yet Late Cretaceous magmatic rocks of the EP, particularly for the east EP and mid-EP, have high-K and shoshonitic tendencies (Figures 6 and 7 and Table 3), a more enriched mantle source (Figure 8), and a clearly marked normal continental arc affinity (Figure 11, ESD 6). We argue that these characteristics indicate roll-back of the north dipping subducting Tethyan slab below EP, especially the east EP and mid-EP. This roll-back and the opening of the EBS were coeval. This roll-back induced the upwelling of asthenospheric mantle in the back-arc domain and caused magma underplating in the lower crust significantly weakening it (Göğüş, 2015; Kim et al., 2015; Menant et al., 2016). Additionally, due to this roll-back, dehydration of the subducting slab contributed to greater mantle source metasomatism. As a consequence, many Late Cretaceous plutons across the EP formed along the active continental margin in an intra-arc extensional environment (Boztuğ et al., 2004; Boztuğ & Harlavan, 2008; Karsli et al., 2010, 2012; Kaygusuz et al., 2009).

Characteristics of Paleogene magmatic rocks in the EP and LC exemplify disparities in collision and postcollision dynamics as well as their timing (Figures 12g–12i). The Paleogene magmatism of the LC (Bolnisi) is dated to the early Eocene (Figure 2). In the LC the end of collision and subsequent suturing of the interplate domain is constrained to the beginning of the Eocene (Lordkipanidze et al., 1988; Sosson et al., 2010; Figure 12h). The magmatic rocks there have high-K and shoshonitic to calc-alkaline tendencies (Figures 6 and 7 and Table 3), originating from an enriched mantle source (Figure 8), with normal arc and adakite-like characteristics (ESD 6) emplaced in a mature continental margin (Figure 11). Following entry of the SAB in the subduction zone, we propose a rapid evolution from roll-back of the subducting slab just prior or during suturing to break-off just after the said suturing in the LC. This model accounts for the coexistence of early Eocene high-K and shoshonitic magmatism with adakite-like tendencies. After the end of the roll-back, slab-pull provoked slab break-off (Sperner et al., 2001) of the north dipping Northern Neotethyan oceanic lithosphere from the SAB (Sokol et al., 2018).

For the EP, the emplacement of the magmatic rocks is divided into two phases: (1) Paleocene-early Eocene (Ypresian) and (2) mid-Eocene (Lutetian). Paleocene-early Eocene (Ypresian) rocks of the mid-EP and west EP rocks exhibit calc-alkaline and shoshonitic tendencies (Figures 6 and 7) originating from an enriched mantle source (Figure 8) with adakite-like characteristics (ESD 6) emplaced in a continental margin setting (Figure 11). The mid-Eocene times (Lutetian) rocks of the mid-EP samples present calc-alkaline and shoshonitic tendencies, but also transitional and some even tholeiitic (Figures 5 and 6) originating from a mantle ranging from mid-ocean ridge basalt (MORB) to more enriched mantle source (Figure 8) with normal arc characteristics in a mature arc setting (Figure 11). East EP samples for this second Paleogene phase are quite different. They exhibit calc-alkaline and tholeiitic tendencies (Figures 5 and 6) from a mantle ranging from depleted MORB to a more enriched mantle source (Figure 8) with normal arc characteristics in a primitive arc setting (Figure 11).

It has been proposed that adakite-like tendencies and the restoration of a primitive arc setting with less evolved magmatic rocks are due to either slab break-off (Aydınçakır & Şen, 2013; Boztuğ & Harlavan, 2008; Dokuz et al., 2010; Karsli et al., 2011) or subduction of a mid-oceanic ridge (Eyüboğlu et al., 2013, 2017; Eyüboğlu, Santosh, & Chung, 2011), creating an asthenospheric window. Alternative models include the initiation of a second subduction creating a convergent double-sided subduction system along both southern and northern margins of the EP (Eyüboğlu et al., 2019) or orogenic root collapse of the EP

(Kaygusuz & Öztürk, 2015). In light of the evolution derived from the LC, we favor a model featuring the slab break-off or westward tear propagation.

In the favored model, roll-back first occurred in the EP during Cretaceous times while in the LC it occurred during the early Eocene. Paleogeographic reconstructions (Barrier et al., 2018; Okay et al., 2001; Sosson et al., 2010) argue that interplate Northern Neotethyan suturing occurred in the LC before suturing in the EP (Figures 12g–12i). This, in turn, argues that break-off occurred first in the LC and propagated westward to the EP. The resulting westward propagating window would be responsible for the adakite-like magmatism. Following this tearing-off of the single north dipping oceanic lithospheric slab, below the LC and EP, and complete suturing in the LC, a short-lived magmatic pulse occurred (Figure 12i). Resulting underplating (roll-up) and dehydration of the remaining oceanic slab attached to the underthrusted TAP and subsequent mantle wedge metasomatism occurred in the east EP and mid-EP during mid-Eocene times.

7. Conclusions

By incorporating new data and observations with geochronological and geochemical data, including paleogeographic reconstructions, a Mesozoic and Cenozoic model is proposed for the evolution of the Caucasus, EP, and Black Sea regions. The Jurassic-Early Cretaceous segments of the arc run from the Sochi-Ritsa/Bechasyn region southeast to the Alaverdi district, continuing to the rest of the SK arc of the LC (Figure 1b). The Late Cretaceous to Cenozoic portion of the arc is evidenced throughout the EP continuing to the Bolnisi district. From east to west, Jurassic and Late Cretaceous to Cenozoic portions of the arc split to the north and south side of the EBS, respectively. The scarcity of Jurassic and Early Cretaceous arc-related magmatic rocks in the EP and Early Cretaceous to Cenozoic arc-related magmatic rocks in the GC (Figure 2) argues for basin opening and important arc migration (formation of a remnant arc) during these times.

The current position of the magmatic rocks and structure of the GC, the LC, the EP, and the EBS best support a model in which they result from a single and continuous north dipping subduction of the northern branch of the Neotethys with opening of the EBS basin in a back-arc to intra-arc setting throughout the Mesozoic and Early Cenozoic. This model implies that there is no south dipping Paleotethyan subduction north of the EP and LC.

Based on all the available geological data, we propose the following model for the evolution of the southern Eurasian margin, along which a magmatic arc was formed during north dipping subduction of the Paleotethyan and Northern Neotethyan domains, affected by collisional to postcollisional tectonics and magmatism after accretion with the SAB and TAP (Figure 12):

1. Jurassic-Paleogene magmatic rocks were emplaced due to a single north dipping interplate boundary (subduction-collision).
2. Emplacement of Jurassic-Early Cretaceous subduction-related magmatic arc.
3. Cretaceous roll-back and onset of the EBS basin opening. The previously emplaced Jurassic magmatic rocks in the EP region are transposed farther north of the SSZ due to the EBS basin opening.
4. Break-off and suturing in the LC during the early Eocene.
5. Propagation of break-off tearing westward to the EP.

Data Availability Statement

Data availability complies with FAIR Data guidelines. New data for this research are included in this paper (Supporting information files are available at https://doi.org/10.5281/zenodo.4028469). Preexisting data sets for this research are available in the references compiled in the caption of Figure 1(Altherr et al., 2008; Arslan & Aslan, 2006; Aydin, 2014; Aydınçakır & Şen, 2013; Boztuğ & Harlavan, 2008; Calder et al., 2019; Delibaş et al., 2016; Dokuz et al., 2010; Eyüboğlu, 2010; Eyüboğlu, Santosh, Dudas, et al., 2011; Eyüboğlu, Santosh, & Chung, 2011; Eyüboğlu et al., 2013; Eyüboğlu et al., 2014; Eyüboğlu et al., 2017; Hess et al., 1995; Karsli et al., 2010, 2011, 2012; Kaygusuz et al., 2009, 2010; Kaygusuz & Şen, 2011; Kaygusuz & Aydinçakir, 2011; Kaygusuz et al., 2013, 2014; Kaygusuz & Öztürk, 2015; McCann et al., 2010; Mederer et al., 2013; Moore et al., 1980; Sadikhov & Shatova, 2016, 2017; Sipahi et al., 2018; Topuz et al., 2011; Yilmaz-Sahin, 2005).

Acknowledgments

This work was carried out within the scope of the Swiss National Science Foundation projects 200020_168996 and 200021_188714. Funding for fieldwork was provided by the Fondation Ernst et Lucie Schmidheiny and the Fonds Général de l'Université de Genève. We thank Jean-Marie Boccard and Fabio Capponi for their involvement in sample preparation and data acquisition, as well as Agathe Martignier for her involvement in SEM-CL image acquisition invaluable for the U-Pb dating.

References

Adamia, S., Alania, V., Chabukiani, A., Chichua, G., Enukidze, O., & Sadradze, N. (2010). Evolution of the Late Cenozoic basins of Georgia (SW Caucasus): A review. *Geological Society, London, Special Publications*, *340*(1), 239–259. https://doi.org/10.1144/SP340.11

Adamia, S., Zakariadze, G., Chkhotua, T., Sadradze, N., Tsereteli, N., Chabukiani, A., & Gventsadze, A. (2011). Geology of the Caucasus: A review. *Turkish Journal of Earth Sciences*, *20*(5), 489–544. http://doi.org/10.3906/yer-1005-11

Adamia, S. A. (1980). Paleomagnetism of Upper Cretaceous rocks of Southern Georgia and its geologic interpretation. *International Geology Review*, *22*(11), 1241–1256. https://doi.org/10.1080/00206818209466995

Adamia, S. A., Belov, A., Kekelia, M., & Shavishvili, I. (1987). Paleozoic tectonic development of the Caucasus and Turkey (Geotraverse C). In H. W. Flugel, F. P. Sassi, & P. Grecula (Eds.), *Pre-Variscan and Variscan events in the Alpine-Mediterranean mountain belts* (pp. 22–50). Alfa Bratislava: Mineralia Slovaca.

Adamia, S. A., Chkhotua, T., Kekelia, M., Lordkipanidze, M., Shavishvili, I., & Zakariadze, G. (1981). Tectonics of Caucasus and adjoining regions: Implications for the evolution of the Tethys ocean. *Journal of Structural Geology*, *3*(4), 437–447. https://doi.org/10.1016/0191-8141(81)90043-2

Adamia, S. A., Lordkipanidze, M. B., & Zakariadze, G. S. (1977). Evolution of an active continental margin as exemplified by the Alpine history of the Caucasus. *Tectonophysics*, *40*(3–4), 183–189. https://doi.org/10.1016/0040-1951(77)90065-8

Afanasenkov, A. P., Skvortsov, M. B., Nikishin, A. M., Murzin, S. M., & Polyakov, A. A. (2008). Geological evolution and petroleum systems in the North Caspian Region. *Moscow University Geology Bulletin*, *63*(3), 131–139. https://doi.org/10.3103/S0145875208030010

Akin, H. (1979). Magmatismus und Lagerstättenbildung im ostpontischen Gebirge/Türkei aus der Sicht der Plattentektonik. *Geologische Rundschau*, *68*(3), 1209–1209. https://doi.org/10.1007/BF01821131

Aliyazicioğlu, I. (1999). Kale (Gümüşhane) yöresi volkanik kayaçlarının petrografi, jeokimyasal ve petrolojik incelenmesi Master Thesis, KTU, Trabzon, 96 pp.

Ali-Zade, A. A. (2005). Geological map of Azerbaijan Republic. National Academy of Sciences of Azerbaijan Republic Geology Institute.

Altherr, R., Topuz, G., Siebel, W., Şen, C., Meyer, H. P., Satır, M., & Lahaye, Y. (2008). Geochemical and Sr-Nd-Pb isotopic characteristics of Paleocene plagioleucitites from the eastern Pontides (NE Turkey). *Lithos*, *105*(1–2), 149–161. https://doi.org/10.1016/j.lithos.2008.03.001

Apkhazava, M. (1988). Late Cretaceous volcanism and volcanic structures of Bolnisi volcano-tectonic depression (Doctoral dissertation). Tbilissi, Georgia: Caucasus Institute of Mineral Resources.

Arslan, M., & Aslan, Z. (2006). Mineralogy, petrography and whole-rock geochemistry of the Tertiary granitic intrusions in the Eastern Pontides, Turkey. *Journal of Asian Earth Sciences*, *27*(2), 177–193. https://doi.org/10.1016/j.bjps.2005.12.048

Asatryan, G., Danelian, T., Seyler, M., Sahakyan, L., Galoyan, G., Sosson, M., et al. (2012). Latest Jurassic-Early Cretaceous Radiolarian assemblages constrain episodes of submarine volcanic activity in the Tethyan oceanic realm of the Sevan ophiolites (Armenia). *Bulletin de la Société Géologique de France*, *183*(4), 319–330. http://doi.org/10.2113/gssgfbull.183.4.319

Asatryan, G., Danelian, T., Sosson, M., Sahakyan, L., & Galoyan, G. (2011). Radiolarian evidence for Early Cretaceous (Late Barremian-Early Aptian) submarine activity in the Tethyan oceanic realm preserved in Karabagh (Lesser Caucasus). *Ofioliti*, *36*(2), 117–123. http://doi.org/10.4454/OFIOLITI.V36.I2.1

Asatryan, G., Danelian, T., Sosson, M., Sahakyan, L., Person, A., Avagyan, A., & Galoyan, G. (2010). Radiolarian ages for the sedimentary cover of Sevan ophiolite (Armenia, Lesser Caucausus). *Ofioliti*, *35*(2), 91–101. https://doi.org/10.4454/OFIOLITI.V36.I2.1

Aydin, F. (2014). Geochronology, geochemistry, and petrogenesis of the Maçka subvolcanic intrusions: Implications for the Late Cretaceous magmatic and geodynamic evolution of the eastern part of the Sakarya Zone, northeastern Turkey. *International Geology Review*, *56*(10), 1246–1275. https://doi.org/10.1080/00206814.2014.933364

Aydınçakır, E., & Şen, C. (2013). Petrogenesis of the post-collisional volcanic rocks from the Borçka (Artvin) area: Implications for the evolution of the Eocene magmatism in the Eastern Pontides (NE Turkey). *Lithos*, *172–173*, 98–117. https://doi.org/10.1016/j.lithos.2013.04.007

Bagdasaryan, G. P., & Melkonyan, R. L. (1968). New data about petrography and geochronology of some volcanogenic and subvolcanic formations of Alaverdi region. *Izvestia Nauki O Zemle (Proceedings of the National Academy of Sciences, Armenian SSR, Earth Sciences)*, *21*, 93–101.

Banks, C. J., Robinson, A. G., & Williams, M. P. (1998). Structure and regional tectonics of the Achara-Trialet fold belt and the adjacent Rioni and Kartli foreland basins. Republic of Georgia. In *Memoir-American Association of Petroleum Geologists* (Vol. 68, pp. 331–346).

Barrett, T. J., & MacLean, W. H. (1994). Chemostratigraphy and hydrothermal alteration in exploration for VHMS deposits in greenstones and younger volcanic rocks. *Geological Association of Canada Short Course Notes*, *11*, 433–467.

Barrett, T. J., & MacLean, W. H. (1999). Volcanic sequences, lithogeochemistry, and hydrothermal alteration in some bimodal volcanic-associated massive sulfide systems. *Reviews in economic geology*, *8*, 101–131.

Barrier, E., & Vrielynck, B. (2008). *Palaeotectonic maps of the Middle East*. Paris: Commission for the Geological Map of the World.

Barrier, E., Vrielynck, B., Brouillet, J. F., & Brunet, M. F., Angiolini, L., Kaveh, F., et al. (2018). Paleotectonic reconstruction of the Central Tethyan Realm. Tectonono-Sedimentary-Palinspastic maps from Late Permian to Pliocene. CCGM/CGMW, Paris, http://www.ccgm.org. Atlas of 20 maps (scale: 1/15 000 000).

Bektaş, O. (1986). Paleostress trajectories and polyphase rifting in arc-back arc of Eastern Pontides. *Bulletin. Mineral Research and Exploration Institute (Turkey)*, *103–104*, 1–15.

Bektaş, O., Şen, C., Atici, Y., & Köprübaşi, N. (1999). Migration of the Upper Cretaceous subduction-related volcanism towards the back-arc basin of the eastern Pontide magmatic arc (NE Turkey). *Geological Journal*, *34*(1–2), 95–106. https://doi.org/10.1002/(SICI)1099-1034(199901/06)34:1/2<95::AID-GJ816>3.0.CO;2-J

Bosworth, W. (1985). Geometry of propagating continental rifts. *Nature*, *316*(6029), 625. https://doi.org/10.1038/316625a0

Boztuğ, D., & Harlavan, Y. (2008). K-Ar ages of granitoids unravel the stages of Neo-Tethyan convergence in the eastern Pontides and central Anatolia, Turkey. *International Journal of Earth Sciences*, *97*(3), 585–599. https://doi.org/10.1007/s00531-007-0176-0

Boztuğ, D., Jonckheere, R. C., Wagner, G. A., & Yeğingil, Z. (2004). Slow Senonian and fast Palaeocene-Early Eocene uplift of the granitoids in the Central Eastern Pontides, Turkey: Apatite fission-track results. *Tectonophysics*, *382*(3–4), 213–228. https://doi.org/10.1016/j.tecto.2004.01.001

Calder, M. F., Moritz, R., Ulyanov, A., Chiaradia, M., Spangenberg, J. E., & Melkonyan, R. L. (2019). Jurassic ore-forming systems during the Tethyan orogeny: Constraints from the Shamlugh deposit, Alaverdi district, Armenia Lesser Caucasus. *Mineralium Deposita*, 1–22. https://doi.org/10.1007/s00126-018-0851-z

Celik, Ö. F. (2007). Metamorphic sole rocks and their mafic dykes in the eastern Tauride belt ophiolites (southern Turkey): Implications for OIB-type magma generation following slab break-off. *Geological Magazine*, *144*(5), 849–866. https://doi.org/10.1017/S0016756807003573

Çelik, Ö. F., Delaloye, M., & Feraud, G. (2006). Precise ^{40}Ar-^{39}Ar ages from the metamorphic sole rocks of the Tauride Belt Ophiolites, southern Turkey: Implications for the rapid cooling history. *Geological Magazine*, *143*(2), 213–227. https://doi.org/10.1017/S0016756805001524

Çelik, Ö. F., Marzoli, A., Marschik, R., Chiaradia, M., Neubauer, F., & Öz, İ. (2011). Early-middle Jurassic intra-oceanic subduction in the İzmir-Ankara-Erzincan Ocean, northern Turkey. *Tectonophysics*, *509*(1–2), 120–134. https://doi.org/10.1016/j.tecto.2011.06.007

Chapman, J. B., Ducea, M. N., DeCelles, P. G., & Profeta, L. (2015). Tracking changes in crustal thickness during orogenic evolution with Sr/Y: An example from the North American Cordillera. *Geology*, *43*(10), 919–922. https://doi.org/10.1130/G36996.1

Chiaradia, M. (2015). Crustal thickness control on Sr/Y signatures of recent arc magmas: An Earth scale perspective. *Scientific Reports*, *5*, 8115. https://doi.org/10.1038/srep08115

Çinku, M. C., Ustaömer, T., Hirt, A. M., Hisarlı, Z. M., Heller, F., & Orbay, N. (2010). Southward migration of arc magmatism during latest Cretaceous associated with slab steepening, East Pontides, N Turkey: New paleomagnetic data from the Amasya region. *Physics of the Earth and Planetary Interiors*, *182*(1–2), 18–29. https://doi.org/10.1016/j.pepi.2010.06.003

Cloetingh, S. A. P. L., Spadini, G., Van Wees, J. D., & Beekman, F. (2003). Thermo-mechanical modelling of Black Sea Basin (de) formation. *Sedimentary Geology*, *156*(1–4), 169–184. https://doi.org/10.1016/S0037-0738(02)00287-7

Çoban, H. (1997). Olucak (Gumushane) ve dolayinin jeolojisi, petrografisi ve jeokimyasi (Doctoral dissertation). Isparta, Turkey: SD Ü. Fen Bilimleri Enstitüsü.

Condie, K. C. (1989). Geochemical changes in baslts and andesites across the Archean-Proterozoic boundary: Identification and significance. *Lithos*, *23*(1–2), 1–18. https://doi.org/10.1016/0024-4937(89)90020-0

Cowgill, E., Forte, A. M., Niemi, N., Avdeev, B., Tye, A., Trexler, C., et al. (2016). Relict basin closure and crustal shortening budgets during continental collision: An example from Caucasus sediment provenance. *Tectonics*, *35*, 2918–2947. https://doi.org/10.1002/2016TC004295

Danelian, T., Asatryan, G., Galoyan, G., Sosson, M., Sahakyan, L., Caridroit, M., & Avagyan, A. (2012). Geological history of ophiolites in the Lesser Caucasus and correlation with the Izmir-Ankara-Erzincan suture zone: Insights from Radiolarian biochronology. *Bulletin de la Société géologique de France*, *183*(4), 331–342. http://doi.org/10.2113/gssgfbull.183.4.331

Danelian, T., Asatryan, G., Sahakyan, L., Galoyan, G. H., Sosson, M., & Avagyan, A. (2010). New and revised Radiolarian biochronology for the sedimentary cover of ophiolites in the Lesser Caucasus (Armenia). *Geological Society, London, Special Publications*, *340*(1), 383–391. https://doi.org/10.1144/SP340.16

Danelian, T., Asatryan, G., Sosson, M., Person, A., Sahakyan, L., & Galoyan, G. (2008). Discovery of Middle Jurassic (Bajocian) Radiolaria from the sedimentary cover of the Vedi ophiolite (Lesser Caucasus, Armenia). *Comptes Rendus Palevol*, *7*(6), 327–334. https://doi.org/10.1016/j.crpv.2008.05.001

Danelian, T., Galoyan, G., Rolland, Y., & Sosson, M. (2007). Palaeontological (Radiolarian) Late Jurassic age constraint for the Stepanavan ophiolite (lesser Caucasus, Armenia). *Bulletin of the Geological Society of Greece*, *40*(1), 31–38. https://doi.org/10.12681/bgsg.16332

Danelian, T., Zambetakis-Lekkas, A., Galoyan, G., Sosson, M., Asatryan, G., Hubert, B., & Grigoryan, A. (2014). Reconstructing Upper Cretaceous (Cenomanian) paleoenvironments in Armenia based on Radiolaria and benthic Foraminifera; Implications for the geodynamic evolution of the Tethyan realm in the Lesser Caucasus. *Palaeogeography, Palaeoclimatology, Palaeoecology*, *413*, 123–132. https://doi.org/10.1016/j.palaeo.2014.03.011

Delibaş, O., Moritz, R., Ulianov, A., Chiaradia, M., Saraç, C., Revan, K. M., & Göç, D. (2016). Cretaceous subduction-related magmatism and associated porphyry-type Cu-Mo prospects in the Eastern Pontides, Turkey: New constraints from geochronology and geochemistry. *Lithos*, *248–251*, 119–137. https://doi.org/10.1016/j.lithos.2016.01.020

Dercourt, J., Gaetani, M., & Vrielynck, B. (Eds.) (2000). Atlas Peri-Tethys, palaeogeographical maps. In: CCGM/CGMW, Paris: 24 Maps and Explanatory Notes: I-XX, pp. 1-269.

Dercourt, J., Ricou, L. E., & Vrielynck, B. (1993). *Atlas Tethys paleoenvironmental maps*. Paris, France: Gauthier-Villars.

Dercourt, J., Zonenshain, L. P., Ricou, L. E., Kazmin, V. G., Le Pichon, X., Knipper, A. L., et al. (1986). Geological evolution of the Tethys belt from the Atlantic to the Pamirs since the Lias. *Tectonophysics*, *123*(1–4), 241–315. https://doi.org/10.1016/0040-1951(86)90199-X

Dokuz, A. (2011). A slab detachment and delamination model for the generation of Carboniferous high-potassium I-type magmatism in the Eastern Pontides, NE Turkey: The Köse composite pluton. *Gondwana Research*, *19*(4), 926–944. https://doi.org/10.1016/j.gr.2010.09.006

Dokuz, A., Aydin, F., & Karslı, O. (2019). Postcollisional transition from subduction-to intraplate-type magmatism in the eastern Sakarya zone, Turkey: Indicators of northern Neotethyan slab breakoff. *GSA Bulletin*, *131*(9–10), 1623–1642. https://doi.org/10.1130/B31993.1

Dokuz, A., Karsli, O., Chen, B., & Uysal, İ. (2010). Sources and petrogenesis of Jurassic granitoids in the Yusufeli area, Northeastern Turkey: Implications for pre-and post-collisional lithospheric thinning of the eastern Pontides. *Tectonophysics*, *480*(1–4), 259–279. https://doi.org/10.1016/j.tecto.2009.10.009

Dokuz, A., Tanyolu, E., & Genç, S. (2006). A mantle-and a lower crust-derived bimodal suite in the Yusufeli (Artvin) area, NE Turkey: Trace element and REE evidence for subduction-related rift origin of Early Jurassic Demirkent intrusive complex. *International Journal of Earth Sciences*, *95*(3), 370–394. https://doi.org/10.1007/s00531-005-0046-6

Dokuz, A., Uysal, İ., Dilek, Y., Karsli, O., Meisel, T., & Kandemir, R. (2015). Geochemistry, Re-Os isotopes and highly siderophile element abundances in the Eastern Pontide peridotites (NE Turkey): Multiple episodes of melt extraction-depletion, melt-rock interaction and fertilization of the Rheic Ocean mantle. *Gondwana Research*, *27*(2), 612–628. https://doi.org/10.1016/j.gr.2013.12.010

Dotduyev, S. I. (1987). Nappe structure of the Greater Caucasus range. *Geotectonics*, *20*(5), 420–430.

Dotduyev, S. I. (1989). Meso-cenozoic geodynamics in the Great Caucasus. In *Geodynamics of Caucasus* (pp. 82–92). Moscow: Nauka.

Eyüboğlu, Y. (2010). Late Cretaceous high-K volcanism in the eastern Pontide orogenic belt: Implications for the geodynamic evolution of NE Turkey. *International Geology Review*, *52*(2–3), 142–186. https://doi.org/10.1080/00206810902757164

Eyüboğlu, Y. (2015). Petrogenesis and U-Pb zircon chronology of felsic tuffs interbedded with turbidites (Eastern Pontides Orogenic Belt, NE Turkey): Implications for Mesozoic geodynamic evolution of the eastern Mediterranean region and accumulation rates of turbidite sequences. *Lithos*, *212*, 74–92. https://doi.org/10.1016/j.lithos.2014.11.006

Eyüboğlu, Y., Bektas, O., & Pul, D. (2007). Mid-Cretaceous olistostromal ophiolitic melange developed in the back-arc basin of the eastern Pontide magmatic arc, northeast Turkey. *International Geology Review*, *49*(12), 1103–1126. https://doi.org/10.2747/0020-6814.49.12.1103

Eyüboğlu, Y., Dudas, F. O., Chatterjee, N., Liu, Z., & Yılmaz-Değerli, S. (2018). Discovery of Latest Cretaceous OIB-type alkaline gabbros in the Eastern Pontides Orogenic Belt, NE Turkey: Evidence for tectonic emplacement of seamounts. *Lithos*, *310*, 182–200. https://doi.org/10.1016/j.lithos.2018.04.013

Eyüboğlu, Y., Dudas, F. O., Santosh, M., Yi, K., Kwon, S., & Akaryali, E. (2013). Petrogenesis and U-Pb zircon chronology of adakitic porphyries within the Kop ultramafic massif (Eastern Pontides Orogenic Belt, NE Turkey). *Gondwana Research*, *24*(2), 742–766. https://doi.org/10.1016/j.gr.2012.11.014

Eyüboğlu, Y., Dudas, F. O., Thorkelson, D., Zhu, D. C., Liu, Z., Chatterjee, N., et al. (2017). Eocene granitoids of northern Turkey: Polybaric magmatism in an evolving arc-slab window system. *Gondwana Research*, *50*, 311–345. https://doi.org/10.1016/j.gr.2017.05.008

Eyüboğlu, Y., Dudas, F. O., Zhu, D. C., Liu, Z., & Chatterjee, N. (2019). Late Cretaceous I-and A-type magmas in eastern Turkey: Magmatic response to double-sided subduction of Paleo-and Neo-Tethyan lithospheres. *Lithos*, *326*, 39–70. https://doi.org/10.1016/j.lithos.2018.12.017

Eyüboğlu, Y., Santosh, M., & Chung, S. L. (2011). Crystal fractionation of adakitic magmas in the crust-mantle transition zone: Petrology, geochemistry and U-Pb zircon chronology of the Seme adakites, Eastern Pontides, NE Turkey. *Lithos*, *121*(1–4), 151–166. https://doi.org/10.1016/j.lithos.2010.10.012

Eyüboğlu, Y., Santosh, M., Dudas, F. O., Chung, S. L., & Akaryalı, E. (2011). Migrating magmatism in a continental arc: Geodynamics of the Eastern Mediterranean revisited. *Journal of Geodynamics*, *52*(1), 2–15. https://doi.org/10.1016/j.jog.2010.11.006

Eyüboğlu, Y., Santosh, M., Yi, K., Tüysüz, N., Korkmaz, S., Akaryali, E., et al. (2014). The Eastern Black Sea-type volcanogenic massive sulfide deposits: Geochemistry, zircon U-Pb geochronology and an overview of the geodynamics of ore genesis. *Ore Geology Reviews*, *59*, 29–54. https://doi.org/10.1016/j.oregeorev.2013.11.009

Finetti, I. (1988). Geophysical study of the Black Sea area. *Bollettino di Geofisica Teorica ed Applicata*, *30*(117), 197–324.

Forte, A. M., Cowgill, E., Bernardin, T., Kreylos, O., & Hamann, B. (2010). Late Cenozoic deformation of the Kura fold-thrust belt, southern Greater Caucasus. *Bulletin*, *122*(3–4), 465–486. https://doi.org/10.1130/B26464.1

Forte, A. M., Cowgill, E., Murtuzayev, I., Kangarli, T., & Stoica, M. (2013). Structural geometries and magnitude of shortening in the eastern Kura fold-thrust belt, Azerbaijan: Implications for the development of the Greater Caucasus Mountains. *Tectonics*, *32*, 688–717. https://doi.org/10.1002/tect.20032

Forte, A. M., Cowgill, E., & Whipple, K. X. (2014). Transition from a singly vergent to doubly vergent wedge in a young orogen: The Greater Caucasus. *Tectonics*, *33*, 2077–2101. https://doi.org/10.1002/2014TC003651

Galoyan, G. (2008). Etudes pétrologiques, géochimiques et géochronologiques des ophiolites du Petit Caucase (Arménie) (Doctoral dissertation). Nice, France.

Galoyan, G., Melkonyan, R., Atayan, L., Chung, S. L., Khorenyan, R. H., Lee, Y. H., & Amiraghyan, S. V. (2018). On the petrology and geochemistry of Jurassic magmatics of the somkheti segment of Somkheto-Karabagh tectonic zone (Northern Armenia). *Bulletin of NAS RA Earth Sciences*, *71*(1), 3–27.

Galoyan, G., Rolland, Y., Sosson, M., Corsini, M., Billo, S., Verati, C., & Melkonyan, R. (2009). Geology, geochemistry and $^{40}Ar/^{39}Ar$ dating of Sevan ophiolites (Lesser Caucasus, Armenia): Evidence for Jurassic Back-arc opening and hot spot event between the South Armenian Block and Eurasia. *Journal of Asian Earth Sciences*, *34*(2), 135–153. https://doi.org/10.1016/j.jseaes.2008.04.002

Gambashidze, R. A. (1974). Stratigraphy of the Upper Cretaceous deposits of Georgia and neighboring areas of Azerbaydzhan and Armenia (Doctoral dissertation). Tbilisi, Georgia.

Gamkrelidze, I. P. (1986). Geodynamic evolution of the Caucasus and adjacent areas in Alpine time. *Tectonophysics*, *127*(3–4), 261–277. https://doi.org/10.1016/0040-1951(86)90064-8

Gamkrelidze, I. P., & Shengelia, D. M. (2007). Pre-Alpine geodynamics of the Caucasus, suprasubduction regional metamorphism and granitoid magmatism. *Bulletin of the Georgian National Academy of Science*, *175*, 57–65.

Ghazaryan, H. A. (1971). *Main features of the magmatism of the Alaverdi ore district. Petrology of intrusive complexes of important ore districts of Armenian SSR* (pp. 7–116). Yerevan: Academy of Sciences of Armenian SSR.

Göğüş, O. H. (2015). Rifting and subsidence following lithospheric removal in continental back arcs. *Geology*, *43*(1), 3–6. https://doi.org/10.1130/G36305.1

Görür, N. (1988). Timing of opening of the Black Sea basin. *Tectonophysics*, *147*(3–4), 247–262. https://doi.org/10.1016/0040-1951(88)90189-8

Graham, R., Kaymakci, N., & Horn, B. W. (2013). The Black Sea: Something different. *Geo Expro*, *10*(5), 57–62.

Gudjabidze, G. E., & Gamkrelidze, I. P. (2003). Geological map of Georgia 1: 500 000. *Georgian State Department of Geology and National Oil Company "Saqnavtobi*.

Gugushvili, V., Bukia, A., Goderdzishvili, N., Javakhidze, D., Zakaraia, D., Muladze, I., et al. (2014). *Bolnisi ore district: Geological development and structure, genesis of mineralization, economic potential and perspectives according to data for April 2014*. Caucasus Mining Group, Tbilisi 55 p (in Russian).

Hässig, M., Rolland, Y., Melis, R., Sosson, M., Galoyan, G., & Bruguier, O. (2019). P-T-t history of the Amasia and Stepanavan sub-ophiolitic metamorphic units (NW Armenia, Lesser Caucasus): Implications for metamorphic sole development and for the obduction process. *Ofioliti*, *44*(1), 43–70. https://doi.org/10.4454/ofioliti.v44i1.464

Hässig, M., Rolland, Y., & Sosson, M. (2017). From seafloor spreading to obduction: Jurassic-Cretaceous evolution of the northern branch of the Neotethys in the Northeastern Anatolian and Lesser Caucasus regions. *Geological Society, London, Special Publications*, *428*(1), 41–60. https://doi.org/10.1144/SP428.10

Hässig, M., Rolland, Y., Sosson, M., Galoyan, G., Müller, C., Avagyan, A., & Sahakyan, L. (2013). New structural and petrological data on the Amasia ophiolites (NW Sevan-Akera suture zone, Lesser Caucasus): Insights for a large-scale obduction in Armenia and NE Turkey. *Tectonophysics*, *588*, 135–153. https://doi.org/10.1016/j.tecto.2012.12.003

Hässig, M., Rolland, Y., Sosson, M., Galoyan, G., Sahakyan, L., Topuz, G., et al. (2013). Linking the NE Anatolian and Lesser Caucasus ophiolites: Evidence for large-scale obduction of oceanic crust and implications for the formation of the Lesser Caucasus-Pontides Arc. *Geodinamica Acta*, *26*(3–4), 311–330. https://doi.org/10.1080/09853111.2013.877236

Hastie, A. R., Kerr, A. C., Pearce, J. A., & Mitchell, S. F. (2007). Classification of altered volcanic island arc rocks using immobile trace elements: Development of the Th-Co discrimination diagram. *Journal of Petrology*, *48*(12), 2341–2357. https://doi.org/10.1093/petrology/egm062

Hess, J. C., Aretz, J., Gurbanov, A. G., Emmermann, R., & Lippolt, H. J. (1995). Subduction-related Jurassic andesites in the northern Great Caucasus. *Geologische Rundschau*, *84*(2), 319–333. https://doi.org/10.1007/BF00260443

Hippolyte, J. C., Müller, C., Sangu, E., & Kaymakci, N. (2017). Stratigraphic comparisons along the Pontides (Turkey) based on new nannoplankton age determinations in the Eastern Pontides: Geodynamic implications. *Geological Society, London, Special Publications*, *428*(1), 323–358. https://doi.org/10.1144/SP428.9

Irvine, T. N. J., & Baragar, W. R. A. (1971). A guide to the chemical classification of the common volcanic rocks. *Canadian Journal of Earth Sciences*, *8*(5), 523–548. https://doi.org/10.1139/e71-055

Kandelaki, D. N., & Kakhazdze, I. R. (1957). *Geological map of the USSR, Caucasus series sheet K-38-XV, scale 1:200,000*. Moscow: Ministry of Geology and Mineral Protection USSR.

Kandemir, R. (2004). Gümüflhane ve Yakın Yörelerindeki Erken-Orta Jura Yafllı fienköy Formasyonunun Çökel Özellikleri ve Birikim Koflulları (Sedimentary Characteristics and Depositional Conditions of Lower-Middle Jurassic fienköy Formation in and around Gümüflhane) (Doctoral dissertation). Trabzon, Turkey: Karadeniz Technical University.

Kandemir, R., & Yılmaz, C. (2009). Lithostratigraphy, facies, and deposition environment of the lower Jurassic Ammonitico Rosso type sediments (ARTS) in the Gümüşhane area, NE Turkey: Implications for the opening of the northern branch of the Neo-Tethys Ocean. *Journal of Asian Earth Sciences*, *34*(4), 586–598. https://doi.org/10.1016/j.jseaes.2008.08.006

Karapetyan, A. I., Amiryan, S. H., Azizbekynam, S., Altunyan, A. Z., Melkonyan, R. L., Guyumjyan, H. P., et al. (1982). Predicting metallogenic map of the Alaverdi-Shamlugh-Akhtala ore junction. *National Academy of Sciences of Armenian SSR, Institute of Geological Sciences*.

Karig, D. E. (1972). Remnant arcs. *Geological Society of America Bulletin*, *83*(4), 1057–1068. https://doi.org/10.1130/0016-7606(1972)83[1057:ra]2.0.co;2

Karsli, O., Caran, Ş., Dokuz, A., Çoban, H., Chen, B., & Kandemir, R. (2012). A-type granitoids from the Eastern Pontides, NE Turkey: Records for generation of hybrid A-type rocks in a subduction-related environment. *Tectonophysics*, *530*, 208–224. https://doi.org/10.1016/j.tecto.2011.12.030

Karsli, O., Chen, B., Aydin, F., & Şen, C. (2007). Geochemical and Sr-Nd-Pb isotopic compositions of the Eocene Dölek and Sariçiçek Plutons, Eastern Turkey: Implications for magma interaction in the genesis of high-K calc-alkaline granitoids in a post-collision extensional setting. *Lithos*, *98*(1–4), 67–96. https://doi.org/10.1016/j.lithos.2007.03.005

Karsli, O., Dokuz, A., Uysal, I., Aydin, F., Chen, B., Kandemir, R., & Wijbrans, J. (2010). Relative contributions of crust and mantle to generation of Campanian high-K calc-alkaline I-type granitoids in a subduction setting, with special reference to the Harşit Pluton, Eastern Turkey. *Contributions to Mineralogy and Petrology*, *160*(4), 467–487. https://doi.org/10.1007/s00410-010-0489-z

Karsli, O., Ketenci, M., Uysal, İ., Dokuz, A., Aydin, F., Chen, B., et al. (2011). Adakite-like granitoid porphyries in the Eastern Pontides, NE Turkey: Potential parental melts and geodynamic implications. *Lithos*, *127*(1–2), 354–372. https://doi.org/10.1016/j.lithos.2011.08.014

Kaygusuz, A., Arslan, M., Siebel, W., Sipahi, F., İlbeyli, N., & Temizel, İ. (2014). LA-ICP MS zircon dating, whole-rock and Sr-Nd-Pb-O isotope geochemistry of the Camiboğazı pluton, Eastern Pontides, NE Turkey: Implications for lithospheric mantle and lower crustal sources in arc-related I-type magmatism. *Lithos*, *192*, 271–290. https://doi.org/10.1016/j.lithos.2014.02.014

Kaygusuz, A., & Aydinçakir, E. (2011). Petrogenesis of a Late Cretaceous composite pluton from the eastern Pontides: The Dağbaşi pluton, NE Turkey. *Neues Jahrbuch für Mineralogie-Abhandlungen: Journal of Mineralogy and Geochemistry*, *188*(3), 211–233. https://doi.org/10.1127/0077-7757/2011/0201

Kaygusuz, A., Chen, B., Aslan, Z., Siebel, W., & Şen, C. (2009). U-Pb zircon SHRIMP ages, geochemical and Sr-Nd isotopic compositions of the Early Cretaceous I-type Sarıosman pluton, Eastern Pontides, NE Turkey. *Turkish Journal of Earth Sciences*, *18*(4), 549–581. https://doi.org/10.3906/yer-0806-1

Kaygusuz, A., & Öztürk, M. (2015). Geochronology, geochemistry, and petrogenesis of the Eocene Bayburt intrusions, Eastern Pontides, NE Turkey: Evidence for lithospheric mantle and lower crustal sources in the high-K calc-alkaline magmatism. *Journal of Asian Earth Sciences*, *108*, 97–116. https://doi.org/10.1016/j.jseaes.2015.04.017

Kaygusuz, A., & Şen, C. (2011). Calc-alkaline I-type plutons in the eastern Pontides, NE Turkey: U-Pb zircon ages, geochemical and Sr-Nd isotopic compositions. *Chemie der Erde-Geochemistry*, *71*(1), 59–75. https://doi.org/10.1016/j.chemer.2010.07.005

Kaygusuz, A., Siebel, W., Ilbeyli, N., Arslan, M., Satır, M., & Şen, C. (2010). Insight into magma genesis at convergent plate margins—A case study from the eastern Pontides (NE Turkey). *Neues Jahrbuch für Mineralogie-Abhandlungen: Journal of Mineralogy and Geochemistry*, *187*(3), 265–287. https://doi.org/10.1127/0077-7757/2010/0178

Kaygusuz, A., Sipahi, F., Ilbeyli, N., Arslan, M., Chen, B., & Aydınçakır, E. (2013). Petrogenesis of the Late Cretaceous Turnagöl intrusion in the eastern Pontides: Implications for magma genesis in the arc setting. *Geoscience Frontiers*, *4*(4), 423–438. https://doi.org/10.1016/j.gsf.2012.09.003

Khain, V. E. (1975). Structure and main stages in the tectono-magmatic development of the Caucasus: An attempt at geodynamic interpretation. *American Journal of Science*, *275-A*, 131–156.

Khain, V. E. (1984). *Regional geotectonics*. Moscow: The Alpine-Mediterranean Belt, Nedra. (in Russian).

Khain, V. E. (1997). Azerbaijan-Greater Caucasus. In *Encyclopedia of European and Asian regional geology* (pp. 60–63). London: Chapman and Hall.

Khriachtchevskaia, O., Stovba, S., & Stephenson, R. (2010). Cretaceous-Neogene tectonic evolution of the northern margin of the Black Sea from seismic reflection data and tectonic subsidence analysis. *Geological Society, London, Special Publications*, *340*(1), 137–157. https://doi.org/10.1144/SP340.8

Kim, H. J., Lee, G. H., Choi, D. L., Jou, H. T., Li, Z., Zheng, Y., et al. (2015). Back-arc rifting in the Korea Plateau in the East Sea (Japan Sea) and the separation of the southwestern Japan Arc from the Korean margin. *Tectonophysics*, *638*, 147–157. https://doi.org/10.1016/j.tecto.2014.11.003

Knipper, A. L. (1975). The oceanic crust in the structure of the Alpine Folded Belt (South Europe, western part of Asia and Cuba). Tr. GIN NAS USSR, 267, 207 (in Russian).

Lebedev, A. P., & Malkhasyan, E. G. (1965). *Jurassic volcanism of Armenia* (p. 167). Moscow: Nauka. (in Russian).

Letouzey, J., Biju-Duval, B., Dorkel, A., Gonnard, R., Kristchev, K., Montadert, L., & Sungurlu, O. (1977). The Black Sea: A marginal basin; geophysical and geological data. In *International Symposium on the Structural History of the Mediterranean Basins 1977 Oct 25* (pp. 363–376). Paris, France: Editions Technip Paris.

Liu, Z., Zhu, D. C., Wang, Q., Eyüboğlu, Y., Zhao, Z. D., Liu, S. A., & Xu, L. J. (2018). Transition from low-K to high-K calc-alkaline magmatism at approximately 84 Ma in the Eastern Pontides (NE Turkey): Magmatic response to slab rollback of the Black Sea. *Journal of Geophysical Research: Solid Earth*, *123*, 7604–7628. https://doi.org/10.1029/2018JB016026

Lordkipanidze, M., Meliksetian, B., & Djerbashian, R. (1988). Mesozoic-Cenozoic magmatic evolution of the Pontian Crimean-Caucasus region. *Mémoire de la Société Géologique de France*, *154*, 103–124.

Maghakyan, R., Zakariadze, G., Dmitriev, L., Kolesov, G., & Korovina, M. (1985). Geochemistry of the Jurassic-Lower cretaceous volcanic assemblage of northern Armenia. *Volcanology and Seismology*, *3*, 39–53.

Mamani, M., Wörner, G., & Sempere, T. (2010). Geochemical variations in igneous rocks of the central Andean orocline (13°S–18°S): Tracing crustal thickening andmagma generation through time and space. *Geological Society of America Bulletin*, *122*(1–2), 162–182. https://doi.org/10.1130/B26538.1

Mauvilly, J., Mosar, J., Koiava, K., Gamkrelidze, I., Enna, N., Lavrishev, V., & Kalberguenova, V. (2018). Tectonics in the Greater Caucasus (Georgia-Russia): From an intracontinental rifted basin to a doubly verging fold-and-thrust belt. In *EGU General Assembly Conference Abstracts* (Vol. 20, p. 4920).

McCann, T., Chalot-Prat, F., & Saintot, A. (2010). The Early Mesozoic evolution of the Western Greater Caucasus (Russia): Triassic-Jurassic sedimentary and magmatic history. *Geological Society, London, Special Publications*, *340*(1), 181–238. https://doi.org/10.1144/SP340.10

Mederer, J., Moritz, R., Ulianov, A., & Chiaradia, M. (2013). Middle Jurassic to Cenozoic evolution of arc magmatism during Neotethys subduction and arc-continent collision in the Kapan Zone, southern Armenia. *Lithos*, *177*, 61–78. https://doi.org/10.1016/j.lithos.2013.06.005

Mederer, J., Moritz, R., Zohrabyan, S., Vardanyan, A., Melkonyan, R., & Ulianov, A. (2014). Base and precious metal mineralization in Middle Jurassic rocks of the Lesser Caucasus: A review of geology and metallogeny and new data from the Kapan, Alaverdi and Mehmana districts. *Ore Geology Reviews*, *58*, 185–207. https://doi.org/10.1016/j.oregeorev.2013.10.007

Meijers, M. J., Smith, B., Kirscher, U., Mensink, M., Sosson, M., Rolland, Y., et al. (2015). A paleolatitude reconstruction of the South Armenian Block (Lesser Caucasus) for the Late Cretaceous: Constraints on the Tethyan realm. *Tectonophysics*, *644*, 197–219. https://doi.org/10.1016/j.tecto.2015.01.012

Melkonyan, R. L. (1976). Petrology, mineralogy and geochemistry of intrusive complexes of the Alaverdi ore field. In *Petrology and geochemistry of some intrusive complexes of the Armenian SSR* (pp. 138–270). Yerevan: Academy of Sciences of the Armenian SSR. (in Russian).

Melkonyan, R. L., & Ghoukassyan, R. H. (2004). On the problem of the age of the KSh intrusive complex. Izvestiya Akademii Nauk Armyanskoi SSR, Nauki O Zemle. *Proceedings of the National Academy of Sciences, Armenian SSR, Earth Sciences*, *1*, 29–35.

Melkonyan, R. L., Moritz, R., Tayan, R. N., Selby, D., Ghoukassyan, R. K., & Hovakimyan, S. E. (2014). Main copper-porphyry systems of Lesser Caucasus. *Izvestia NAN RA, Nauki o Zemle*, *67*(1), 3–29. (in Russian).

Menant, A., Sternai, P., Jolivet, L., Guillou-Frottier, L., & Gerya, T. (2016). 3D numerical modeling of mantle flow, crustal dynamics and magma genesis associated with slab roll-back and tearing: The eastern Mediterranean case. *Earth and Planetary Science Letters*, *442*, 93–107. https://doi.org/10.1016/j.epsl.2016.03.002

Milanovsky, E. E. (1991). *Geology of the USSR, Part* (Vol. 3, pp. 1–272). Moscow, Russia: Moscow University Press.

Milanovsky, E. E., & Khain, V. E. (1963). *Geological structure of the Caucasus. Essay of Regional Geology of the USSR*. Moscow: Moscow State University. in Russian

Milanovsky, E. E., Koronovsky, N. V., Baranov, G. I., Skhirtladze, N. J., Mrevlishvili, N. J., & Alpaidze, V. S. (1984). The geological structure of the Mountain Crimea and Great Caucasus. In *Guidebook for Excursions on the Ukranian Soviet Socialist Republic Of International Geological Congress, 27th, Moscow* (pp. 33–80).

Moore, W. J., McKee, E. H., & Akıncı, Ö. (1980). Chemistry and geochronology of plutonic rocks in the Pontide mountains, Northern Turkey. *European Copper Deposits*, 209–216.

Moritz, R., Melkonyan, R., Selby, D., Popkhadze, N., Gugushvili, V., Tayan, R., & Ramazanov, V. (2016). Metallogeny of the Lesser Caucasus: From arc construction to post-collision evolution. *Special publications of the Society of Economic Geologists*, *19*, 157–192.

Moritz, R., Rezeau, H., Ovtcharova, M., Tayan, R., Melkonyan, R., Hovamkimyan, S., et al. (2016). Long-lived, stationary magmatism and pulsed porphyry systems during Tethyan subduction to post-collision evolution in the southernmost Lesser Caucasus, Armenia and Nakhitchevan. *Gondwana Research*, *37*, 465–503.

Mosar, J., Kangarli, T., Bochud, M., Glasmacher, U. A., Rast, A., Brunet, M. F., & Sosson, M. (2010). Cenozoic-Recent tectonics and uplift in the Greater Caucasus: A perspective from Azerbaijan. *Geological Society, London, Special Publications*, *340*(1), 261–280. https://doi.org/10.1144/SP340.12

Muratov, M. V., Arkhipov, I. V., & Uspenskaya, Y. A. (1984). Structural evolution of the Crimean Mountains and comparison with the western Caucasus and the eastern Balkan ranges. *International Geology Review*, *26*(11), 1259–1266. https://doi.org/10.1080/00206818409466646

Nalivkin, D. V. (1973). Geology of the USSR.

Nalivkin, V. D. (1976). Dynamics of the development of the Russian platform structures. *Developments in Geotectonics*, *12*, 247–262.

Nikishin, A. M., Alekseev, A. S., Baraboshkin, E. J., Kopaevich, L. F., Gabdullin, R. R., & Badulina, N. V. (2008). The Cretaceous history of the Bakhchisaray area, southern Crimea (Ukraine). *Bulletin de l'Institut Royal des Sciences Naturelles de Belgique: Sciences de la Terre*, *78*, 75–85.

Nikishin, A. M., Cloetingh, S. A. P. L., Bolotov, S. N., Baraboshkin, E. Y., Kopaevich, L. F., Nazarevich, B. P., et al. (1998). Scythian platform: Chronostratigraphy and polyphase stages of tectonic history. *Mémoires du Muséum national d'histoire naturelle (1993)*, *177*, 151–162.

Nikishin, A. M., Cloetingh, S. A. P. L., Brunet, M. -F., Stephenson, R. A., Bolotov, S. N., & Ershov, A. V. (1998). Scythian platform, Caucasus and Black Sea region: Mesozoic-Cenozoic tectonic history and dynamics. *Peri-Tethys Memoir*, *3*, 163–176.

Nikishin, A. M., Ershov, A. V., & Nikishin, V. A. (2010). Geological history of western Caucasus and adjacent foredeeps based on analysis of the regional balanced section. *Doklady Earth Sciences*, *430*(2), 155–157. https://doi.org/10.1134/S1028334X10020017

Nikishin, A. M., Korotaev, M. V., Ershov, A. V., & Brunet, M. F. (2003). The Black Sea basin: Tectonic history and Neogene-Quaternary rapid subsidence modelling. *Sedimentary Geology*, *156*(1–4), 149–168. https://doi.org/10.1016/S0037-0738(02)00286-5

Nikishin, A. M., Okay, A., Tüysüz, O., Demirer, A., Wannier, M., Amelin, N., & Petrov, E. (2015b). The Black Sea basins structure and history: New model based on new deep penetration regional seismic data. Part 2: Tectonic history and paleogeography. *Marine and Petroleum Geology*, *59*, 656–670. https://doi.org/10.1016/j.marpetgeo.2014.08.018

Nikishin, A. M., Okay, A. I., Tüysüz, O., Demirer, A., Amelin, N., & Petrov, E. (2015a). The Black Sea basins structure and history: New model based on new deep penetration regional seismic data. Part 1: Basins structure and fill. *Marine and Petroleum Geology*, *59*, 638–655. https://doi.org/10.1016/j.marpetgeo.2014.08.017

Nikishin, A. M., Ziegler, P. A., Bolotov, S. N., Mazarevich, B. P., Panov, D. I., Brunet, M. -F., et al. (2001). Mesozoic and Cenozoic evolution of the Scythian platform-Black Sea-Caucasus domain. *Mémoires du Muséum national d'histoire naturelle*, *186*, 295–346.

Nzegge, O. M., Satir, M., Siebel, W., & Taubald, H. (2006). Geochemical and isotopic constraints on the genesis of the Late Palaeozoic Deliktaş and Sivrikaya granites from the Kastamonu granitoid belt (Central Pontides, Turkey). *Neues Jahrbuch für Mineralogie-Abhandlungen: Journal of Mineralogy and Geochemistry*, *183*(1), 27–40. https://doi.org/10.1127/0077-7757/2006/0057

Okay, A. I. (1997). Jadeite-K-feldspar rocks and jadeitites from northwest Turkey. *Mineralogical Magazine*, *61*(409), 835–843. https://doi.org/10.1180/minmag.1997.061.409.06

Okay, A. I., & Nikishin, A. M. (2015). Tectonic evolution of the southern margin of Laurasia in the Black Sea region. *International Geology Review*, *57*(5–8), 1051–1076. https://doi.org/10.1080/00206814.2015.1010609

Okay, A. I., & Şahintürk, Ö. (1997). Geology of the eastern Pontides. *Regional and Petroleum Geology of the Black Sea and Surrounding Region: American Association of Petroleum Geologists Memoir*, *68*, 291–311. https://doi.org/10.1306/M68612C15

Okay, A. I., Şahintürk, Ö., & Yakar, H. (1997). Stratigraphy and tectonics of the Pulur (Bayburt) region in the eastern Pontides. *Mineral Research and Exploration Bulletin*, *119*, 1–24.

Okay, A. I., Şengör, A. M. C., & Görür, N. (1994). Kinematic history of the opening of the Black Sea and its effect on the surrounding regions. *Geology*, *22*(3), 267–270. https://doi.org/10.1130/0091-7613(1994)022<0267:KHOTOO>2.3.CO;2

Okay, A. I., Sunal, G., Sherlock, S., Alt, D., Tüysüz, O., Kylander-Clark, A. R., & Aygül, M. (2013). Early Cretaceous sedimentation and orogeny on the active margin of Eurasia: Southern Central Pontides, Turkey. *Tectonics*, *32*, 1247–1271. https://doi.org/10.1002/tect.20077

Okay, A. I., Tansel, I., & Tüysüz, O. (2001). Obduction, subduction and collision as reflected in the Upper Cretaceous-Lower Eocene sedimentary record of western Turkey. *Geological Magazine*, *138*(2), 117–142. https://doi.org/10.1017/S0016756801005088

Okay, A. I., & Tüysüz, O. (1999). Tethyan sutures of northern Turkey. *Geological Society, London, Special Publications*, *156*(1), 475–515. https://doi.org/10.1144/GSL.SP.1999.156.01.22

Okay, A. I., Tüysüz, O., Satır, M., Ozkan-Altiner, S., Altiner, D., Sherlock, S., & Eren, R. H. (2006). Cretaceous and Triassic subduction-accretion, high-pressure-low-temperature metamorphism, and continental growth in the Central Pontides, Turkey. *Geological Society of America Bulletin*, *118*(9–10), 1247–1269. https://doi.org/10.1130/B25938.1

Parlak, O., Çolakoğlu, A., Dönmez, C., Sayak, H., Yildirim, N., Türkel, A., & Odabaşi, İ. (2012). Geochemistry and tectonic significance of ophiolites along the İzmir-Ankara-Erzincan Suture Zone in northeastern Anatolia. *Geological Society, London, Special Publications*, *372*(1), 75–105. https://doi.org/10.1144/SP372.7

Parlak, O., & Delaloye, M. (1999). Precise $^{40}Ar/^{39}Ar$ ages from the metamorphic sole of the Mersin ophiolite (southern Turkey). *Tectonophysics*, *301*(1–2), 145–158. https://doi.org/10.1016/S0040-1951(98)00222-4

Pearce, J. A. (1982). Trace element characteristics of lavas from destructive plate boundaries. *Andesites*, *8*, 525–548.

Pearce, J. A. (1983). The role of sub-continental lithosphere in magma genesis at destructive plate margins. In C. J. Hawkesworth, M. J. Norry (Eds.), *Continental basalts and mantle xenoliths* (pp. 230–249). Nantwich, Cheshire: Shiva Publications.

Pearce, J. A., Harris, N. B., & Tindle, A. G. (1984). Trace element discrimination diagrams for the tectonic interpretation of granitic rocks. *Journal of Petrology*, *25*(4), 956–983. https://doi.org/10.1093/petrology/25.4.956

Philip, H., Cisternas, A., Gvishiani, A., & Gorshkov, A. (1989). The Caucasus: An actual example of the initial stages of continental collision. *Tectonophysics*, *161*(1–2), 1–21. https://doi.org/10.1016/0040-1951(89)90297-7

Popkhadze, N., Moritz, R., & Gugushvili, V. (2014). Architecture of Upper Cretaceous rhyodacitic hyaloclastite at the polymetallic Madneuli deposit, Lesser Caucasus, Georgia. *Central European Journal of Geosciences*, *6*(3), 308–329. https://doi.org/10.2478/s13533-012-0182-z

Razvetaev, L. M. (1977). The Mountain Crimea and Northern Black Sea area. In *Faults and horizontal movements of mountain chain in the U.S.S.R.* (pp. 95–107). Moscow: Nauka.

Razvetaev, L. M. (1989). Shifts and alpine geodynamics inthe Caucasus region. In A. A. Belov, & M. A. Satian (Eds.), *Geodynamics of Caucasus* (pp. 106–113). Moscow: Nauka. (in Russian).

Rezeau, H., Moritz, R., Leuthold, J., Hovakimyan, S., Tayan, R., & Chiaradia, M. (2017). 30 Myr of Cenozoic magmatism along the Tethyan margin during Arabia-Eurasia accretionary orogenesis (Meghri-Ordubad pluton, southernmost Lesser Caucasus). *Lithos*, *288*, 108–124. https://doi.org/10.1016/j.lithos.2017.07.007

Rezeau, H., Moritz, R., Wotzlaw, J. F., Tayan, R., Melkonyan, R., Ulianov, A., et al. (2016). Temporal and genetic link between incremental pluton assembly and pulsed porphyry Cu-Mo formation in accretionary orogens. *Geology*, *44*(8), 627–630. https://doi.org/10.1130/G38088.1

Rice, S. P., Robertson, A. H., & Ustaömer, T. (2006). Late Cretaceous-Early Cenozoic tectonic evolution of the Eurasian active margin in the Central and Eastern Pontides, northern Turkey. *Geological Society, London, Special Publications*, *260*(1), 413–445. https://doi.org/10.1144/GSL.SP.2006.260.01.17

Rice, S. P., Robertson, A. H., Ustaömer, T., Inan, N., & Tasli, K. (2009). Late Cretaceous-Early Eocene tectonic development of the Tethyan suture zone in the Erzincan area, Eastern Pontides, Turkey. *Geological Magazine*, *146*(4), 567–590. https://doi.org/10.1017/S0016756809006360

Richards, J. P., & Kerrich, R. (2007). Adakite-like rocks: Their diverse origins and questionable role in metallogenesis. *Economic Geology*, *102*(4), 537–576. https://doi.org/10.2113/gsecongeo.102.4.537

Ricou, L. E., Dercourt, J., Geyssant, J., Grandjacquet, C., Lepvrier, C., & Biju-Duval, B. (1986). Geological constraints on the Alpine evolution of the Mediterranean Tethys. *Tectonophysics*, *123*(1–4), 83–122. https://doi.org/10.1016/0040-1951(86)90194-0

Robertson, A., Parlak, O., Ustaömer, T., Taslı, K., İnan, N., Dumitrica, P., & Karaoğlan, F. (2013). Subduction, ophiolite genesis and collision history of Tethys adjacent to the Eurasian continental margin: New evidence from the Eastern Pontides, Turkey. *Geodinamica Acta*, *26*(3–4), 230–293. https://doi.org/10.1080/09853111.2013.877240

Robertson, A. H. (2002). Overview of the genesis and emplacement of Mesozoic ophiolites in the Eastern Mediterranean Tethyan region. *Lithos*, *65*(1–2), 1–67. https://doi.org/10.1016/S0024-4937(02)00160-3

Robertson, A. H., Parlak, O., & Ustaömer, T. (2013). Late Palaeozoic-Early Cenozoic tectonic development of Southern Turkey and the easternmost Mediterranean region: Evidence from the inter-relations of continental and oceanic units. *Geological Society, London, Special Publications*, *372*(1), 9–48. https://doi.org/10.1144/SP372.22

Robertson, A. H. F., & Dixon, J. E. (1984). Introduction: Aspects of the geological evolution of the Eastern Mediterranean. *Geological Society, London, Special Publications*, *17*(1), 1–74. https://doi.org/10.1144/GSL.SP.1984.017.01.02

Robinson, A., Spadini, G., Cloetingh, S., & Rudat, J. (1995). Stratigraphic evolution of the Black Sea: Inferences from basin modelling. *Marine and Petroleum Geology*, *12*(8), 821–835. https://doi.org/10.1016/0264-8172(95)98850-5

Robinson, A. G., Banks, C. J., Rutherford, M. M., & Hirst, J. P. P. (1995). Stratigraphic and structural development of the Eastern Pontides, Turkey. *Journal of the Geological Society*, *152*(5), 861–872. https://doi.org/10.1144/gsjgs.152.5.0861

Robinson, A. G., & Kerusov, E. (1997). Stratigraphic and structural development of the Gulf of Odessa, Ukrainian Black Sea: Implications for petroleum explorations. *American Association of Petroleum Geologists Memoirs*, *68*, 369–380.

Robinson, A. G., Rudat, J. H., Banks, C. J., & Wiles, R. L. F. (1996). Petroleum geology of the Black Sea. *Marine and Petroleum Geology*, *13*(2), 195–223. https://doi.org/10.1016/0264-8172(95)00042-9

Rolland, Y., Billo, S., Corsini, M., Sosson, M., & Galoyan, G. (2009). Blueschists of the Amassia-Stepanavan suture zone (Armenia): linking Tethys subduction history from E-Turkey to W-Iran. *International Journal of Earth Sciences*, *98*(3), 533–550. https://doi.org/10.1007/s00531-007-0286-8

Rolland, Y., Galoyan, G., Bosch, D., Sosson, M., Corsini, M., Fornari, M., & Verati, C. (2009). Jurassic back-arc and Cretaceous hot-spot series In the Armenian ophiolites—Implications for the obduction process. *Lithos*, *112*(3–4), 163–187. https://doi.org/10.1016/j.lithos.2009.02.006

Rolland, Y., Galoyan, G., Sosson, M., Melkonyan, R., & Avagyan, A. (2010). The Armenian Ophiolite: Insights for Jurassic back-arc formation, Lower Cretaceous hot spot magmatism and Upper Cretaceous obduction over the South Armenian Block. *Geological Society, London, Special Publications*, *340*(1), 353–382. https://doi.org/10.1144/SP340.15

Rolland, Y., Hässig, M., Bosch, D., Meijers, M. J. M., Sosson, M., Bruguier, O., et al. (2016). A review of the plate convergence history of the East Anatolia-Transcaucasus region during the Variscan: Insights from the Georgian basement and its connection to the Eastern Pontides. *Journal of Geodynamics*, *96*, 131–145. https://doi.org/10.1016/j.jog.2016.03.003

Sadikhov, E. A., & Shatova, N. V. (2016). Geochemical characteristics and isotopic U-Pb dating of plagiogranite plutonic complex rocks from the Lok-Garabakh zone of the Lesser Caucasus (Azerbaijan) Region. *Geologiya i Metallogeniya*, *66*, 67–74. (In Russian).

Sadikhov, E. A., & Shatova, N. V. (2017). U-Pb dating (SHRIMP II) and geodynamic condition of intrusions of the gabbro-tonalite complexes of the Lok-Karabakh, Lesser Caucasus (Azerbaijan) Region. *Geologiya i Metallogeniya*, *69*, 49–60. (In Russian).

Saintot, A., & Angelier, J. (2002). Tectonic paleostress fields and structural evolution of the NW-Caucasus fold-and-thrust belt from Late Cretaceous to Quaternary. *Tectonophysics*, *357*(1–4), 1–31. https://doi.org/10.1016/S0040-1951(02)00360-8

Saintot, A., Brunet, M. F., Yakovlev, F., Sébrier, M., Stephenson, R., Ershov, A., et al. (2006). The Mesozoic-Cenozoic tectonic evolution of the Greater Caucasus. *Geological Society, London, Memoirs*, *32*(1), 277–289. https://doi.org/10.1144/GSL.MEM.2006.032.01.16

Sarıfakıoğlu, E., Dilek, Y., & Sevin, M. (2017). New synthesis of the Izmir-Ankara-Erzincan suture zone and the Ankara mélange in northern Anatolia based on new geochemical and geochronological constraints. *Geological Society of America Special Papers*, *525*, 613–675. https://doi.org/10.1130/2017.2525(19)

Sartori, R. (2003). The Tyrrhenian back-arc basin and subduction of the Ionian lithosphere. *Episodes*, *26*(3), 217–221. https://doi.org/10.18814/epiiugs/2003/v26i3/011

Sayıt, K., & Göncüoglu, M. C. (2013). Geodynamic evolution of the Karakaya Mélange Complex, Turkey: A review of geological and petrological constraints. *Journal of Geodynamics*, *65*, 56–65. https://doi.org/10.1016/j.jog.2012.04.009

Şen, C. (2007). Jurassic volcanism in the Eastern Pontides: Is it rift related or subduction related? *Turkish Journal of Earth Sciences*, *16*(4), 523–539.

Şen, C., Arslan, M., & Van, A. (1999). Geochemical and petrological characteristics of the Eastern Pontide Eocene (?) alkaline volcanic province, NE Turkey. *Turkish Journal of Earth Sciences*, *7*(3), 231–240.

Sengör, A. M. C. (1989). Cimmeride orogenic system and the tectonics of Eurasia. *Geological Society of America, Special Paper*, *195*, 1–82. https://doi.org/10.1130/SPE195-p1

Şengör, A. M. C., Özeren, S., Genç, T., & Zor, E. (2003). East Anatolian high plateau as a mantle-supported, north-south shortened domal structure. *Geophysical Research Letters*, *30*, 8045. https://doi.org/10.1029/2003GL017858

Şengör, A. M. C., & Yilmaz, Y. (1981). Tethyan evolution of Turkey: A plate tectonic approach. *Tectonophysics*, *75*(3–4), 181–241. https://doi.org/10.1016/0040-1951(81)90275-4

Shengelia, D. M., Tsutsunava, T. N., & Shubitidze, L. G. (2006). New data on structure, composition, and regional metamorphism of the Tsakhkunyats and Akhum-Asrikchai massifs, the lesser Caucasus. *Doklady Earth Sciences*, *409*(2), 900–904. https://doi.org/10.1134/S1028334X06060146

Sheremet, Y., Sosson, M., Muller, C., Gintov, O., Murovskaya, A., & Yegorova, T. (2017). Key problems of stratigraphy in the Eastern Crimea Peninsula: Some insights from new dating and structural data. *Geological Society, London, Special Publications*, *428*(1), 265–306. https://doi.org/10.1144/SP428.14

Shillington, D. J., White, N., Minshull, T. A., Edwards, G. R., Jones, S. M., Edwards, R. A., & Scott, C. L. (2008). Cenozoic evolution of the eastern Black Sea: A test of depth-dependent stretching models. *Earth and Planetary Science Letters*, *265*(3–4), 360–378. https://doi.org/10.1016/j.epsl.2007.10.033

Sholpo, V. N. (1993). Strucure of inversion anticlinoria in the core of the Greater Caucasus: An advection hypothesis. *Geotectonics*, *23*, 245–251.

Sipahi, F., Kaygusuz, A., Saydam Eker, Ç., Vural, A., & Akpınar, İ. (2018). Late Cretaceous arc igneous activity: The Eğrikar Monzogranite example. *International Geology Review*, *60*(3), 382–400. https://doi.org/10.1080/00206814.2017.1336120

Sokol, K., Halama, R., Meliksetian, K., Savov, I. P., & Sudo, M. (2018). Alkaline magmas in zones of continental convergence: The Tezhsar volcano-intrusive ring complex Armenia. *Lithos*, *320–321*, 172–119. https://doi.org/10.1016/j.lithos.2018.08.028

Somin, M. L. (2011). Pre-Jurassic basement of the Greater Caucasus: Brief overview. *Turkish Journal of Earth Sciences*, *20*(5), 545–610.

Sopko, P. F. (1961). *Geology of pyrite deposits in the Alaverdi Ore District* (Vol. 170). Yerevan: Academy of Sciences of the Armenian SSR.

Sosson, M., Rolland, Y., Müller, C., Danelian, T., Melkonyan, R., Kekelia, S., et al. (2010). Subductions, obduction and collision in the Lesser Caucasus (Armenia, Azerbaijan, Georgia), new insights. *Geological Society, London, Special Publications*, *340*(1), 329–352. https://doi.org/10.1144/SP340.14

Sosson, M., Stephenson, R., & Adamia, S. (2017). Tectonic evolution of the Eastern Black Sea and Caucasus: An introduction. *Geological Society, London, Special Publications*, *428*(1), 1–9. https://doi.org/10.1144/SP428.16

Sosson, M., Stephenson, R., Adamia, S., Avagyan, A., Kangarli, T., Starostenko, V., et al. (2018). The Meso-Cenozoic Tectonic evolution of Eastern Black Sea and Caucasus domain: State of the art and perspectives of research. EGU General Assembly Conference Abstracts, *20*, 15212.

Sosson, M., Stephenson, R., Sheremet, Y., Rolland, Y., Adamia, S., Melkonian, R., et al. (2016). The eastern Black Sea-Caucasus region during the Cretaceous: New evidence to constrain its tectonic evolution. *Comptes Rendus Geoscience*, *348*(1), 23–32. https://doi.org/10.1016/j.crte.2015.11.002

Spadini, G., Robinson, A., & Cloetingh, S. (1996). Western versus Eastern Black Sea tectonic evolution: Pre-rift lithospheric controls on basin formation. *Tectonophysics*, *266*(1–4), 139–154. https://doi.org/10.1016/S0040-1951(96)00187-4

Speranza, F., Minelli, L., Pignatelli, A., & Chiappini, M. (2012). The Ionian Sea: The oldest in situ ocean fragment of the world? *Journal of Geophysical Research*, *117*, B12101. http://doi.org/10.1029/2012JB009475

Sperner, B., Lorenz, F., Bonjer, K., Hettel, S., Müller, B., & Wenzel, F. (2001). Slab break-off-abrupt cut or gradual detachment? New insights from the Vrancea Region (SE Carpathians, Romania). *Terra Nova*, *13*(3), 172–179. https://doi.org/10.1046/j.1365-3121.2001.00335.x

Stampfli, G. M., Borel, G. D., Cavazza, W., Mosar, J., & Ziegler, P. A. (2001). The paleotectonic atlas of the Peritethyan domain-CD ROM.

Stephenson, R., & Schellart, W. P. (2010). The Black Sea back-arc basin: Insights to its origin from geodynamic models of modern analogues. *Geological Society, London, Special Publications*, *340*(1), 11–21. https://doi.org/10.1144/SP340.2

Streckeisen, A. (1976). To each plutonic rock its proper name. *Earth-science reviews*, *12*(1), 1–33. https://doi.org/10.1016/0012-8252(76)90052-0

Sun, S. S., & McDonough, W. F. (1989). Chemical and isotopic systematics of oceanic basalts: Implications for mantle composition and processes. *Geological Society, London, Special Publications*, *42*(1), 313–345. https://doi.org/10.1144/GSL.SP.1989.042.01.19

Sydorenko, G., Stephenson, R., Yegorova, T., Starostenko, V., Tolkunov, A., Janik, T., et al. (2017). Geological structure of the northern part of the Eastern Black Sea from regional seismic reflection data including the DOBRE-2 CDP profile. *Geological Society, London, Special Publications*, *428*(1), 307–321. https://doi.org/10.1144/SP428.15

Tokel, S. (1977). Eocene calc-alkaline andesites and geotectonism in the Eastern Black Sea region. *Geological Society of Turkey Bulletin*, *20*, 49–54.

Topuz, G., Altherr, R., Kalt, A., Satır, M., Werner, O., & Schwarz, W. H. (2004). Aluminous granulites from the Pulur complex, NE Turkey: A case of partial melting, efficient melt extraction and crystallisation. *Lithos*, *72*(3–4), 183–207. https://doi.org/10.1016/j.lithos.2003.10.002

Topuz, G., Altherr, R., Schwarz, W. H., Dokuz, A., & Meyer, H. P. (2007). Variscan amphibolite-facies rocks from the Kurtoğlu metamorphic complex (Gümüşhane area, Eastern Pontides, Turkey). *International Journal of Earth Sciences*, *96*(5), 861. https://doi.org/10.1007/s00531-006-0138-y

Topuz, G., Altherr, R., Schwarz, W. H., Siebel, W., Satır, M., & Dokuz, A. (2005). Post-collisional plutonism with adakite-like signatures: The Eocene Saraycık granodiorite (Eastern Pontides, Turkey). *Contributions to Mineralogy and Petrology*, *150*(4), 441–455. https://doi.org/10.1007/s00410-005-0022-y

Topuz, G., Göçmengil, G., Rolland, Y., Çelik, Ö. F., Zack, T., & Schmitt, A. K. (2013). Jurassic accretionary complex and ophiolite from northeast Turkey: No evidence for the Cimmerian continental ribbon. *Geology*, *41*(2), 255–258. https://doi.org/10.1130/G33577.1

Topuz, G., Okay, A. I., Altherr, R., Schwarz, W. H., Siebel, W., Zack, T., et al. (2011). Post-collisional adakite-like magmatism in the Ağvanis Massif and implications for the evolution of the Eocene magmatism in the Eastern Pontides (NE Turkey). *Lithos*, *125*(1–2), 131–150. https://doi.org/10.1016/j.lithos.2011.02.003

Ustaömer, T., & Robertson, A. H. (2010). Late Palaeozoic-Early Cenozoic tectonic development of the Eastern Pontides (Artvin area), Turkey: Stages of closure of Tethys along the southern margin of Eurasia. *Geological Society, London, Special Publications*, *340*(1), 281–327. https://doi.org/10.1144/SP340.13

Vincent, S. J., Allen, M. B., Ismail-Zadeh, A. D., Flecker, R., Foland, K. A., & Simmons, M. D. (2005). Insights from the Talysh of Azerbaijan into the Paleogene evolution of the South Caspian region. *Geological Society of America Bulletin*, *117*(11–12), 1513–1533. https://doi.org/10.1130/B25690.1

Vincent, S. J., Morton, A. C., Carter, A., Gibbs, S., & Barabadze, T. G. (2007). Oligocene uplift of the Western Greater Caucasus: An effect of initial Arabia-Eurasia collision. *Terra Nova*, *19*(2), 160–166. https://doi.org/10.1111/j.1365-3121.2007.00731.x

Wright, I. C. (1997). Morphology and evolution of the remnant Colville and active Kermadec arc ridges south of 33°30′S. *Marine Geophysical Researches*, *19*(2), 177–193. https://doi.org/10.1023/A:1004266932113

Wright, I. C., Parson, L. M., & Gamble, J. A. (1996). Evolution and interaction of migrating cross-arc volcanism and backarc rifting: An example from the southern Havre Trough (35°20′–37°S). *Journal of Geophysical Research*, *101*(B10), 22,071–22,086. https://doi.org/10.1029/96JB01761

Yegorova, T., & Gobarenko, V. (2010). Structure of the Earth's crust and upper mantle of the West-and East-Black Sea Basins revealed from geophysical data and its tectonic implications. *Geological Society, London, Special Publications*, *340*(1), 23–42. https://doi.org/10.1144/SP340.3

Yilmaz, S., & Boztuğ, D. (1996). Space and time relations of three plutonic phases in the Eastern Pontides, Turkey. *International Geology Review*, *38*(10), 935–956. https://doi.org/10.1080/00206819709465373

Yilmaz-Sahin, S. (2005). Transition from arc-to post-collision extensional setting revealed by K-Ar dating and petrology: An example from the granitoids of the Eastern Pontide Igneous Terrane, Araklı-Trabzon, NE Turkey. *Geological Journal*, *40*(4), 425–440. https://doi.org/10.1002/gj.1020

Zakariadze, G. S., Dilek, Y., Adamia, S. A., Oberhänsli, R. E., Karpenko, S. F., Bazylev, B. A., & Solov'eva, N. (2007). Geochemistry and geochronology of the Neoproterozoic Pan-African Transcaucasian Massif (Republic of Georgia) and implications for island arc evolution of the late Precambrian Arabian-Nubian Shield. *Gondwana Research*, *11*(1–2), 92–108. https://doi.org/10.1016/j.gr.2006.05.012

Zonenshain, L. P., Kuz'min, M. I., & Natapov, L. M. (1990). Geology of the USSR: A plate tectonic synthesis. *Geodynamics Series*, *21*, 13–242. https://doi.org/10.1029/GD021

Zonenshain, L. P., & Pichon, X. (1986). Deep basins of the Black Sea and Caspian Sea as remnants of Mesozoic back-arc basins. *Tectonophysics*, *123*(1–4), 181–211. https://doi.org/10.1016/0040-1951(86)90197-6

References From the Supporting Information

Hastie, A. R., Mitchell, S. F., Treloar, P. J., Kerr, A. C., Neill, I., & Barfod, D. N. (2013). Geochemical components in a Cretaceous island arc: The Th/La-$(Ce/Ce^*)_{Nd}$ diagram and implications for subduction initiation in the inter-American region. *Lithos*, *162–164*, 57–69. https://doi.org/10.1016/j.lithos.2012.12.001

Jackson, S. E. (2008). Lamtrace data reduction software for LA-ICP-MS. *Mineralogical Association of Canada, Short Course Series*, *40*, 305–307.

Jackson, S. E., Pearson, N. J., Griffin, W. L., & Belousova, E. A. (2004). The application of laser ablation-inductively coupled plasma-mass spectrometry to in situ U-Pb zircon geochronology. *Chemical Geology*, *211*(1–2), 47–69. https://doi.org/10.1016/j.chemgeo.2004.06.017

Ludwig, K. R. (2008). *User's manual for Isoplot 3.70. A geochronological toolkit for Microsoft Excel*, *Special publication* (Vol. 4). Berkeley, California: Berkeley Geochronology Center.

Miller, J. S., Matzel, J. E., Miller, C. F., Burgess, S. D., & Miller, R. B. (2007). Zircon growth and recycling during the assembly of large, composite arc plutons. *Journal of Volcanology and Geothermal Research*, *167*(1–4), 282–299. https://doi.org/10.1016/j.jvolgeores.2007.04.019

Pearce, N. J., Perkins, W. T., Westgate, J. A., Gorton, M. P., Jackson, S. E., Neal, C. R., & Chenery, S. P. (1997). A compilation of new and published major and trace element data for NIST SRM 610 and NIST SRM 612 glass reference materials. *Geostandards Newsletter*, *21*(1), 115–144. https://doi.org/10.1111/j.1751-908X.1997.tb00538.x

Sláma, J., Košler, J., Condon, D. J., Crowley, J. L., Gerdes, A., Hanchar, J. M., et al. (2008). Plešovice zircon—A new natural reference material for U-Pb and Hf isotopic microanalysis. *Chemical Geology*, *249*(1–2), 1–35. https://doi.org/10.1016/j.chemgeo.2007.11.005

Ulianov, A., Müntener, O., Schaltegger, U., & Bussy, F. (2012). The data treatment dependent variability of U-Pb zircon ages obtained using mono-collector, sector field, laser ablation ICPMS. *Journal of Analytical Atomic Spectrometry*, *27*(4), 663–676. http://doi.org/10.1039/c2ja10358c

Wendt, I., & Carl, C. (1991). The statistical distribution of the mean squared weighted deviation. *Chemical Geology: Isotope Geoscience Section*, *86*(4), 275–285. https://doi.org/10.1016/0168-9622(91)90010-T